

**Dynamic Mode Decomposition
and Network Motif Evolution**

A Thesis
Presented to the
Faculty of
San Diego State University

In Partial Fulfillment
of the Requirements for the Degree
Master of Science in Applied Mathematics
with a Concentration in
Dynamical Systems

by
Robert Simpson
Spring 2021

SAN DIEGO STATE UNIVERSITY

The Undersigned Faculty Committee Approves the

Thesis of Robert Simpson:

Dynamic Mode Decomposition

and Network Motif Evolution

Christopher Curtis, Chair
Department of Mathematics and Statistics

Christopher O'Neill
Department of Mathematics and Statistics

Xialu Liu
Department of Management Information Systems

Approval Date

Copyright © 2021
by
Robert Simpson

DEDICATION

To my family, who have been wholly supportive.

ABSTRACT OF THE THESIS

Dynamic Mode Decomposition
and Network Motif Evolution

by
Robert Simpson

Master of Science in Applied Mathematics with a Concentration in Dynamical Systems
San Diego State University, 2021

Complex networks are structurally non-trivial and require a large set of tools to analyze their characteristics. In this thesis, we implement standard statistical correlation and covariance methods. In addition, we implement the data-driven methods, Dynamic Mode Decomposition (DMD), and Kernel Dynamic Mode Decomposition (KDMD). These methods are grounded in Koopman Theory and give us a dynamical systems perspective into network development. With feature matrices built from snapshots of motif counts throughout a network's development, we characterize the local network structure. Using our data-driven methods, we identify sets of DMD and KDMD modes. The DMD and KDMD modes show low mode-error by the Rowley criterion and are good approximations to the true Koopman modes.

TABLE OF CONTENTS

	PAGE
ABSTRACT	v
LIST OF TABLES	ix
LIST OF FIGURES	x
ACKNOWLEDGMENTS	xvi
CHAPTER	
1 Network Theory	1
1.1 An Introduction	1
1.2 Complex Networks	1
1.3 Network Analysis.....	2
1.4 The Social Network Twitter	3
2 Motifs.....	5
2.1 Graph Theory	5
2.2 Non-Simple Cycle Motifs	10
3 Barabási–Albert Model.....	13
4 The Thij Model	20
5 Barabási–Albert Model Motif and Thij <i>T</i> 2 Event Motif Dynamics	36
5.1 H3	36
5.2 H4	37
5.3 H5	37
5.4 H6	39
5.5 H7	40
5.6 H8	42
5.7 H9	43
5.8 H10.....	44
5.9 H11	46
5.10 H12	46
5.11 H13	48
5.12 Summary of Preferential Attachment and <i>T</i> 2 Event Motif Evolution ...	49

6	Twitter Model Specific Motif Evolution	50
6.1	H3	50
6.2	H4	51
6.3	H5	51
6.4	H6	52
6.5	H7	53
6.6	H8	54
6.7	H9	55
6.8	H10	57
6.9	H11	58
6.10	H12	59
6.11	H13	60
6.12	In summary of the T_3 events	61
7	Motif Correlation	62
8	Dynamic Mode Decomposition	75
8.1	The Koopman Operator	75
8.2	Dynamic Mode Decomposition	76
8.3	Kernel Dynamic Mode Decomposition	79
8.4	Accuracy Criterion	80
9	Results	82
9.1	Preprocessing Data	82
9.2	DMD: Barabási-Albert $m=1$	82
9.3	KDMD: Barabási-Albert $m=1$	87
9.4	DMD: Barabási-Albert $m=2$	89
9.5	KDMD: Barabási-Albert $m=2$	92
9.6	DMD: Thij Model with $\lambda = 0.2, p = 0.2$	94
9.7	KDMD: Thij Model with $\lambda = 0.2, p = 0.2$	97
9.8	DMD: Thij Model with $\lambda = 0.2, p = 0.8$	99
9.9	KDMD: Thij Model with $\lambda = 0.2, p = 0.8$	102
9.10	DMD: Thij Model with $\lambda = 0.8, p = 0.2$	104
9.11	KDMD: Thij Model with $\lambda = 0.8, p = 0.2$	107
9.12	DMD: Thij Model with $\lambda = 0.8, p = 0.8$	109

9.13	KDMD: Thij Model with $\lambda = 0.8, p = 0.8$	112
9.14	Accuracy of Methods	114
10	Discussion	118
11	Conclusion	120
	BIBLIOGRAPHY	121

LIST OF TABLES

	PAGE
5.1 The rows denote counts of isomorphisms that can be found in either motif. The H_3 , a four walk, can be found twice in the modified H_3 in event one by starting the walk at either end. In the graph produced again we can only find two H_3 's.....	37
5.2 Motif Counts of the H_4 motif and the possible motifs given a T_2 event.	37
5.3 Motif counts of the possible T_2 events on the H_5 motif.	39
5.4 Motif counts for variations of the T_2 event on the H_6 motif.	40
5.5 Motif counts of the H_7 motif and the possible additions of T_2 event nodes. .	41
5.6 Motif counts graphs formed by possible T_2 events on the H_8 motif.	43
5.7 Motif counts graphs formed by possible T_2 events on the H_9 motif.	43
5.8 Motifs counts of the possible T_2 event on the H_{10} motif.....	45
5.9 Motif counts of the graphs generated by possible T_2 events on the H_{11} motif.	46
5.10 Variations of the T_2 event on the H_{12} motif.....	48
5.11 Motif counts of the possible T_2 events on the H_{13} motif	49
6.1 Motif counts of the possible T_3 events on the H_3 motif.....	51
6.2 Motif counts of the T_3 event on the H_4 motif	51
6.3 Motif counts of the graphs produced by a T_3 event on the H_5 motif.....	52
6.4 Motif counts of graph produced by a T_3 event on the H_6 motif.	53
6.5 Motif counts of the two possible graphs produced by the T_3 event on the H_7 motif	54
6.6 Motif counts of the possible T_3 event on the H_8 motif.....	54
6.7 Motif counts of the possible T_3 event on the H_9 motif.....	56
6.8 Motif counts of the graphs given by a T_3 event on the H_{10} motif	58
6.9 Motif counts of the single graph produced by a T_3 event on the H_{11} motif..	59
6.10 Motif counts of the possible T_3 event on the H_{12} motif.....	59
6.11 Motif counts of the graph given by a T_3 event on the H_{13} motif.....	61

LIST OF FIGURES

	PAGE
1.1 All the circles represent nodes or users in this Twitter network. The edges between the nodes denote follows. The red node is a single user in the Twitter network following Tesla, Dogecoin, and Grimes (denoted by the red edges), but no others. The red user receives all tweets and retweets from Tesla, Dogecoin, and Grimes. This user may retweet these messages outside the network potentially bringing in more users to the network. Note the red node and its adjacents are isomorphic to, S_3 or $H4$	4
2.1 A homomorphism from G to H	6
2.2 An isomorphism between G and H	7
2.3 Example of subgraphs and induced subgraphs on G	8
2.4 A simple cycle of length five.	9
2.5 The star S_4	9
2.6 The first four non-simple motifs. This set is comprised of three-walk ($H3$), a star S_3 ($H4$), the star S_3 with two vertices attached ($H5$), and finally an S_3 with two edges added.	10
3.1 This Barabási–Albert model is initialized with $m = 8$ nodes. At each time-step a new node enters and is attached to $k = 1$ nodes by the preferential attachment mechanism. Only for the motifs who have a node of degree one, can their respective counts increase given $k = 1$. All simulations are terminated after the network reaches a size of 300 nodes.	14
3.2 Statistics characterizing the development of the Barabási–Albert model for $k = 1$. Edges and nodes grow linearly. We also see as Barabási noted, the edge density and clustering coefficients decrease asymptotically.	15
3.3 The Barabási–Albert model for $k = 1$ at the final time-step. The color and size of the nodes reflect the degree centrality of each node.	16
3.4 This Barabási–Albert model is initialized with $m = 5$ nodes. At each time-step a new node enters and is attached to $k = 2$ nodes. We see that different motif appearances correlate for the $k = 2$ simulation and other motif appearances, like those of C_3 and C_5 , can be generated.	17

3.5	Statistics characterizing the development of the Barabási–Albert model for $k = 2$. Edges and nodes grow linearly, with 2 edges added at each time-step. The histogram at the final time also shows that the vast majority of nodes, approximately 220, have two or three attachments while three vertices have a degree greater than 35.....	18
3.6	The Barabási–Albert model for $k = 2$ at the final time-step. Once again the color and size reflect the degree-centrality of each node.	19
4.1	We see the $T1$, $T2$, and $T3$ events on a simple graph. In the $T1$ case we see a new message node $U3$ appears. It has yet to be connected to anything at all. In $T2$ we see a new node $V4$. This is a retweet of the message $U1$. Finally in the last plot we see a $T3$ event. Here the user $V3$, who has already retweeted $U2$, now retweets message $U1$	22
4.2	Here we see that $H8$'s lead with $H9$'s and $H10$'s. These motifs are closely correlated with one another throughout the time series. $H7$'s and $H3$'s have the next highest counts where $H7$ movement prima facie appears to correlate with $H8$ counts, while $H3$ counts steadily increases throughout time.	23
4.3	Compared to the Barabási–Albert model, neither edge count nor node count grow strictly linear at each time-step. The edge density tends toward zero, although a $T3$ event amounts to a small increase in edge density. Finally, we see a final time degree histogram that is similar	24
4.4	The network for $\lambda = 0.2$, $p = 0.2$ at the final time-step.....	25
4.5	For high λ we see many new message nodes appear ($T1$ events), but with low p we should see many $T3$ events. $H3$ motifs are the most prevalent followed by $H8$'s and $H4$'s.	26
4.6	The edges and nodes travel tightly together with roughly a ratio of one-to-one. Here we see many, many nodes unattached with degree zero. For those that are attached, we do see a power law describing degree distribution, but one that is not quite as strong as those found in other simulations.....	27
4.7	The network for $\lambda = 0.8$, $p = 0.2$ at the final time-step.....	28
4.8	Small λ decreases the likelihood of new message nodes appearing, but high p means a greater likelihood of $T2$ events which we speculate lead to a large count of $H4$'s. C_3 's exist around the center where all these $H4$'s overlap. Although $C3$'s are not prevalent here, a combinatorial effect generates many $H7$'s and $H4$'s.	29
4.9	Here, we see two nodes with degrees greater than seventy but an abundance of nodes with only one or two connections. We can see this reflected in the graph of the network in figure 4.10.	30

4.10	The network for $\lambda = 0.2, p = 0.8$ at the final time-step.....	31
4.11	Here, like the simulation directly in figure 4.9, we see a prominence of $H4$'s. The scales of the counts between simulations are separated by several orders of magnitude. In this simulation there is a relatively high count of $H3$'s. We can explain the difference in magnitude due to many $T1$ events introducing many nodes, but the occurrence of $T2$ events is still sufficient to make $H4$ the motif of highest count.....	32
4.12	This Twitter simulation produces many more nodes than edges, because of the frequency of $T1$ events. The vast majority of nodes only have degrees of one or two, while we see a single node with 25 connections. This might suggest many small clusters of nodes with a single larger cluster around a single message node.....	33
4.13	The network for $\lambda = 0.8, p = 0.8$ at the final time-step.....	34
5.1	The possible graphs generated by adding a node to the $H3$ graph and connecting it to an existing node.....	36
5.2	The possible graphs generated by adding a node to the $H4$ graph and connecting it to an existing node.....	37
5.3	The possible graphs generated by adding a node to the $H5$ graph and connecting it to an existing node.....	38
5.4	The possible graphs generated by adding a node to the $H6$ graph and connecting it to an existing node.....	39
5.5	The possibly graphs generated by adding a node to the $H7$ graph and connecting it to an existing node.....	41
5.6	The possible graphs generated by adding a node to the $H8$ graph and connecting it to an existing node.....	42
5.7	The possible graphs generated by adding a node to the $H9$ graph and connecting it to an existing node.....	44
5.8	The possible graphs generated by adding a node to the $H10$ graph and attaching it to an existing node.....	45
5.9	The possibly graphs generated by adding a node to the $H11$ graph and connecting it to an existing node.....	46
5.10	The possibly graphs generated by adding a node to the $H12$ graph and connecting it to an existing node.....	47
5.11	The $H13$ graph and possible node attachments up to symmetry.....	48
6.1	The possible graphs generated by adding an edge to the $H3$ graph.....	50

6.2	The possible graphs generated by adding an edge to the $H4$ graph. By connecting the two outer edges we find a C_4 and by connecting an outer vertex to an inner vertex we generate a $H5$	51
6.3	The possible graphs generated by adding an edge to the $H5$ graph.....	52
6.4	The possible graphs generated by adding an edge to the $H6$ graph.....	53
6.5	The possible graphs generated by adding an edge to the $H7$ graph.....	53
6.6	The possible graphs generated by adding an edge to the $H8$ graph.....	55
6.7	The possible graphs generated by adding an edge to the $H9$ graph.....	56
6.8	The possible graphs generated by adding an edge to the $H10$ graph.	57
6.9	The possible graphs generated by adding an edge to the $H11$ graph.	58
6.10	The possible graphs generated by adding an edge to the $H12$ graph.	60
6.11	The possible graph generated by a $T3$ event on the $H13$	61
7.1	Barabási–Albert model with eight initial nodes and $m = 1$. The model is capable of only producing certain motifs due to the limita- tions of attaching a single edge and a single node at every time-step. We also see that $H7$'s and $H8$'s correlate together. However, appear- ances of those motifs depend upon the initialization of the graph itself.	62
7.2	Barabási–Albert model with eight initial nodes and $m = 1$. Here we once again see that the $H7$ and $H8$ motifs have a much higher covariance than any other pair of motifs.	63
7.3	Here we have the Barabási–Albert model with $m = 3$ initial nodes and $k = 2$. Here we see that all motifs are present. They all have fairly high correlation coefficients, but we see that the $H7$'s and $H8$'s are highly correlated as is $H7$ and $H8$ with $H3$	64
7.4	Barabási–Albert model with $m = 3$ initial nodes and $k = 2$. The covariance offers a different perspective from that of the correlation figure. The $H7$ and $H8$ motif counts exhibit high covariance, and once again there is a relationship between $H8$, $H7$, $H3$, $H4$. Other motifs have a much smaller covariances.	65
7.5	$\lambda = 0.2$ and $p = 0.2$. We recall low λ reduces the chance of only adding a new node ($T1$) and low p reduces the chance of adding a new node and a new edge. Thus probabilistically this simulation should be overall adding only edges between existing nodes.	66
7.6	$\lambda = 0.2$ and $p = 0.2$. Here we see once again a strong covariance relationship between $H7$, $H8$, $H9$, $H10$. In this particular graph it's insightful to see these correlate together given these parameters are less likely to produce the induced star subgraph we expect to see for higher p	67

7.7	$\lambda = 0.2$ and $p = 0.8$. Here in the correlation coefficients we see that there is a strong correlation between $H7$, $H8$, but otherwise a much larger spread over the motifs. We also see that no $H6$ or $H13$ motifs appeared throughout this simulation.	68
7.8	$\lambda = 0.2$ and $p = 0.8$. Here the covariance is relatively very small, except for the $H4$ variance. This is suggestive of the high p generating that induced star subgraph.....	69
7.9	$\lambda = 0.8$ and $p = 0.2$. Once again we see a familiar structure in the correlation matrix. Here though we do see strong correlations across a wider selection of motifs: $C3$, $C4$, $C5$, $H3$, $H4$, $H5$, $H7$, $H8$, $H9$, $H10$. It appears the $H6$'s are not easily produced by any of the parameters chosen or the Barabási–Albert model.	70
7.10	$\lambda = 0.8$ and $p = 0.2$. We do see strong covariance around the $H4$ with other motifs. There is possibly multiple induced star subgraphs connected that could drive this phenomena generating many $H4$'s along with other motifs.	71
7.11	$\lambda = 0.8$ and $p = 0.8$. Here we have a higher likelihood of adding a new node or a new edge and node. Here we do not see any new $H6$'s or $H8$'s produced after the initialization of the graph. Any block structures that we saw in earlier correlation matrices are not as apparent, although there is still strong $H7$ - $H8$ correlation.	72
7.12	$\lambda = 0.8$ and $p = 0.8$. The covariances formed by this simulation suggest once again an overlapping of $H4$'s, but there are clearly more nodes attached to the outer edges of this induced subgraph. This could lead to the covariance we see between $H3$ and $H4$	73
9.1	Smooth motif counts for Barabási–Albert model $k = 1$	84
9.2	Mode eigenvalues for Barabási–Albert model with $k = 1$	85
9.3	DMD modes for Barabási–Albert model with $k = 1$	86
9.4	Mode eigenvalues by KDMD for Barabási–Albert model with $k = 1$	87
9.5	KDMD modes for Barabási–Albert model with $k = 1$	88
9.6	Smooth motif counts for the Barabási–Albert model with $k = 2$	89
9.7	DMD modes for the Barabási–Albert model with $k = 2$	90
9.8	KDMD modes for the Barabási–Albert model with $k = 2$	91
9.9	Mode eigenvalues by KDMD for the Barabási–Albert model with $k = 2$	92
9.10	KDMD modes for the Barabási–Albert model with $k = 2$	93
9.11	Smooth motif counts for the Thij model with $\lambda = 0.2$, $p = 0.2$	94
9.12	Mode eigenvalues by DMD for the Thij model with $\lambda = 0.2$, $p = 0.2$	95

9.13	DMD modes for the Thij model with $\lambda = 0.2, p = 0.2$	96
9.14	Mode eigenvalues by KDMD for the Thij model with $\lambda = 0.2, p = 0.2$	97
9.15	KDMD modes for the Thij model with $\lambda = 0.2, p = 0.2$	98
9.16	Motif counts for the Thij model with $\lambda = 0.2, p = 0.8$	99
9.17	Mode eigenvalues by DMD for the Thij model with $\lambda = 0.2, p = 0.8$	100
9.18	DMD modes for the Thij model with $\lambda = 0.2, p = 0.8$	101
9.19	Mode eigenvalues by KDMD for the Thij model with $\lambda = 0.2, p = 0.8$	102
9.20	KDMD modes for the Thij model with $\lambda = 0.2, p = 0.8$	103
9.21	Motif counts for the Thij simulation with $\lambda = 0.8, p = 0.2$	104
9.22	Mode eigenvalues by DMD for the Thij model with $\lambda = 0.8, p = 0.2$	105
9.23	DMD modes for the Thij model with $\lambda = 0.8, p = 0.2$	106
9.24	Mode eigenvalues by KDMD for the Thij model with $\lambda = 0.8, p = 0.2$	107
9.25	KDMD modes for the Thij model with $\lambda = 0.8, p = 0.2$	108
9.26	Motif counts for the Thij model with $\lambda = 0.8, p = 0.8$	109
9.27	Mode eigenvalues by DMD for the Thij model with $\lambda = 0.8, p = 0.8$	110
9.28	DMD modes for the Thij model with $\lambda = 0.8, p = 0.8$	111
9.29	Mode eigenvalues by KDMD for the Thij model with $\lambda = 0.8, p = 0.8$	112
9.30	KDMD modes for the Thij model with $\lambda = 0.8, p = 0.8$	113
9.31	In orange, have the reconstruction error of the DMD results and in cyan the KDMD results. The DMD performs much better with regard to reconstruction error, by several scales of magnitude.	114
9.32	DMD also seems to produce modes with lower mode error. The scale on this figure is linear, so the differences are not as large as in figure 9.31.	115
9.33	DMD and KDMD reconstruction errors across Thij simulations. DMD again has very low reconstruction errors compared to KDMD.	116
9.34	DMD and KDMD mode errors across simulations. DMD does seem to produce better results, but KDMD has the advantage of being able to produce more Koopman modes. The KDMD results for $\lambda = 0.2, p = 0.2$ is a noticeable outlier with very low mode error.	116

ACKNOWLEDGMENTS

I would like to thank Chris Curtis for his invaluable insight and mentorship throughout the making of this thesis. I would also like to thank Professor Chris O'Neill and Professor Xialu Liu for taking part as members of the thesis committee. Finally, a thank you to the Professors of the SDSU Department of Mathematics and Statistics, who have encouraged my learning and development in applied mathematics these last several years.

This thesis is partially protected against the evil forces of the Montezuma Publishing thesis reviewers by the magic of the Department of Mathematics and Statistics Master's Thesis L^AT_EX Template.

CHAPTER 1

Network Theory

1.1 An Introduction

The social network has taken on new meaning with the advent of the computer, particularly with mobile technology. Social media allows for information (and misinformation) to spread rapidly within and across communities. These communities and their interactions are well-modeled by network theory, an extension of graph theory. Individuals are represented as nodes in these networks, and their connections as edges. These nodes and their connections form patterns in the networks. These patterns, or motifs, offer a way to characterize the local structure of the network making them informational features. These motif counts change over time as users enter and leave the network. The dynamic behavior of these motif counts, and how they correlate with one another, offers a way to understand how the network changes locally in time. This analysis can extend easily beyond social networks into other domains. In the following section, we first establish some of the fundamentals of network theory.

1.2 Complex Networks

The terms "network" and "graph" are often used interchangeably as networks are represented via vertices and edges, but networks are graphs in specific context. In its most general sense a network is comprised of objects and connections between those objects. These connections may be directed, undirected, weighted - representing any number of different relationships. The versatility and effectiveness of this approach has encouraged network modeling in a variety of fields: physics, sociology, biology, economy, chemistry. Some networks are small and simple. Most networks are large containing many nodes and connections and many of these are topologically (or structurally) non-trivial. These we refer to as complex networks and they are commonly found in those fields mentioned previously.

Complex networks differ from other networks as edges are found between vertices in patterns neither completely random nor regular. Such networks often have degree distributions that are fat-tailed meaning a few nodes are of relatively high degree, while most other nodes are not. These networks are commonly called scale-free

networks. The Barabási–Albert model we examine later will fall under this category. These networks also cluster, which correlates with the scale-free property.

1.3 Network Analysis

Network science has many statistical measures to differentiate networks from one another. These measures offer different levels of insight into a network and its structure. One such measure is the notion of centrality. There are several different types of centrality, but each represents a way to denote the most important vertices within a given network. One such measure is degree centrality. Aptly named, degree centrality assigns a weight to each vertex determined by its degree d_i . In chapter 3 and chapter 4, degree centrality is useful as the preferential attachment model’s dynamics directly depend on it. The centrality measures are informative about the connectivity of the network, but leave much to be desired in the way of understanding structure. We make use of the clustering coefficient in chapters 3 and 4 to characterize graph dynamics. Thij [33] notes that clustering coefficients are a way to understand how a network’s density changes over time. He further notes that future study of the proposed Twitter model found should include an analysis of its temporal clustering coefficients. To define the clustering coefficient we first define the neighborhood of a vertex N_i .

$$N_i = \{v_j : e_{i,j} \in E \vee e_{j,i} \in E\}$$

The local clustering coefficient of a node v_i in the undirected graph G is defined as

$$C_i = \frac{2|p_i|}{k_i(k_i - 1)}$$

where we define p_i

$$p_i = \{e_{jk} : e_j, e_k \in N_i, e_{j,k} \in E\}$$

This can also be calculated by way of the adjacency matrix described in definition 2.

$$C_i = \frac{1}{k_i(k_i - 1)} \sum_{j,k} a_{i,j} a_{j,k} a_{i,k}$$

The average clustering coefficient is calculated by arithmetic mean.

$$\bar{C} = \frac{1}{|V|} \sum_i C_i$$

The global clustering coefficient is simply

$$C_G = \frac{\text{Total Number of Triangles}}{\text{Total Possible Triangles}}$$

Clustering allows us to understand how dense a network is relative to a complete graph.

1.4 The Social Network Twitter

Twitter is now, as of 2021, an eminent example of complex networks in social media. As of 2019, there are 330 million monthly active users on Twitter, thirteen years after the platform was established in 2006. However, according to Pew Research, the top ten percent of Twitter users tweet 138 tweets per month, while the bottom ninety percent of Twitter users only tweet twice per month. The top ten percent of users have a median of 387 followers while the bottom ninety percent have only a median of 19 followers. The top ten percent also follow more users, a median of 456 accounts, compared to a median of 74 accounts for the bottom ninety percent [36]. This itself is suggestive of a Twitter being a scale-free network, but analysis confirms this [5]. Twitter, as a network with vertices as users and edges as signifying follows, exhibits a fat-tailed degree distribution. Moreover, its estimated average clustering coefficient is two-hundred-fifty-six-thousand times larger than expected for a random graph.

Twitter's status as a complex network aside, the platform is also notable for its position among social networks not only for its size, but also its influence on culture and politics. During the 2016 election, a survey of thirty million tweets from two million users, linked articles that were found to be spreading false information. Moreover, this information spread based on community structure within an inclusive left-right influencer network. Twitter is cliquey and the communities form around shared interests. In online communities where exposure to the same memetic theme occurs frequently, facts and rumors may spread easily and quickly [8].

Twitter also has a substantial economic impact. Twitter sentiment is known to precede fluctuations in the stock market [11] and Bitcoin prices [32]. Only a handful of Twitter users actually have influence, although groups of people could theoretically be enough to influence market prices [30]. Elon Musk is one such person who, as of March 2021, has influenced multiple markets driving Tesla's share price up and down [16], as well as causing jumps in cryptocurrency prices [13] [14]. Musk is as of 2021, the forty-third largest Twitter account giving him much more influence than the vast majority of users.

Twitter's suitability as a subject of network science is clear. The users and follows (and retweets) are naturally described in by vertices and edges. One can generate networks from Twitter in a two ways. First, there are the user accounts which are linked to one another through followers and follows, in-degrees and out-degrees. An

example of this is given in Figure 1.1. One can also construct networks of tweets and retweets as discussed in chapter 4. A user posts a message, which is retweeted by a portion of their followers, which is then again retweeted by a portion of their followers. It is this latter case we will consider in the Thij model.

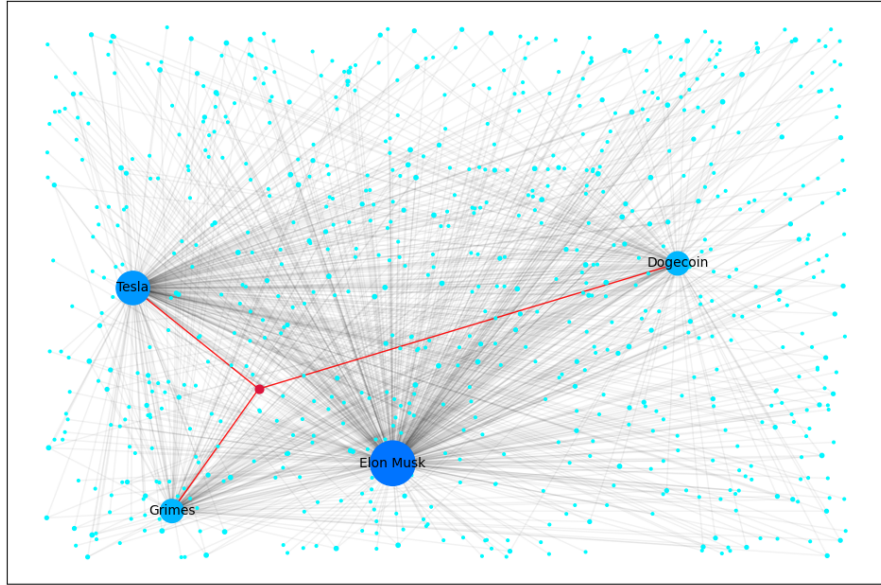


Figure 1.1. All the circles represent nodes or users in this Twitter network. The edges between the nodes denote follows. The red node is a single user in the Twitter network following Tesla, Dogecoin, and Grimes (denoted by the red edges), but no others. The red user receives all tweets and retweets from Tesla, Dogecoin, and Grimes. This user may retweet these messages outside the network potentially bringing in more users to the network. Note the red node and its adjacents are isomorphic to, S_3 or $H4$.

CHAPTER 2

Motifs

Motifs are the primary object of interest as a way of characterizing the local structure of a network. The dynamic motif count indicates the network and the communities within are evolving according to certain rules. In the context of static networks, the frequency of motifs has been shown to highlight system properties in biological networks [28] [1].

Motifs are the fundamental components of complex systems. The topological structure of complex networks is tied to the frequency and distribution of motifs. Initially, the counting of these motifs was treated as a static problem where the frequencies of motifs affect functions on networks [21]. As the significance of motifs has become more apparent authors have begun examining the emergence of motifs via temporal edges [26]. Our motifs will act as a vector of features characterizing the network at each point in time. Before we examine our specific motifs we must first define common objects of graph theory such as cycles, paths, and stars which will aid us in understanding the motifs we would like to examine.

2.1 Graph Theory

In the pursuit of counting our particular motifs, we require some ideas from graph theory. There is no reason some of these objects could not be motifs on their own. We will count three-cycles, four-cycles, and five-cycles as motifs themselves, but we require the non-simple cycle motifs. Much of the literature on motifs focuses on directed triangle motifs [26] [24] [29], but the motifs can take on other shapes. The motifs in this thesis are undirected but more varied in edge and node count. Motifs are generally best described by graphs.

Definition 1. *Let $G = (V, E)$ be a graph with V being a set of vertices (or nodes), and E , a set of edges. If v is a vertex of G we write $v \in V(G)$. If $u, v \in V(G)$ and there is an edge between them we write $\{u, v\} \in E(G)$*

Graphs may be directed or undirected. For directed graphs $\{u, v\} \in E(G)$ is taken to mean there exists an edge from u to v in G . Undirected meaning the edge between u and v to have no notion of direction.

Definition 2. The adjacency matrix for any graph G with $n = |V|$ vertices is a matrix of size $n \times n$. The element a_{ij} is defined to be

$$a_{ij} = \begin{cases} 1 & e_{ij} \in E(G) \\ 0 & \text{otherwise} \end{cases}$$

The adjacency matrix is critical to all of our calculations to come. It renders any graph amenable to the tools of linear algebra.

Definition 3. We call $f : G \rightarrow H$ a homomorphism, if f maps endpoints in

$G = (V(G), E(G))$ to endpoints in $H = (V(H), E(H))$. i.e.

$$\forall u, v \in V(G) \quad \{u, v\} \in E(G) \Rightarrow \{f(u), f(v)\} \in E(H).$$

For example, in Figure 2.1 we can define a mapping f such that:

$$f(0) = A$$

$$f(1) = A$$

$$f(2) = B$$

$$f(3) = C$$

Thus f is a homomorphism by the definition presented in definition 3. We now define particular cases of the homomorphism.

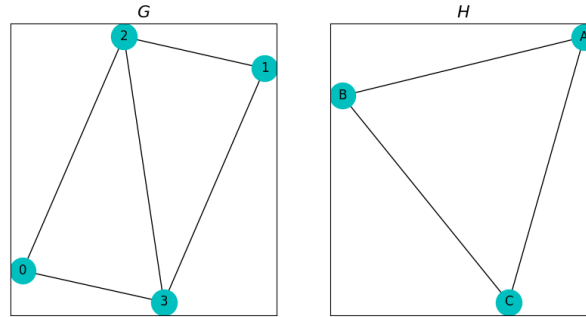


Figure 2.1. A homomorphism from G to H .

Definition 4. We call $f : G \rightarrow H$ an isomorphism, if f is a homomorphism and is bijective.

We can define an isomorphism f for between G and H in the figure 2.2 such that:

$$g(0) = B$$

$$g(1) = A$$

$$g(2) = C$$

$$g(3) = D$$

Definition 5. An automorphism is an isomorphism between a graph G and itself. The automorphism is edge-preserving, $\{u, v\} \in G \implies \{f(v), f(u)\} \in G$.

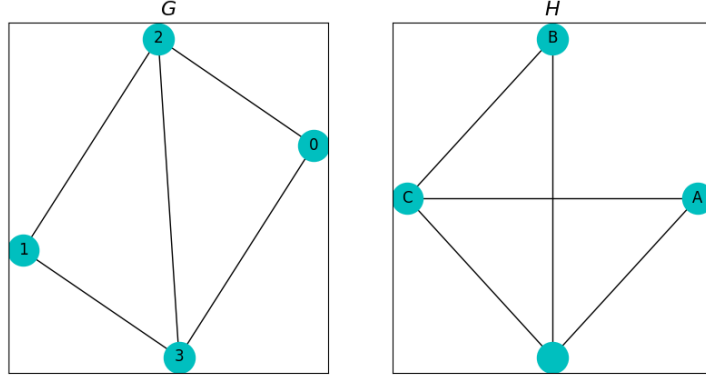


Figure 2.2. An isomorphism between G and H .

Automorphisms represent the symmetries of a graph. For instance, a C_3 with vertices $\{A, B, C\}$ and the set of undirected edges $\{A, B\}, \{B, C\}, \{C, A\}$, has six possible automorphisms - three from rotation and three from reflection of the graph. Below when counting motifs on graphs, the algorithms only count up to symmetry. For instance, where we find an induced subgraph isomorphic to the C_3 we count the single appearance.

Definition 6. Let $G = (V, E)$ be a graph. We call $G' = (V', E')$ a subgraph, denoted $G' \subset G$, if $V' \subseteq V \wedge E' \subseteq E \cap (V' \times V')$. Furthermore we call G' an induced subgraph of G if for the edges $\{u, v\}$ of G' we have $\{u, v\} \in E$, for $u, v \in V'$.

Induced subgraphs are vital to our understanding of how motifs interact as we add edges or nodes to a given graph. In Figure 2.3, G has a subgraph which does not

include the edge $\{1, 2\}$. If the edge is included in the set then we have an induced subgraph of G .

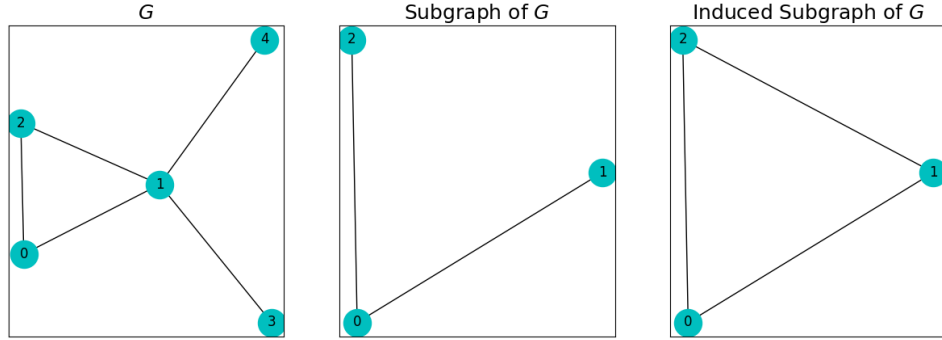


Figure 2.3. Example of subgraphs and induced subgraphs on G .

Definition 7. Let $G'' \subset G$ and furthermore let there exist an isomorphism between G'' and G' . We call G'' an appearance of G' . Provided the number of appearances of G' is greater than some N we call G' a motif or pattern.

Definition 8. A walk $W = \{v_0, e_1, v_1, \dots, v_n\}$ is a sequence of edges and vertices of G such that for $0 \leq k \leq n - 1$ the edge $e_i = \{v_k, v_{k+1}\}$.

Definition 9. A cycle is a walk whose first and last vertex is the same.

Cycles are often also referred to by the geometric objects they resemble. A three-cycle is a triangle, and a four-cycle is a square. The three-cycle, four-cycle, and five-cycle will feature as motifs in our feature vectors. A five-cycle is featured in Figure 2.4.

Definition 10. A bipartite graph is a graph whose nodes may be separated into two disjoint sets U and V such that there exists an edge between all vertices in U and all vertices in V .

The $C3$ and $C4$ motif counts are themselves a measurement of clustering the graph. In fact, the global clustering coefficient defined in chapter one explicitly requires the $C3$ count in its calculation. We count few bipartite motifs, but do count star graphs whose definition relies on the definition of a bipartite graph. However, the definition of a star graph S_k is very useful, because some of the motif counts increase exponentially due to the motifs that are generated as a new node or a new edge is added to the S_k graph. An example of S_4 can be found in Figure 2.5.

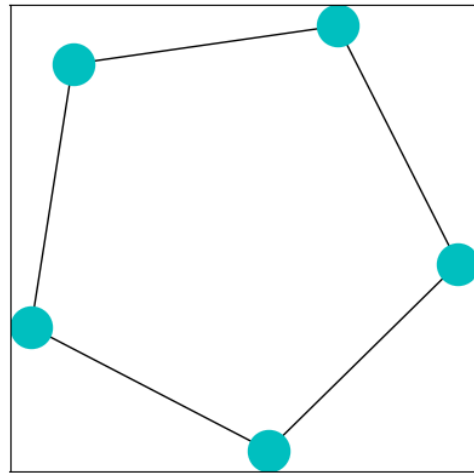


Figure 2.4. A simple cycle of length five.

Definition 11. A star S_n denotes the complete bipartite graph $K_{1,n}$. In other words a tree with one internal node, but n branches.

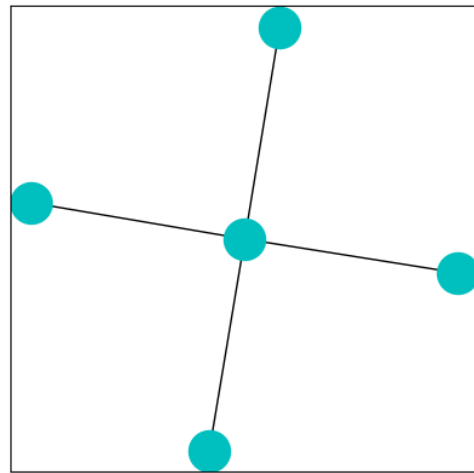


Figure 2.5. The star S_4 .

2.2 Non-Simple Cycle Motifs

We wish to consider motifs that we refer to as H_3 up to H_{13} . These motifs, and their enumerations, are described in [4]. In Figure 2.6, are the graphs of all eleven motifs.

Definition 12. Let f be a homomorphism between graphs G and H . We say that H is a homomorphic image of G provided f is surjective.

Definition 13. A graph $H = (V_H, E_H)$ is said to be k -cyclic, for $k > 3$, if it is a homomorphic image of the cycle C_k . The number of different homomorphisms from C_k to H is denoted by $C_k(H)$. H is k -cyclic if and only if $C_k(H) > 0$.

These motifs are non-simple cycles. For the motifs in figures 2.6 we can classify them according to which cycle each graph is a homomorphic image. H_3 , H_4 , H_6 , H_9 , and H_{11} are all six-cyclic. H_5 is the only five-cyclic graph. However H_5 , H_6 , H_7 , H_8 , H_{10} , H_{12} , and H_{13} are all seven-cyclic.

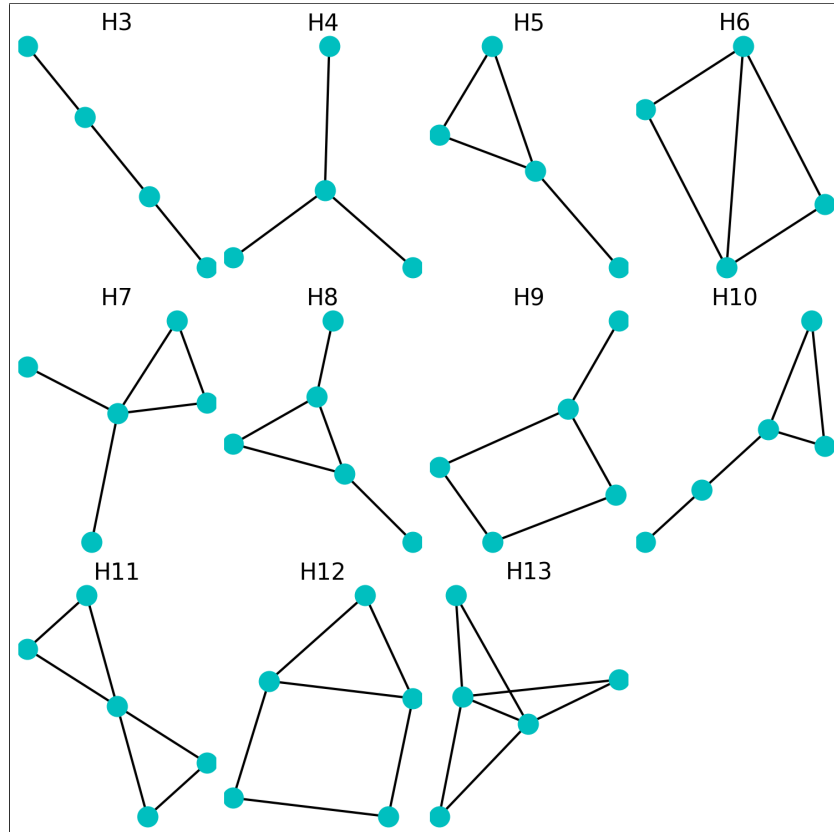


Figure 2.6. The first four non-simple motifs. This set is comprised of three-walk (H_3), a star S_3 (H_4), the star S_3 with two vertices attached (H_5), and finally an S_3 with two edges added.

We will also consider the simple cycles of C_3 , C_4 , C_5 . Motif counts can be generated from a network's adjacency matrix in the following ways. Let A be the adjacency matrix of some arbitrary network with greater than four nodes. Let $N_m(A)$ denote the total count of motif m in the network.

When counting motifs, we let E denote the set of edges in the network, e_i, j denotes a particular edge between the i 'th and j 'th nodes. d_i denotes the degree of the i 'th node. A is the adjacency matrix of the graph G . Finally, $a_{i,j}^{(k)}$ denotes the k th power of the matrix element at the i 'th row and j 'th column of matrix A . The formulae for motif counts are as follows:

$$\begin{aligned}
N_G(C3) &= \frac{1}{6} \text{tr}(A^3) \\
N_G(C4) &= \frac{1}{8} \left(\text{tr}(A^4) - 4 \sum_{i=1}^n \binom{d_i}{2} - 2 \sum_{i,j \in E} e_{i,j} \right) \\
N_G(C5) &= \frac{1}{2} \sum_{(i,j) \in E} (d_i - 1)(d_j - 1) - 3N_{C3} \\
N_G(H4) &= \sum_{i=1}^n \binom{d_i}{3} \\
N_G(H5) &= \frac{1}{2} \sum_{i=1}^n a_{i,i}^{(3)} (d_i - 2) \\
N_G(H6) &= \sum_{(i,j) \in E} \binom{a_{i,j}^{(2)}}{2} \\
N_G(H7) &= \frac{1}{2} \sum_{i=1}^n a_{i,i}^{(3)} \binom{d_i - 2}{2} \\
N_G(H8) &= \sum_{(i,j) \in E} a_{i,j}^{(2)} (d_i - 2)(d_j - 2) - 2N_G(H6) \\
N_G(H9) &= \sum_{i=1}^n (d_i - 2) \sum_{j \neq i} \binom{a_{i,j}^{(2)}}{2} \\
N_G(H10) &= \frac{1}{2} \sum_{i=1}^n a_{i,i}^{(3)} \sum_{j \neq i} a_{i,j}^{(2)} - 3N_G(C3) - 2N_G(H5) - 4N_G(H6) \\
N_G(H11) &= \sum_{i=1}^n \binom{\frac{1}{2} a_{i,i}^{(3)}}{2} - 2N_G(H6) \\
N_G(H12) &= \sum_{(i,j) \in E} a_{i,j}^{(2)} a_{i,j}^{(3)} - 9N_G(C3) - 2N_G(H5) - 4N_G(H6) \\
N_G(H13) &= \sum_{(i,j) \in E} \binom{a_{i,j}^{(2)}}{3}
\end{aligned}$$

We want to understand how each motif count affects another given the addition of new nodes or edges in any simulation. Some motifs contain an appearance of another motif and this will affect how they interact with one another. In chapter 5, an analysis of edge addition on the motif graphs shows simple changes to a motif's graph may cause a combinatorial effect generating a large number of new motif appearances.

CHAPTER 3

Barabási–Albert Model

The early models of networks failed to capture the characteristics that appear in empirical data. An early model proposed by Paul Erdős and Alfréd Rényi, appropriately called the Erdős–Rényi model, generates graphs of fixed node count where each pair of nodes has the same probability to have an edge between them. Réka Albert and Albert Barabási recognized the Erdős–Rényi model was incapable of modeling most real-world phenomena as the Erdős–Rényi model does not add in new nodes or edges through a temporal process. In three key areas, real network structure differs from the Erdős–Rényi model [7]. First, real networks often have degree distributions that are not explainable according to a Poisson distribution. Second, real networks have a sizable largest connected component - a large cluster of nodes inside the network, forming a hub of activity. Finally, the local clustering coefficient of most networks decreases as the node degree decreases, but is independent of overall graph size.

Réka Albert and Albert Barabási developed a model of complex networks encompassing those we find common in practice. They found the dynamic addition of new nodes and new edges to a network generate the network's defining characteristics. Edges were found to follow a preferential attachment mechanism, which ascribes probabilities of attachment, based upon the relative degree of the nodes in a network. Moreover, most networks are scale-free and their degree distributions follow a power law. The preferential attachment mechanism of the Barabási–Albert model generates this power law. A network is said to follow a power law if the fraction of nodes P having k edges is

$$P(N) \approx k^{-\gamma}, \quad 2 < \gamma < 3$$

To model such a network, we begin at $t = 0$ by initializing m nodes and randomly distribute a number of edges between them according to a uniform distribution. Then at each time-step $t > 0$, we introduce a new node and k edges between that node and the existing nodes. We assign probabilities of attachment to the n th node via the probability distribution:

$$\Pi(n) = \frac{d_n}{\sum_{i=1}^N d_i}$$

where d_i is the degree of the i th node and N is the total number of nodes at $t - 1$.

Nodes which have a high degree are probabilistically more likely to be attached to new nodes.

In Figure 3.1, we see that only certain motifs can be generated in the $k = 1$ BA model. Motif counts in the Barabási–Albert model are dependent upon the initialization of the m nodes and the choice of k . For example, if $k = 1$ the model cannot complete any new cycles. If the initial graph at $t = 0$ does not contain any C_3 or C_4 appearances then any motif which has an induced subgraph isomorphic to C_3 or C_4 cannot appear. The BA model for $k = 1$ can only attach nodes to the existing C_3 or C_4 appearances and in that way generate new $H7$'s, $H8$'s, $H9$'s. The BA model with $k = 2$ is capable of generating those new C_3 , C_4 , and C_5 appearances in the network quite easily in Figure 3.4.

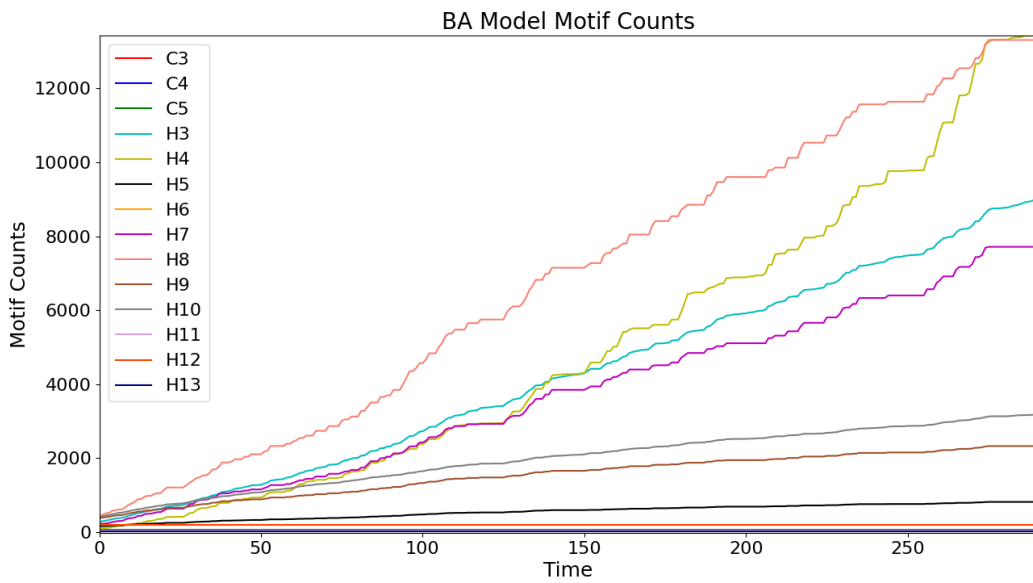


Figure 3.1. This Barabási–Albert model is initialized with $m = 8$ nodes. At each time-step a new node enters and is attached to $k = 1$ nodes by the preferential attachment mechanism. Only for the motifs who have a node of degree one, can their respective counts increase given $k = 1$. All simulations are terminated after the network reaches a size of 300 nodes.

The Barabási–Albert model exhibits a few characteristics that differentiate it from the Erdős–Rényi model. If we consider its diameter, the maximum distance in the network, for $k > 1$ and sufficiently large time we can write the diameter analytically. Let N be the total number of nodes in the network.

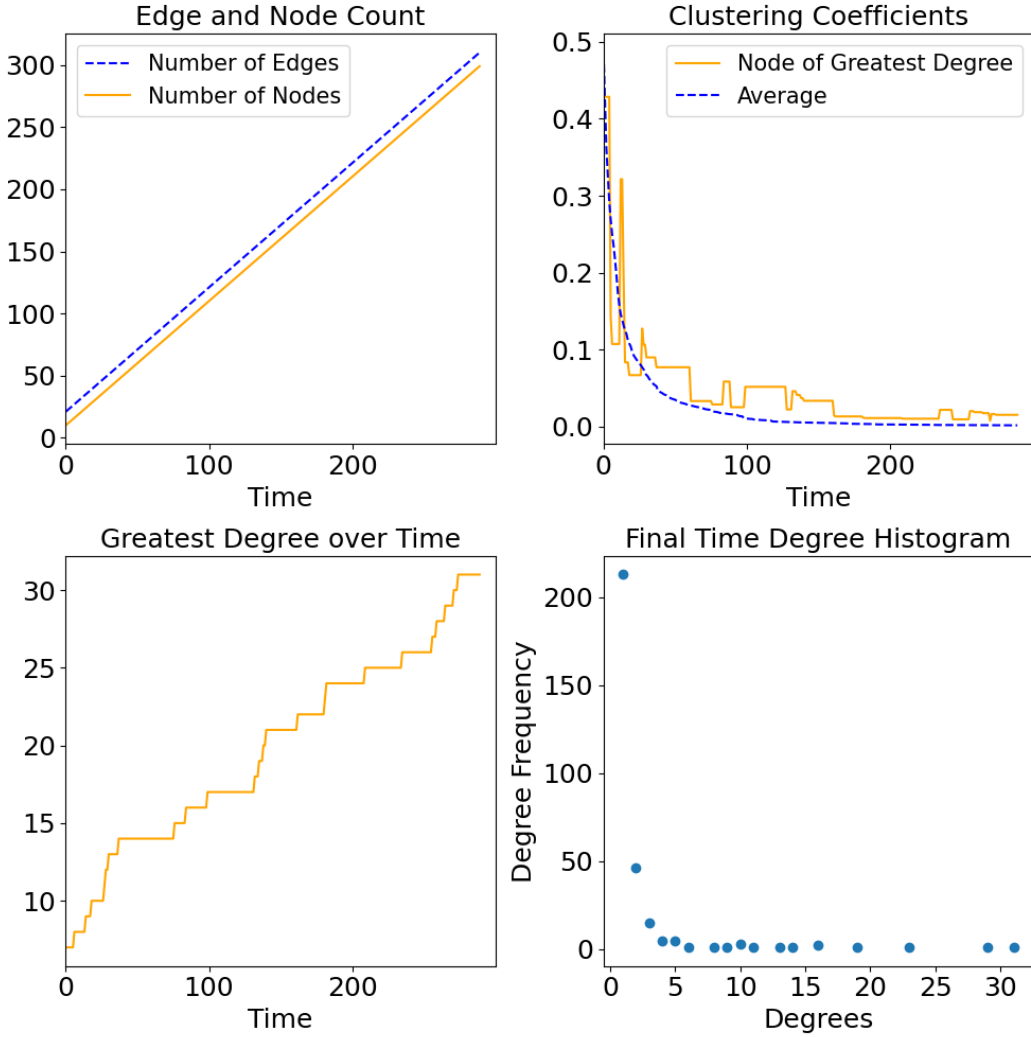


Figure 3.2. Statistics characterizing the development of the Barabási–Albert model for $k = 1$. Edges and nodes grow linearly. We also see as Barabási noted, the edge density and clustering coefficients decrease asymptotically.

$$\text{diam}(G) = \frac{\ln(N)}{\ln(\ln(N))}$$

The diameter grows slower than $\ln(N)$ or the rate of growth for the Erdős–Rényi model’s diameter. We can also examine the clustering coefficient of the model. The clustering coefficients for the preferential attachment model grows according to [22].

$$C(G) = \frac{(\ln(N))^2}{N}$$

This differs from the Erdős–Rényi model by the term $(\ln(N))^2$, which increases the clustering coefficient for large N . Still, as N grows large, both clustering coefficients

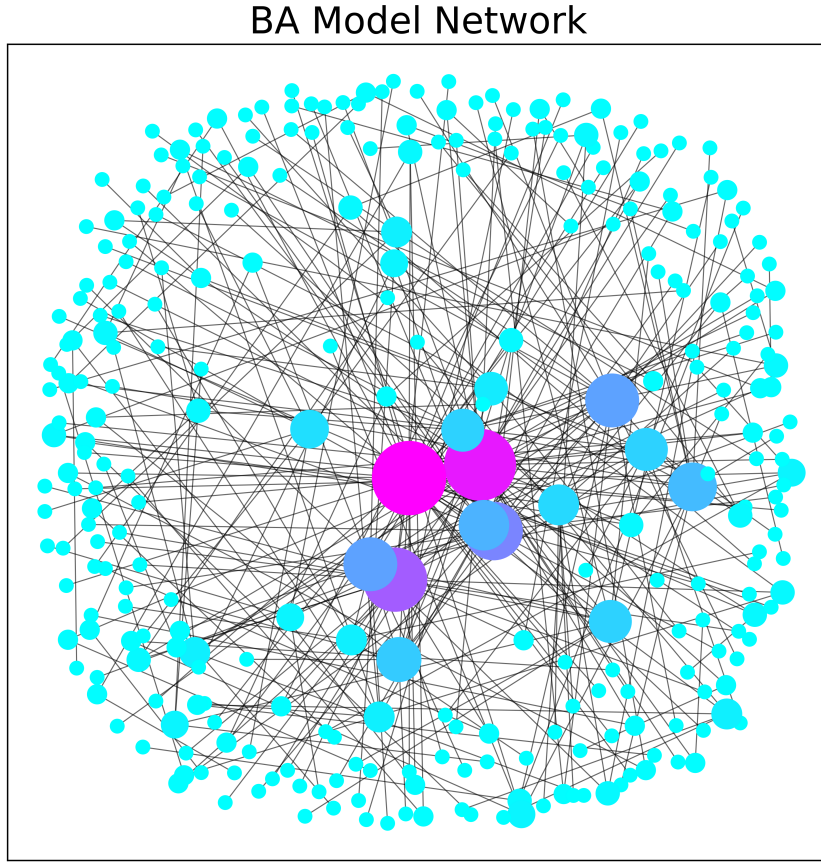


Figure 3.3. The Barabási–Albert model for $k = 1$ at the final time-step. The color and size of the nodes reflect the degree centrality of each node.

decrease, asymptotically approaching zero. The Barabási-Albert network is locally more clustered than a random network for all N [7].

The Barabási–Albert model is a good candidate to compare to the Thij model, given that the Thij model incorporates a preferential attachment mechanism itself. The Thij model is more complex and the study of how motifs interact in the Thij model is much more difficult. The Barabási–Albert model represents a simpler, non-trivial model, which is widely acknowledged as a useful tool for understanding networks across a variety of disciplines. We should note the limitations to the Barabási–Albert model. The nodes and edges are restricted to growing linear which may fail to capture certain phenomena that appear empirically. The model is also incapable of removing nodes, a

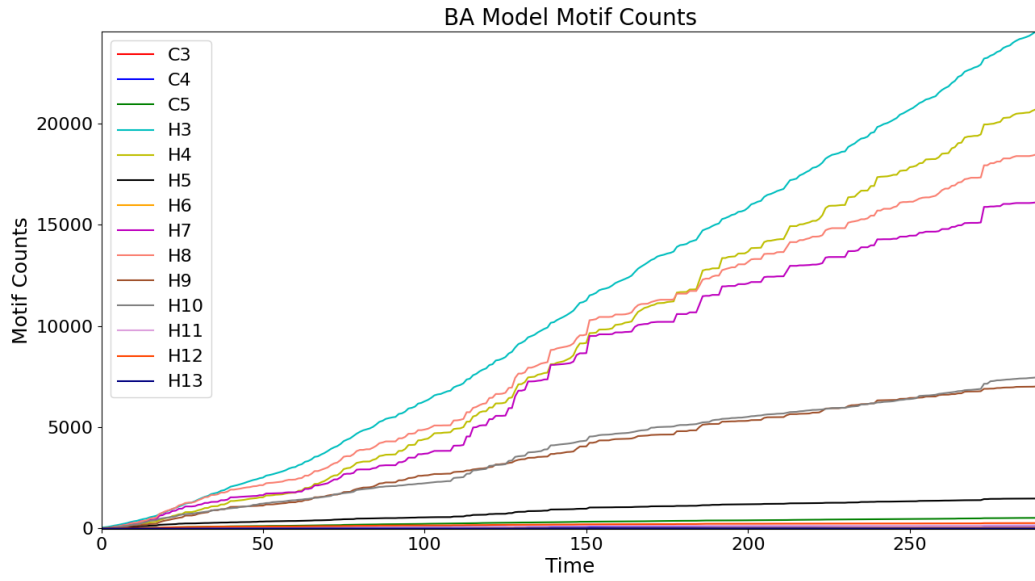


Figure 3.4. This Barabási–Albert model is initialized with $m = 5$ nodes. At each time-step a new node enters and is attached to $k = 2$ nodes. We see that different motif appearances correlate for the $k = 2$ simulation and other motif appearances, like those of C_3 and C_5 , can be generated.

point on which Barabási himself has elaborated. The following model does account for the first of these limitations at the cost of increased complexity.

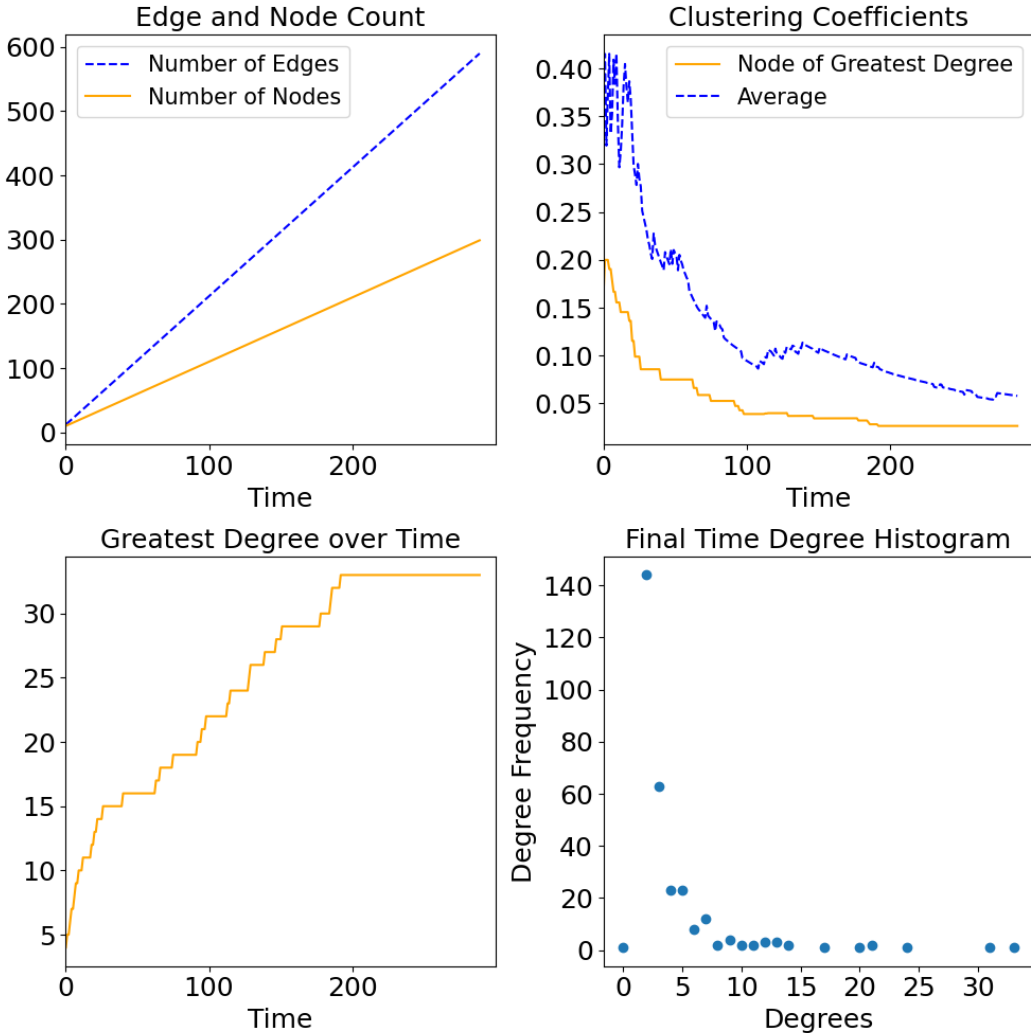


Figure 3.5. Statistics characterizing the development of the Barabási–Albert model for $k = 2$. Edges and nodes grow linearly, with 2 edges added at each time-step. The histogram at the final time also shows that the vast majority of nodes, approximately 220, have two or three attachments while three vertices have a degree greater than 35.

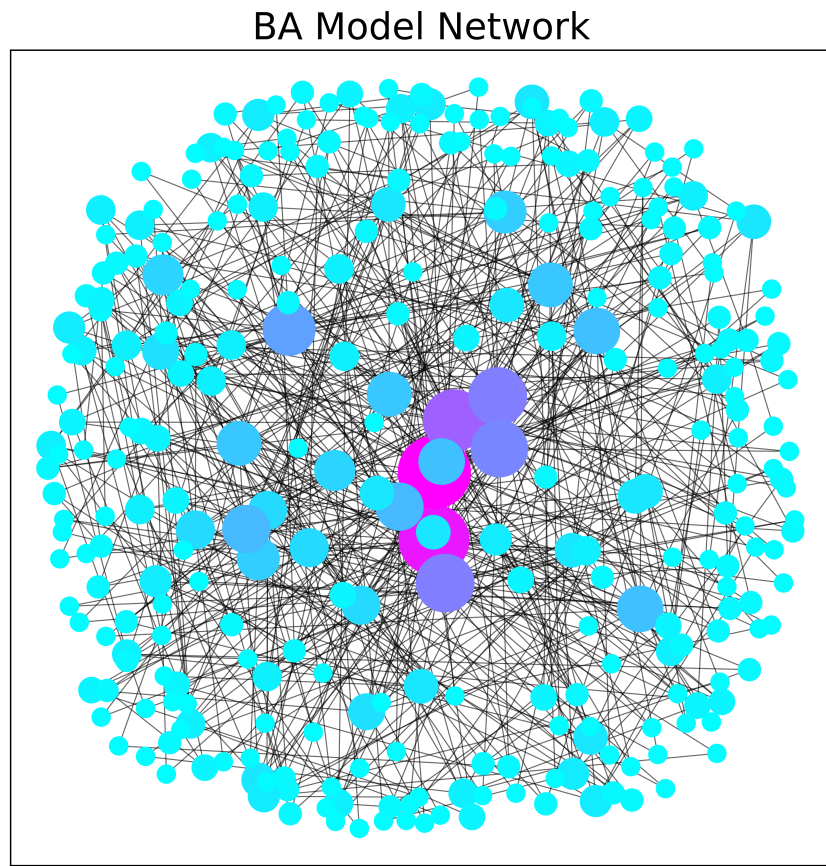


Figure 3.6. The Barabási–Albert model for $k = 2$ at the final time-step. Once again the color and size reflect the degree-centrality of each node.

CHAPTER 4

The Thij Model

The Thij model is a particular random graph that seeks to model the development of a Twitter network [33]. Twitter offers a platform where a user may post a message to all of their followers' feeds. Those followers may then ignore, like, reply (comment), or retweet (quote tweet) that message. In the instance they choose to retweet the message, that message is then posted to their respective feed and their own followers now have the opportunity to then retweet that same message. If a message has received a significant number of retweets the message is more likely to be seen, and thus retweeted again. A preferential attachment mechanism drives the popularity of the most popular tweets [5].

A user can retweet different original messages at different times, meaning edges can be generated between existing nodes in the network. Accounting for this, one can produce a model better suited to Twitter simulations than the Barabási–Albert model described in chapter 3.

We wish to simulate a network of retweets. There are the original message nodes from users u_i and retweets from users v_i . All users are capable of retweeting or posting original messages. For clarity, we make a distinction between the posts of original messages and retweets. v_i may be a simple retweet, or a quote tweet, meaning v_i may reasonably retweet v_k who may have added commentary to the original message. The simulation starts with an initial message node from user u_0 at time $t = 0$. For all time-steps, there is now the possibility of three events: $T1$, $T2$, and $T3$.

T1: A new message node from user u_k appears.

T2: A user v_k enters the retweet network and retweets an existing user, either a u_i who has posted an original message or v_i with $i \neq k$ who has simply retweeted another user in the network. This user v_k retweets an original message node u_i with probability q and any other node with probability $\frac{1-q}{N}$. N is the total number of nodes in the network.

T3: An existing user v_i retweets another existing user u_i or v_j . The retweeter retweets a message node with probability q and all other message or retweet nodes with probability $\frac{1-q}{N}$.

We must also note that there will be multiple message nodes in the retweet graph, and thus, we have to decide for any given event which particular message node should be assigned the q probability. Here we introduce a preferential attachment mechanism. At any time t , given a $T2$ or $T3$ event occurring, the probability of a particular message node being chosen is almost the same mechanism described in the Barabási–Albert model. Instead, a message node is chosen by its total descendants and not by the degree of the message node itself. In essence, a message node is selected based upon the number of those who have retweeted the message and all those who have retweeted retweets of that message.

We now must assign probabilities of $T1$, $T2$, and $T3$ events. Let $\lambda \geq 0$ and $1 \geq p \geq 0$,

$$\begin{aligned} P(T1) &= \frac{\lambda}{1 + \lambda} \\ P(T2) &= \frac{p}{1 + \lambda} \\ P(T3) &= \frac{1 - p}{1 + \lambda} \end{aligned}$$

Our choices of λ and p will drastically affect the dynamics of the graph, as well as the motif counts that make up its structure. We want to consider a series of cases for different probabilities allowing us to make informed predictions about the graph's development over time. The motif counts for various parameters help demonstrate the differences in scale and structure which arise from different probability distributions. Consider the case when $0.5 > \lambda > 0$ and $0.5 \gg p > 0$. In this case, it is the $T3$ event expected to be the most prevalent. For these parameter values, we see in figure 4.2 the first four greatest motif counts almost everywhere in order are $H8, H10, H9$, and $H7$. The $T3$ mechanism allows for more C_3 's and C_4 's to form within the network.

Next, consider $1 > \lambda > 0.5$ and $0.5 \gg p > 0$. Here the $T1$ event should dominate the dynamics with many new message nodes introduced to the overall retweet network. In this scenario, we have a greater likelihood of $T3$ events. This means those nodes without connections are likely to become connected to other message nodes. In figures 4.5 and 4.7 we can visualize the motif development and the overall network. Looking at the final time degree distribution in figure 4.6, we see the majority of nodes are still unconnected.

What about the case $0 < \lambda \ll 0.5$ and $1 > p \gg 0.5$? The probability distribution is such that adding a new node with an edge is the most likely outcome. These

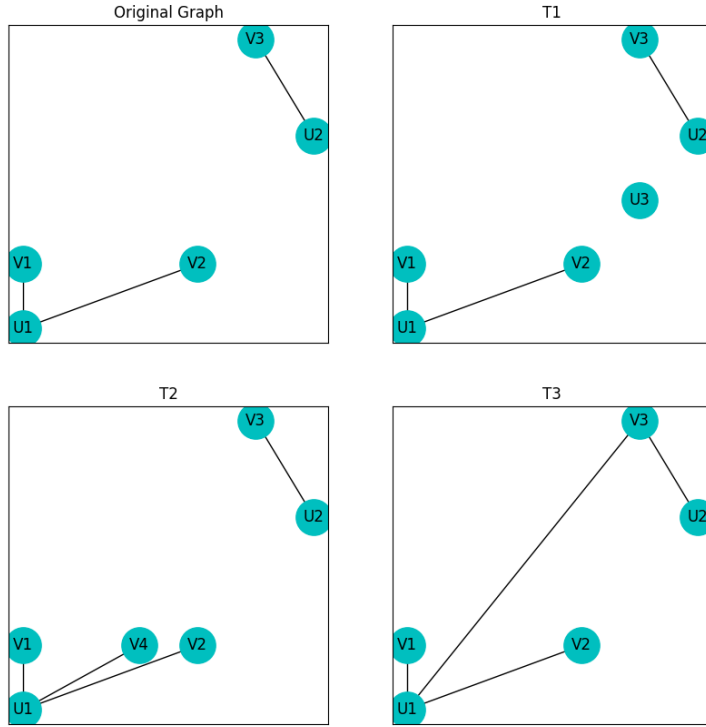


Figure 4.1. We see the T_1 , T_2 , and T_3 events on a simple graph. In the T_1 case we see a new message node U_3 appears. It has yet to be connected to anything at all. In T_2 we see a new node V_4 . This is a retweet of the message U_1 . Finally in the last plot we see a T_3 event. Here the user V_3 , who has already retweeted U_2 , now retweets message U_1 .

parameter choices combines with the superstar parameter $q = 0.9$ means that T_2 and T_3 attachments are very likely to target the root message node. In figure 4.8, we see the resulting star pattern in the motif counts and the end-result in figure 4.10. The preferential attachment mechanism encourages an induced subgraph S_k to form with $k \gg 1$. For any $k \gg 3$ S_k itself has many appearances of H_4 and for every increase in k we see an increase in the probability of yet another increase in k .

Last, $1 > \lambda > 0.5$ and $1 > p \gg 0.5$, we see an increased chance of adding many new root messages, but still a good possibility of introducing a new node with a new edge, but a decreased possibility of adding in only new edges. For an example of the resulting motif counts we can look to figure 4.11.

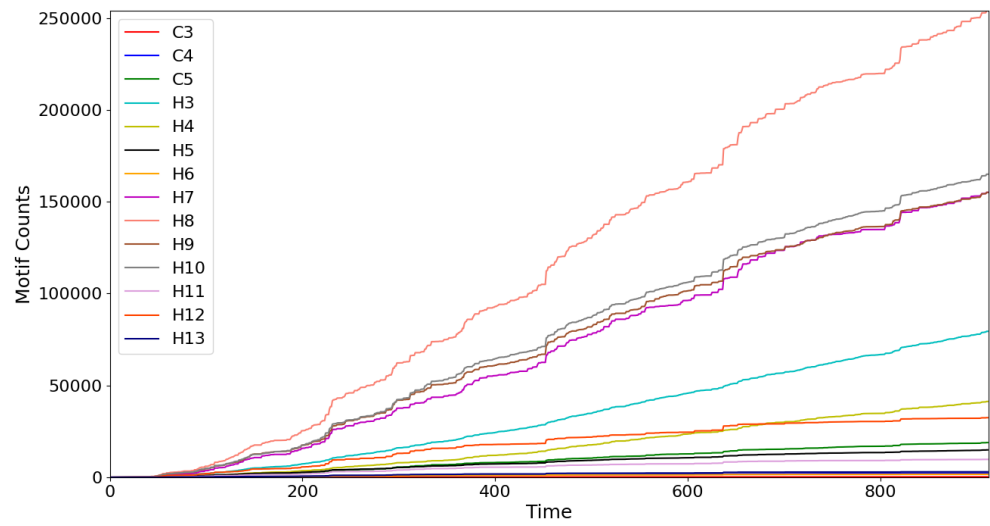


Figure 4.2. Here we see that H_8 's lead with H_9 's and H_{10} 's. These motifs are closely correlated with one another throughout the time series. H_7 's and H_3 's have the next highest counts where H_7 movement *prima facie* appears to correlate with H_8 counts, while H_3 counts steadily increases throughout time.

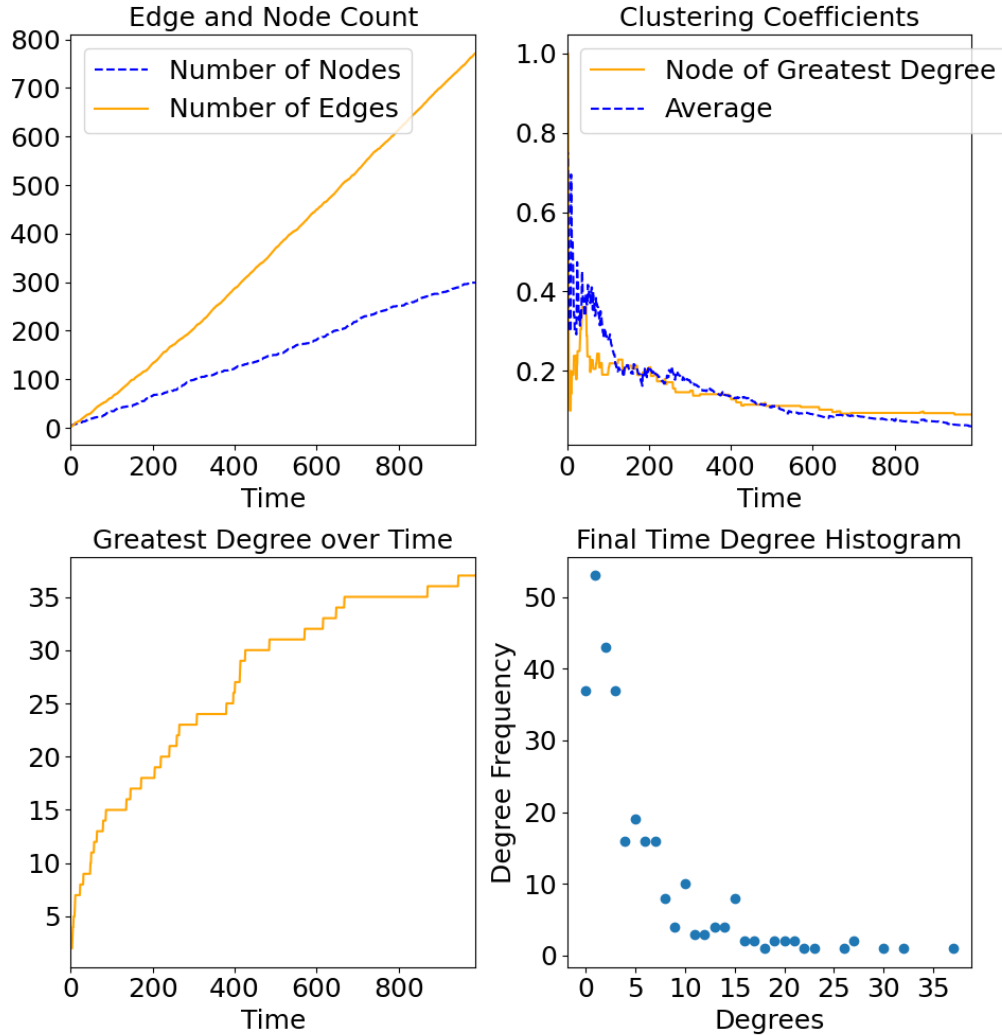


Figure 4.3. Compared to the Barabási–Albert model, neither edge count nor node count grow strictly linear at each time-step. The edge density tends toward zero, although a T_3 event amounts to a small increase in edge density. Finally, we see a final time degree histogram that is similar.

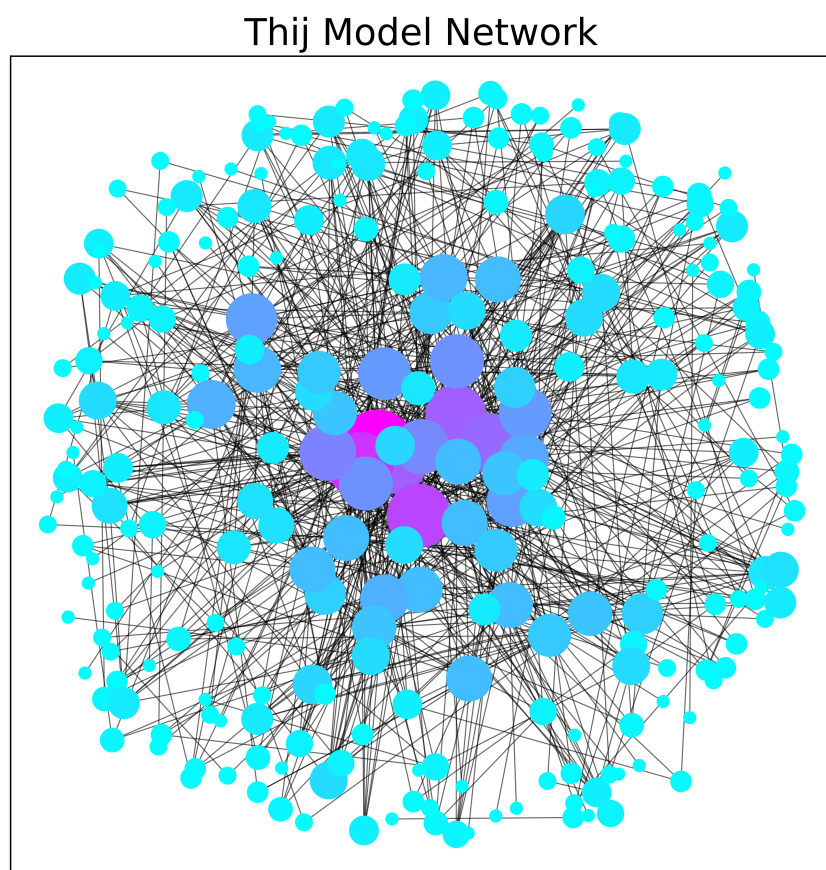


Figure 4.4. The network for $\lambda = 0.2$, $p = 0.2$ at the final time-step.

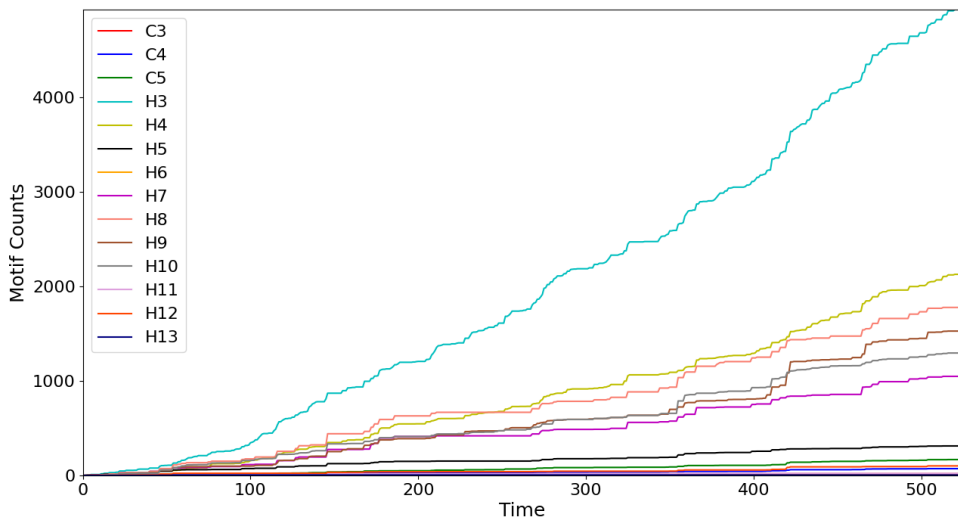


Figure 4.5. For high λ we see many new message nodes appear (T_1 events), but with low p we should see many T_3 events. H_3 motifs are the most prevalent followed by H_8 's and H_4 's.

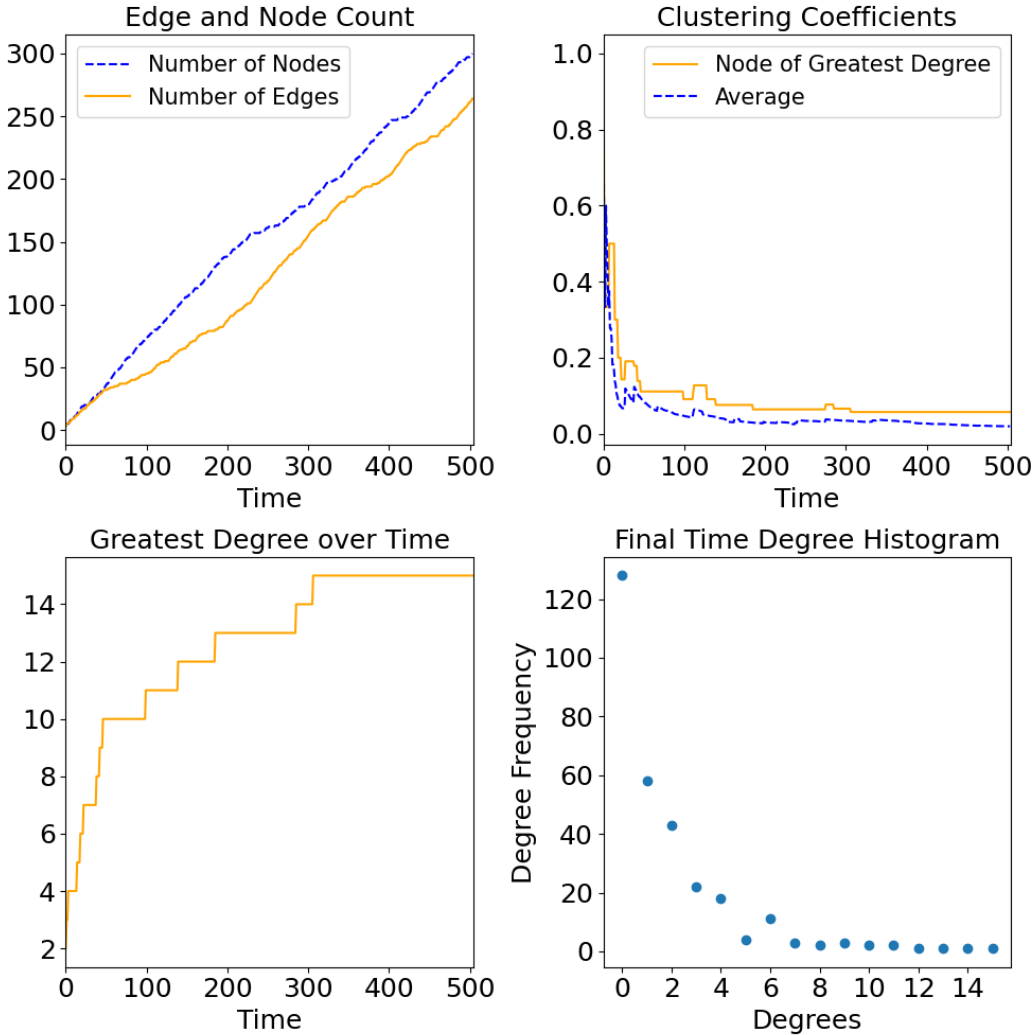


Figure 4.6. The edges and nodes travel tightly together with roughly a ratio of one-to-one. Here we see many, many nodes unattached with degree zero. For those that are attached, we do see a power law describing degree distribution, but one that is not quite as strong as those found in other simulations.

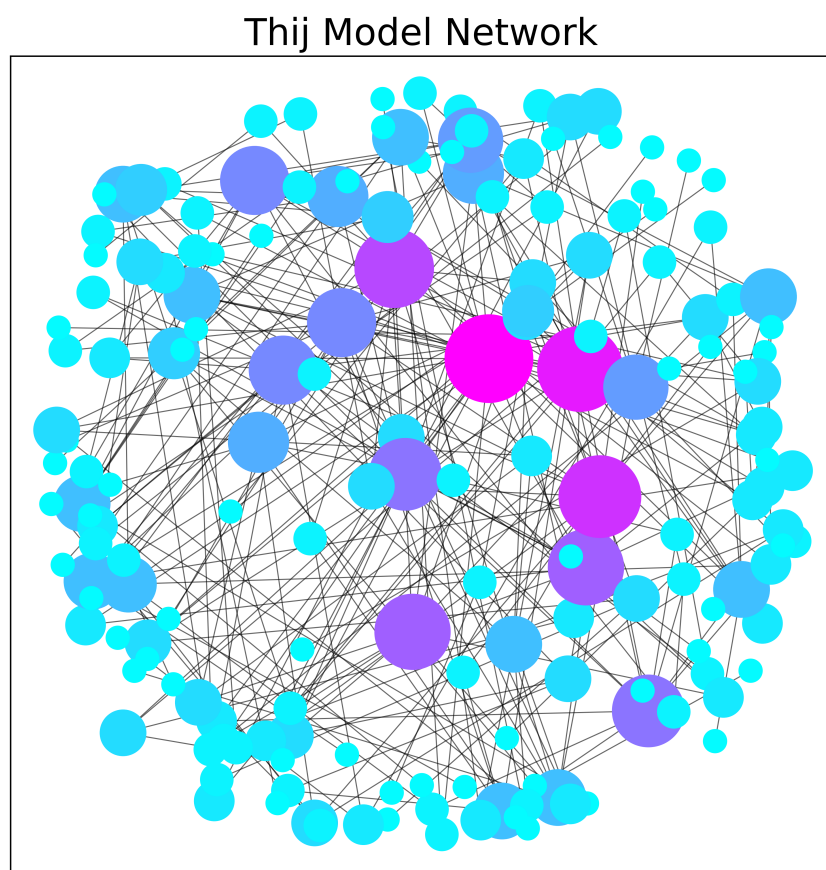


Figure 4.7. The network for $\lambda = 0.8$, $p = 0.2$ at the final time-step.

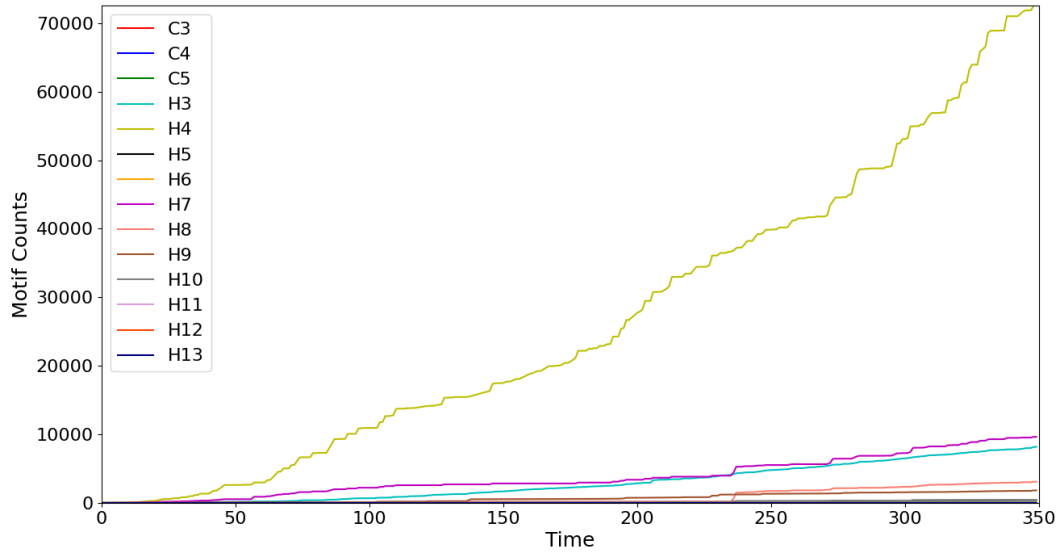


Figure 4.8. Small λ decreases the likelihood of new message nodes appearing, but high p means a greater likelihood of T_2 events which we speculate lead to a large count of H_4 's. C_3 's exist around the center where all these H_4 's overlap. Although C_3 's are not prevalent here, a combinatorial effect generates many H_7 's and H_4 's.

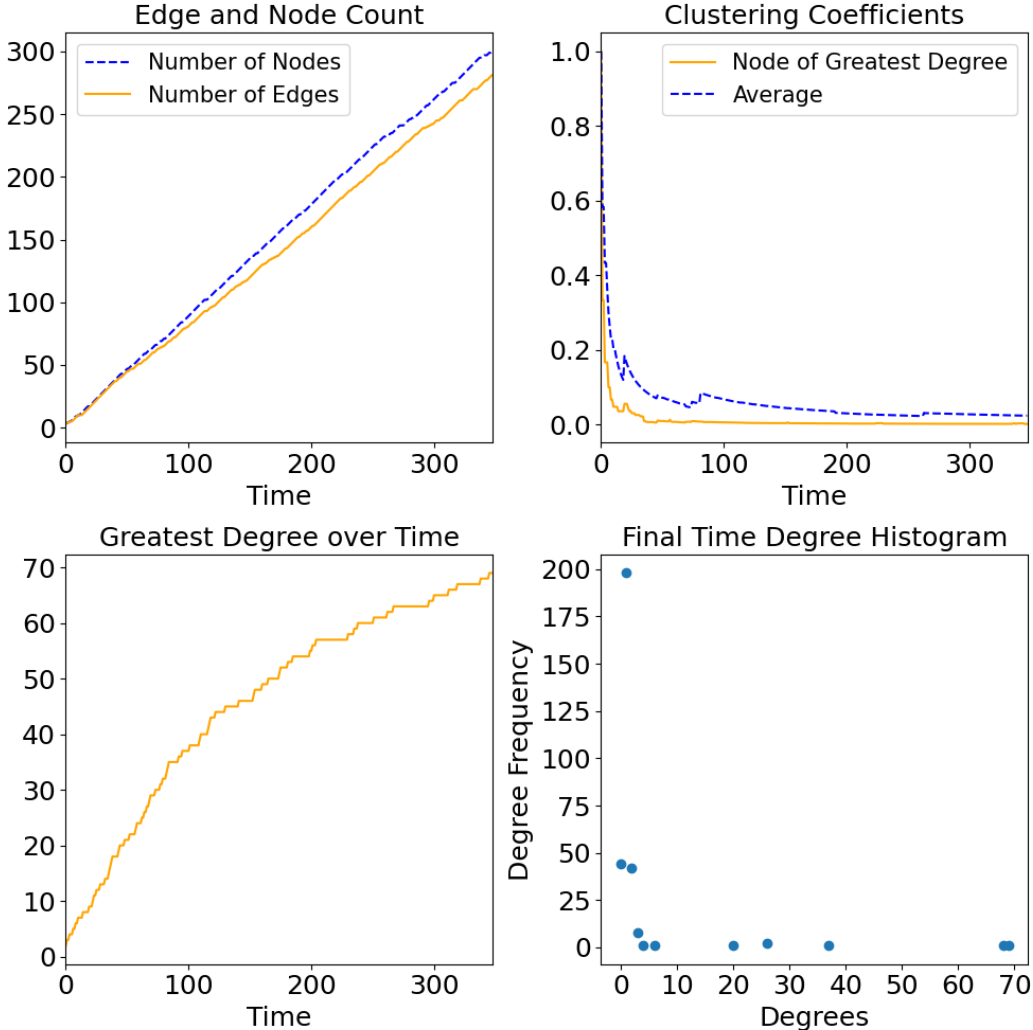


Figure 4.9. Here, we see two nodes with degrees greater than seventy but an abundance of nodes with only one or two connections. We can see this reflected in the graph of the network in figure 4.10.

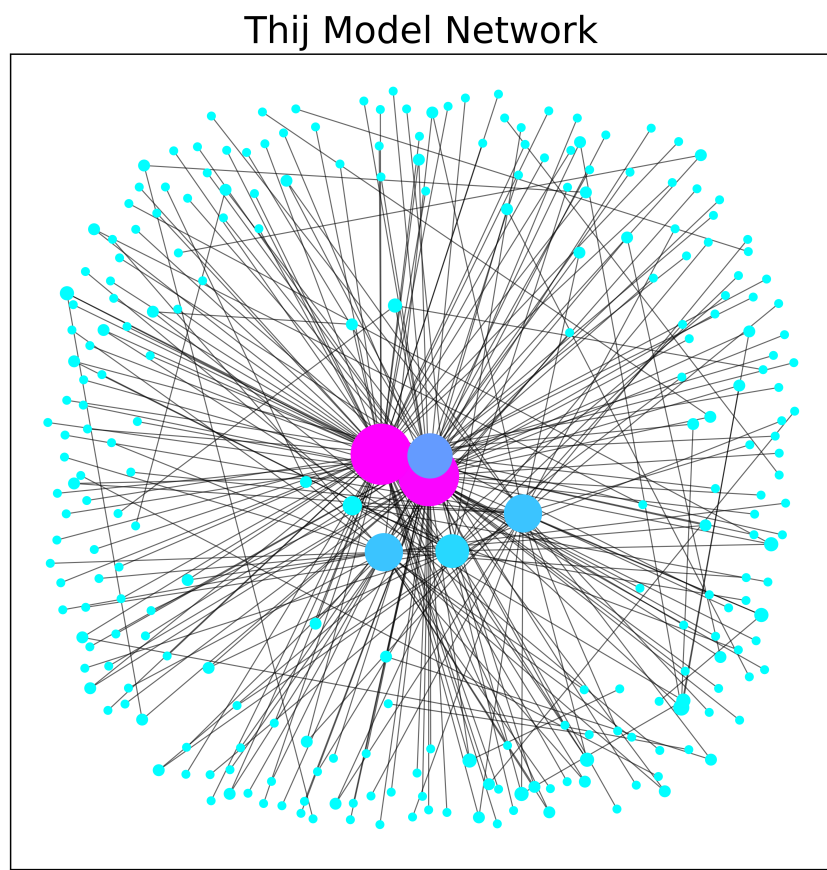


Figure 4.10. The network for $\lambda = 0.2$, $p = 0.8$ at the final time-step.

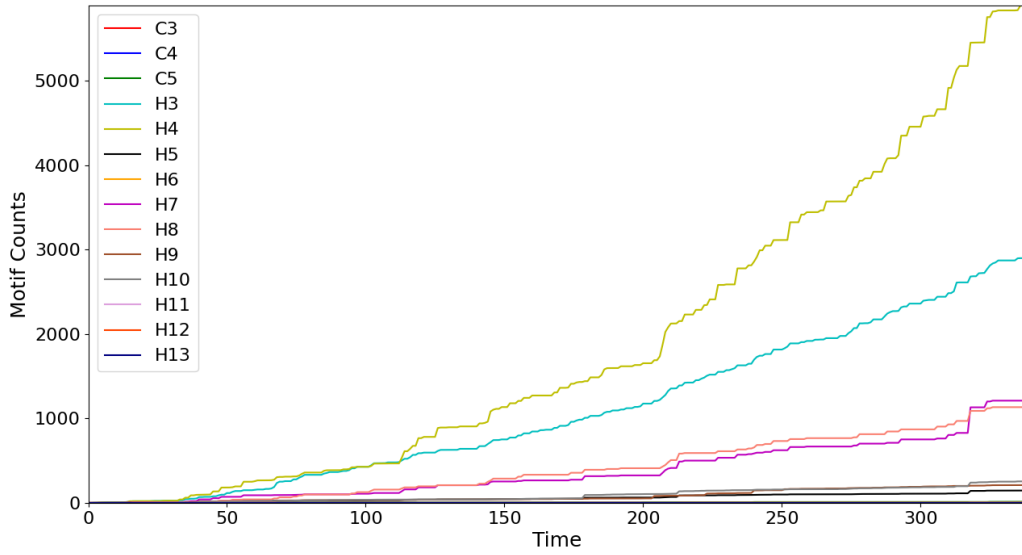


Figure 4.11. Here, like the simulation directly in figure 4.9, we see a prominence of H_4 's. The scales of the counts between simulations are separated by several orders of magnitude. In this simulation there is a relatively high count of H_3 's. We can explain the difference in magnitude due to many T_1 events introducing many nodes, but the occurrence of T_2 events is still sufficient to make H_4 the motif of highest count.

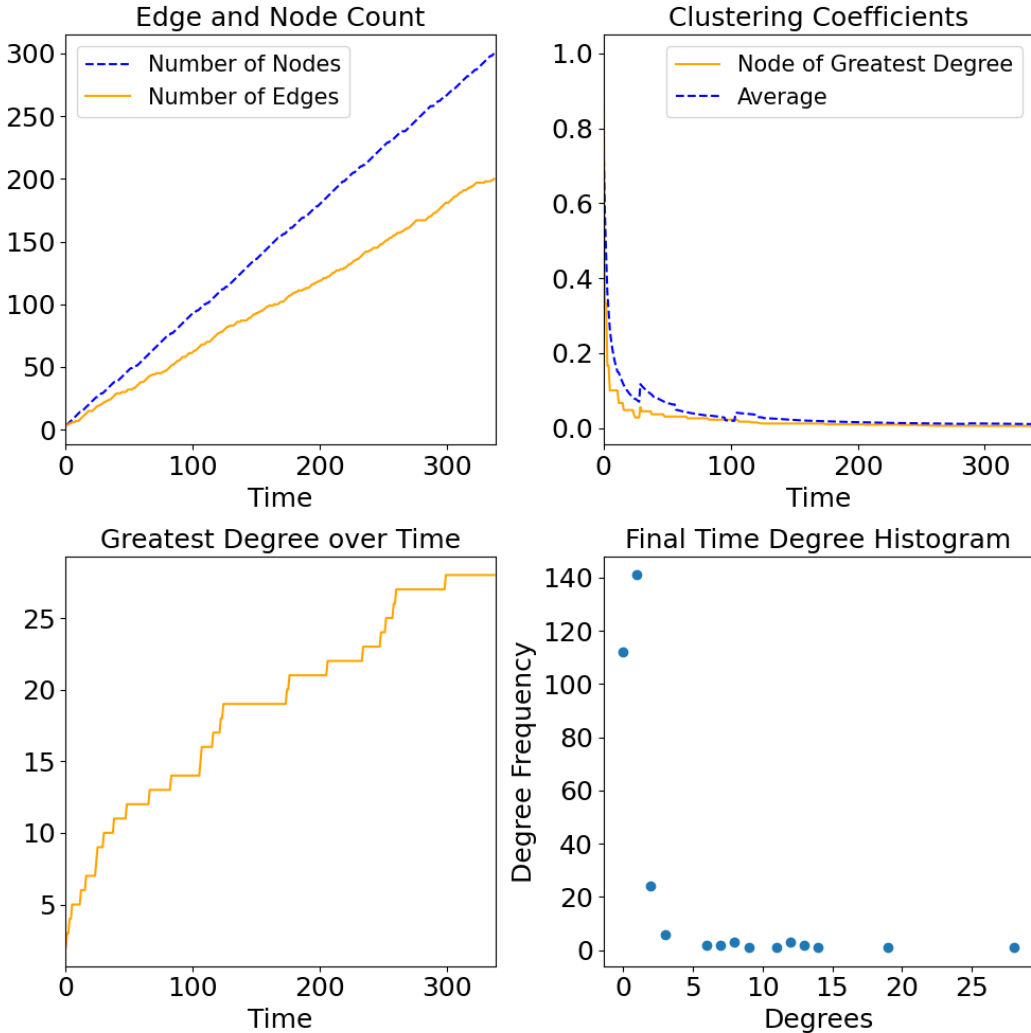


Figure 4.12. This Twitter simulation produces many more nodes than edges, because of the frequency of $T1$ events. The vast majority of nodes only have degrees of one or two, while we see a single node with 25 connections. This might suggest many small clusters of nodes with a single larger cluster around a single message node.

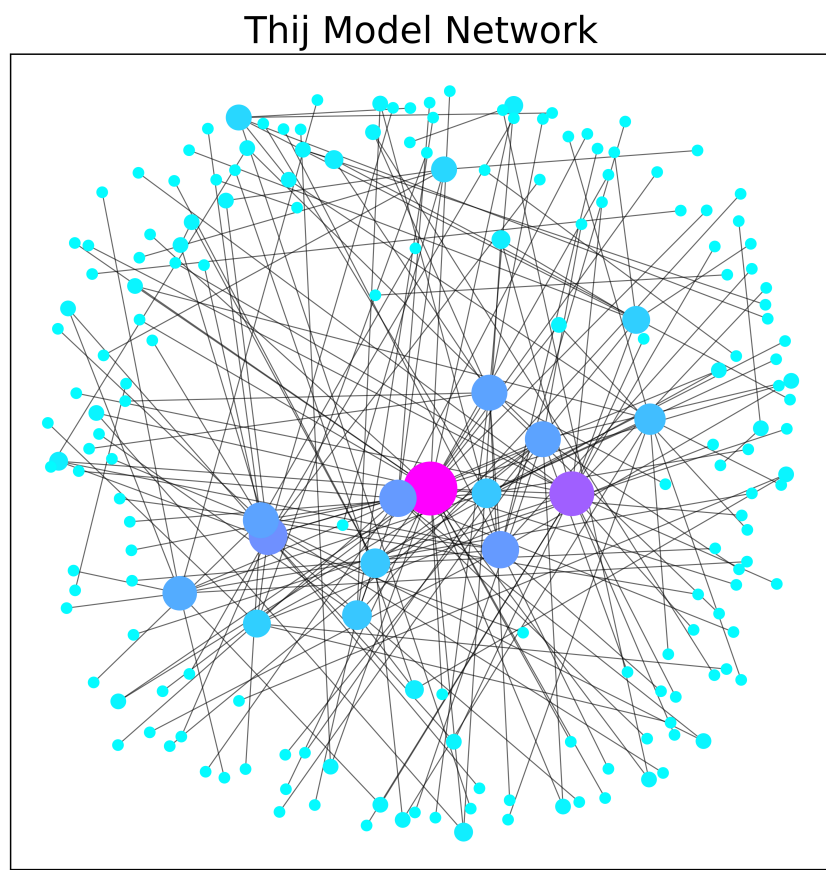


Figure 4.13. The network for $\lambda = 0.8$, $p = 0.8$ at the final time-step.

The dynamics and end state of the network vary across parameter choices. Given greater p values and smaller λ values, the degree distribution will obey stronger power laws. The ratio of edges to vertices for the Twitter model varies much more than the Barabási–Albert model. This is expected given the probabilistic nature of how many edges may be added in a given turn (0 or 1) compared to the given m edges of the Barabási–Albert model. This affects not only the network structure, but the time-scale over which the network grows.

Each graph spans over *very* different time frames. Each graph was allowed to grow to a maximum of three hundred nodes, same as the sampled Barabási–Albert run, before ending the simulation. Ending the simulation with a size threshold makes a comparison of the topology of the networks more feasible. For $\lambda = 0.2$ and $p = 0.8$, the model was able to reach three-hundred nodes very quickly, in approximately three-hundred time-steps, whereas for $\lambda = 0.2$, $p = 0.2$ it took nearly a thousand time-steps. This is consequent of how λ controls how often a new node enters without a new edge and p controls the rate at which new nodes are added without attached edges or if only new edges are introduced.

CHAPTER 5

Barabási–Albert Model Motif and Thij $T2$

Event Motif Dynamics

To gain insight into graph dynamics, we analyze how the composition of motifs change upon the addition of a node to a given motif, and attaching that node to an existing node. The tables below count the isomorphisms of a motif in the present graph, but not automorphisms. For example, in the figure 5.2, the $H4$ motif has six automorphisms, but we only count the identity automorphism as an appearance of $H4$. After adding a node to the root of the star, we count four appearances of $H4$ as the motif $H4$ is isomorphic to four induced subgraphs in the newly generated motif.

5.1 H3

We begin by considering the $H3$ motif. The $H3$ motif is simply a four-path. A preferential attachment mechanism on this motif will most likely connect a new node to one of the center nodes with probability $p = 0.67$, and to an outer node happens with a probability of $p = 0.33$. In the Thij model, this change is based upon which node has the superstar quality.

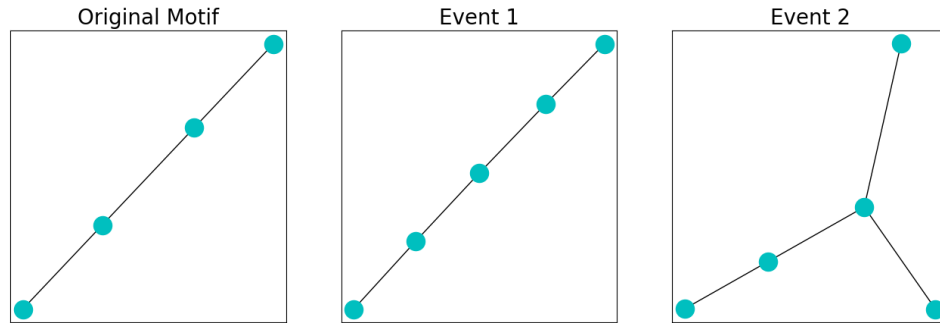


Figure 5.1. The possible graphs generated by adding a node to the $H3$ graph and connecting it to an existing node.

Motif Count	Original Motif	Event 1	Event 2
H3	1	2	2
H4	0	0	1

Table 5.1. The rows denote counts of isomorphisms that can be found in either motif. The H_3 , a four walk, can be found twice in the modified H_3 in event one by starting the walk at either end. In the graph produced again we can only find two H_3 's.

5.2 H4

The H_4 motif is one of the motifs that are of primary interest given that for any star S_k with $k \geq 3$ we will find $\binom{k}{3}$ appearances of the motif. For large clusters of H_4 motifs the H_4 motif count will grow rapidly in time. Adding a single node and connecting it produces k new H_4 appearances in S_k . The probability for an event one on the single motif is 0.5, and for the event two 0.5. A significant difference in the occurrence of event one's over event two's will encourage more event ones in the future.

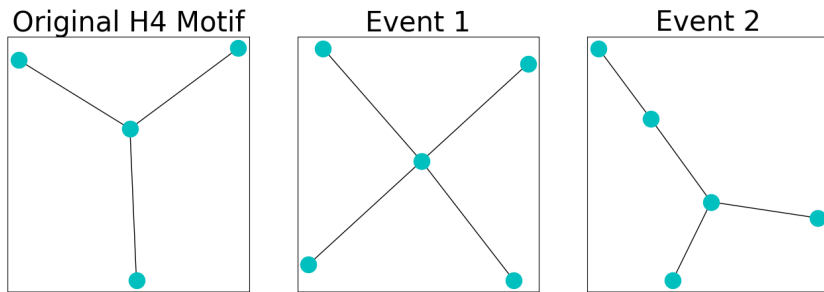


Figure 5.2. The possible graphs generated by adding a node to the H_4 graph and connecting it to an existing node.

Motif Count	Original Motif	Event 1	Event 2
H3	0	0	2
H4	1	4	1
H5	0	0	0

Table 5.2. Motif Counts of the H_4 motif and the possible motifs given a T_2 event.

5.3 H5

H_5 's are of interest due to the relationship they carry to the H_4 motif and the H_7 and H_8 motifs. The C_3 isomorphism in the motif means we find two appearances H_5 in the H_7 and H_8 motifs. The H_4 is isomorphic to an induced subgraph of the H_5 . The probabilities, given by a preferential attachment mechanism, of the events in figure 5.3 event one, $p = 0.375$, for event two, $p = 0.125$, and event three, $p = 0.5$. The last event only has the highest probability due to symmetry.

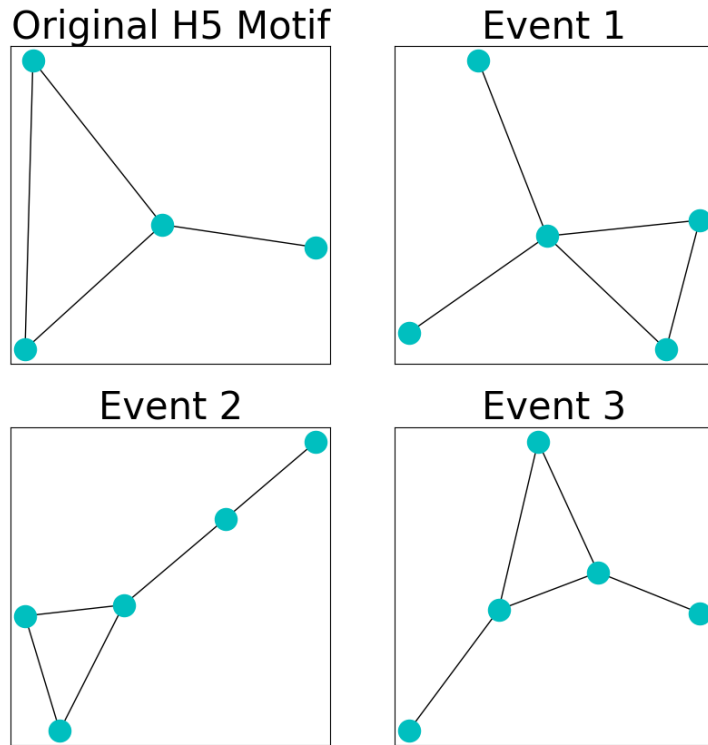


Figure 5.3. The possible graphs generated by adding a node to the H_5 graph and connecting it to an existing node

Motif Count	Original Motif	Event 1	Event 2	Event 3
H3	2	4	4	5
H4	1	4	1	2
H5	1	2	1	2
H6	0	0	0	0
H7	0	1	0	0
H8	0	0	0	1
H9	0	0	1	0

Table 5.3. Motif counts of the possible T_2 events on the H_5 motif.

5.4 H6

The H_6 motif is formed starting with an H_4 and adding two edges between the three outer nodes. It is almost a complete four-node graph. The H_6 motif count is not relatively high when compared to other motifs in the Thij model because it would require exact T_3 events to generate them. Moreover, this T_3 event has to occur between what are likely non-root nodes. However, in the preferential attachment model for $m > 2$ it is more likely to see many H_6 appearances because of how the preferential attachment model adds multiple edges from a single new node.

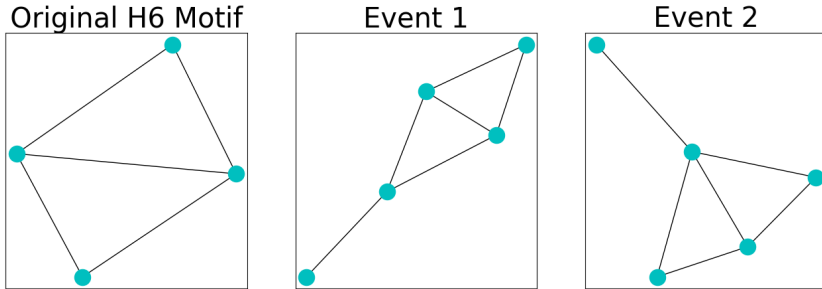


Figure 5.4. The possible graphs generated by adding a node to the H_6 graph and connecting it to an existing node

Motif Count	Original Motif	Event 1	Event 2
H3	6	10	10
H4	2	3	5
H5	4	5	6
H6	1	1	1
H7	0	0	2
H8	0	2	2
H9	0	1	1
H10	0	2	0

Table 5.4. Motif counts for variations of the $T2$ event on the $H6$ motif.

5.5 H7

$H7$ motifs feature prominently given certain parameters in the Thij model. This is another consequence of S_k induced subgraphs in the networks. Connecting any two of the outer edges of S_k will generate $\binom{k-2}{2}$ $H7$ motifs. If we generalize it and assume a network has formed with nodes attached across to all three vertices of a C_3 the $H7$ count is the sum of $\binom{d_i-2}{2}$ for $i = 1, 2, 3$. Adding a node to any one of those vertices, assuming $d_i \geq 4$, will generate $d_i - 2$ new $H7$ appearances.

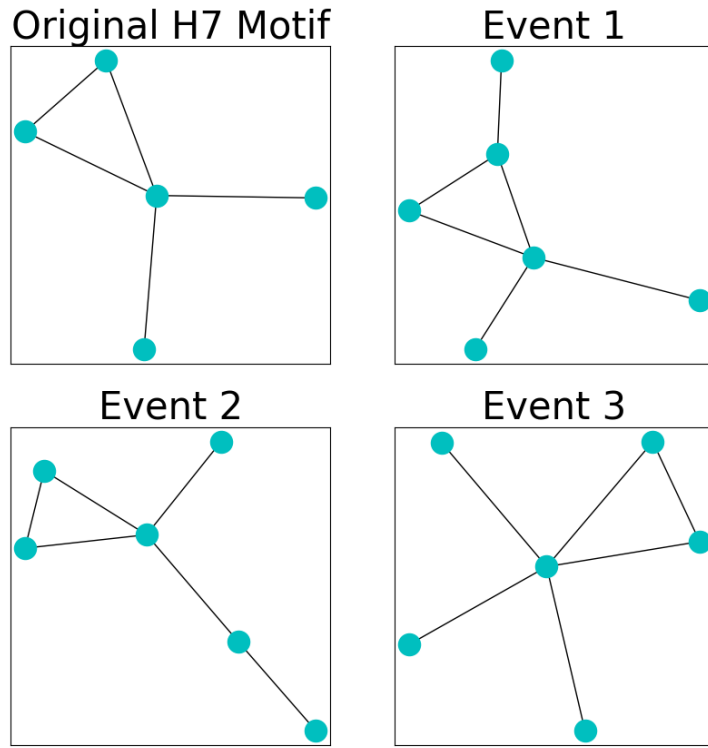


Figure 5.5. The possibly graphs generated by adding a node to the $H7$ graph and connecting it to an existing node

Motif Count	Original Motif	Event 1	Event 2	Event 3
H3	4	8	7	6
H4	4	5	4	10
H5	2	3	2	3
H6	0	0	0	0
H7	1	1	1	3
H8	0	2	0	0
H9	0	0	0	0
H10	0	0	1	0

Table 5.5. Motif counts of the $H7$ motif and the possible additions of $T2$ event nodes.

5.6 H8

The $H8$ motif is another we expect to appear fairly often. The $H8$ is two $H4$'s sharing an edge and a node. We can also characterize it as C_3 with two nodes attached to distinct vertices on the C_3 . For the $H8$ it is relatively easy to characterize growth as nodes connect to the vertices of the C_3 . Given a C_3 with at-least one node attached to each vertex we have $(d_i - 2)(d_j - 2)(d_k - 2)$ $H8$'s. The number of new $H8$'s by connecting a node to vertex v_i is given by $(d_j - 2)(d_k - 2)$.

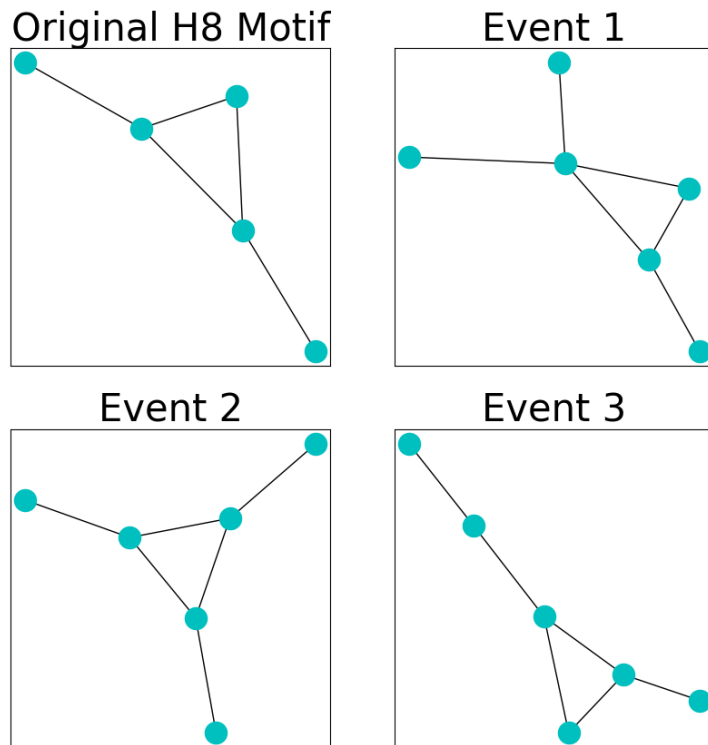


Figure 5.6. The possible graphs generated by adding a node to the $H8$ graph and connecting it to an existing node

Motif Count	Original Motif	Event 1	Event 2	Event 3
H3	5	8	9	7
H4	2	5	3	2
H5	2	3	3	2
H6	0	0	0	0
H7	0	1	0	0
H8	1	2	3	1
H9	0	0	0	0
H10	0	0	0	1

Table 5.6. Motif counts graphs formed by possible T_2 events on the H_8 motif.

5.7 H9

The H_9 motifs do not form around stars in the same way we might expect H_7 's and H_8 's to do so. The H_9 motif could develop in a way similar to the H_5 . This is because the H_9 has an induced subgraph isomorphic to the C_4 . The H_9 is produced by attaching a node to any one of those vertices in the induced subgraph. Given a C_4 and attachment of new nodes to any of its four vertices, the count of H_9 's is simply the sum of the degrees of each vertex minus 2. The growth is additive, not combinatorial in the manner of H_7 's or H_8 's.

Motif Count	Original Motif	Event 1	Event 2	Event 3	Event 4
H3	6	8	8	9	8
H4	1	1	4	2	2
H5	0	0	0	0	0
H6	0	0	0	0	0
H7	0	0	0	0	0
H8	0	0	0	0	0
H9	1	1	2	2	2

Table 5.7. Motif counts graphs formed by possible T_2 events on the H_9 motif.

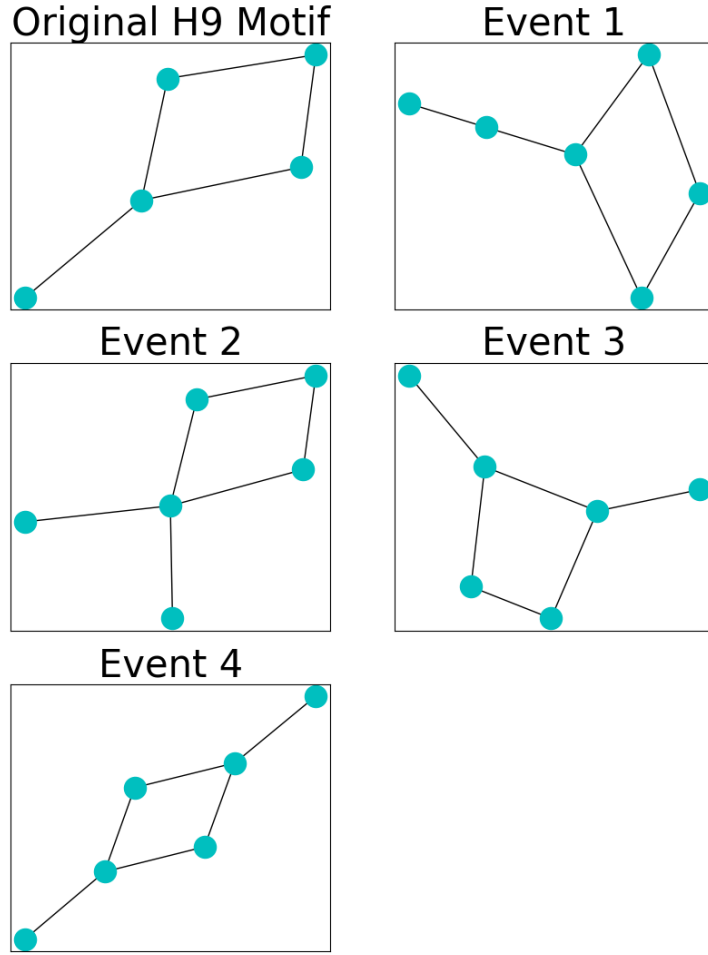


Figure 5.7. The possible graphs generated by adding a node to the $H9$ graph and connecting it to an existing node

5.8 H10

The $H10$ is the $H9$ with an extra vertex and an edge between that vertex to the single vertex of degree one in the $H9$. Many $H10$ appearances could be generated from a single $H9$ if vertices attach to the single vertex of degree one in the $H9$ motif. A star graph would form with that vertex at the center. The growth for the $H10$ in the preferential mechanism with $k = 1$ is additive. For $k > 1$, it is possible clusters of triangles could form causing $H10$ motif count to increase faster than by the addition of a single node and edge at each time-step.

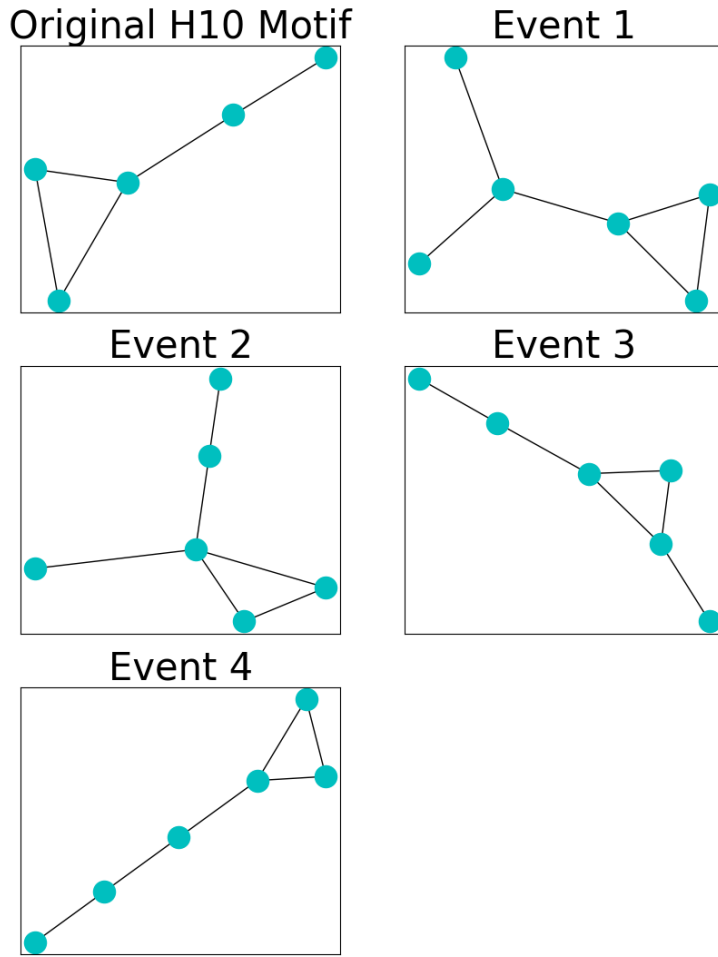


Figure 5.8. The possible graphs generated by adding a node to the H_{10} graph and attaching it to an existing node.

Motif Count	Original Motif	Event 1	Event 2	Event 3	Event 4
H3	4	6	7	7	5
H4	1	2	4	2	1
H5	1	1	2	2	1
H6	0	0	0	0	5
H7	0	0	1	0	0
H8	0	0	0	1	0
H9	0	0	0	0	0
H10	1	2	1	1	1

Table 5.8. Motifs counts of the possible T_2 event on the H_{10} motif.

5.9 H11

The H_{11} motif, shaped like a bow-tie, is formed by two three-walks that share a common vertex. This motif does need $k \geq 2$ in the Barabási–Albert Model or a T_3 event to form an edge between two existing nodes. The H_{11} motif does not appear commonly without those necessary criteria.

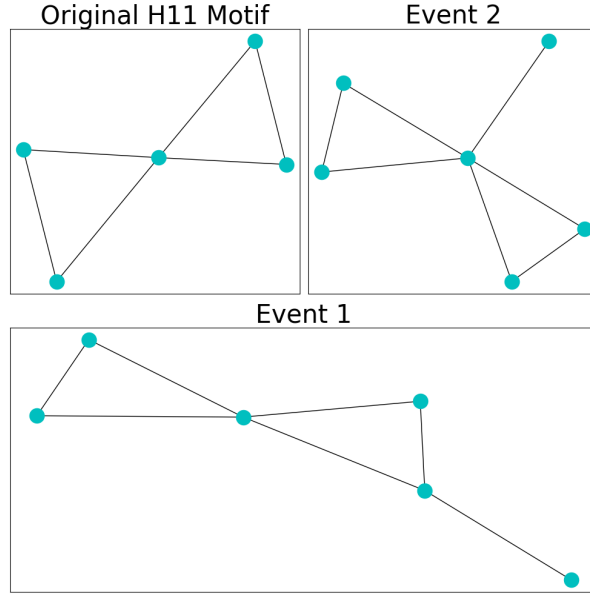


Figure 5.9. The possibly graphs generated by adding a node to the H_{11} graph and connecting it to an existing node.

Motif Count	Original Motif	Event 1	Event 2
H3	8	12	12
H4	4	5	10
H5	0	5	6
H6	0	0	0
H7	2	2	6
H8	0	2	0
H9	0	0	0
H10	4	5	4
H11	1	1	1

Table 5.9. Motif counts of the graphs generated by possible T^2 events on the H_{11} motif.

5.10 H12

H_{12} , shaped like a house, contains five nodes, six edges, with an induced subgraph isomorphic to C_4 and a single vertex attached to two vertices they connected. The H_{12} , like other motifs, contains an induced subgraph isomorphic to C_4 is not a priori expected to have a relatively large count given the preferential attachment mechanism.

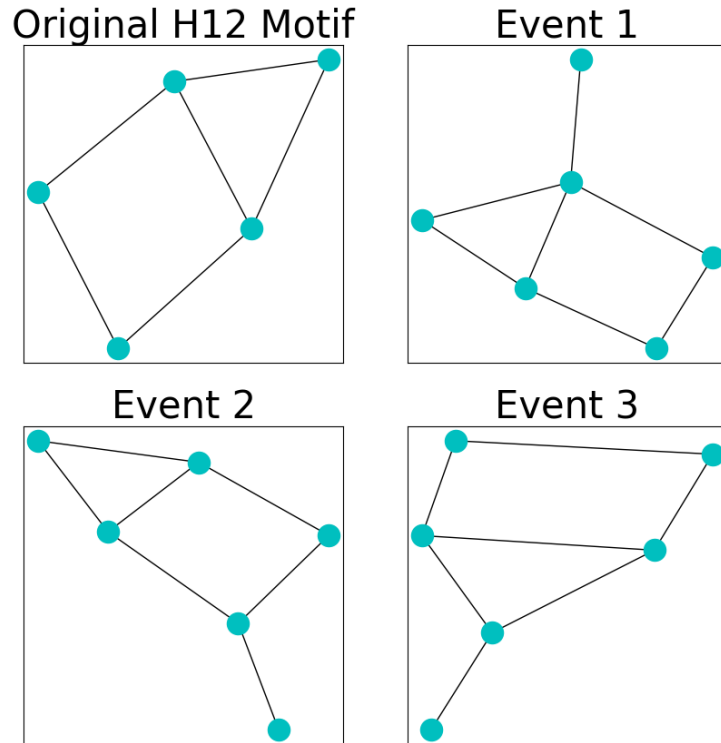


Figure 5.10. The possibly graphs generated by adding a node to the H_{12} graph and connecting it to an existing node.

Motif Count	Original Motif	Event 1	Event 2	Event 3
H3	10	14	13	14
H4	2	5	3	3
H5	2	3	2	3
H6	0	0	0	0
H7	0	1	0	0
H8	1	2	1	3
H9	2	3	3	2
H10	2	2	3	2
H11	0	0	0	0
H12	1	1	1	1

Table 5.10. Variations of the T_2 event on the H_{12} motif

5.11 H13

The H_{13} could plausibly form in the $k \geq 2$ case for the Barabási–Albert model, but it would require a new node being consistently attached to the same two nodes repeatedly. If this process of generating new H_{13} 's, the increase in the motif counts is additive. Thus for the Barabási–Albert model of $0 < k < 3$, the presence of an H_{13} is sensitive to the initial graph and its early development when there might still be a 'more uniform' probability of attachment.

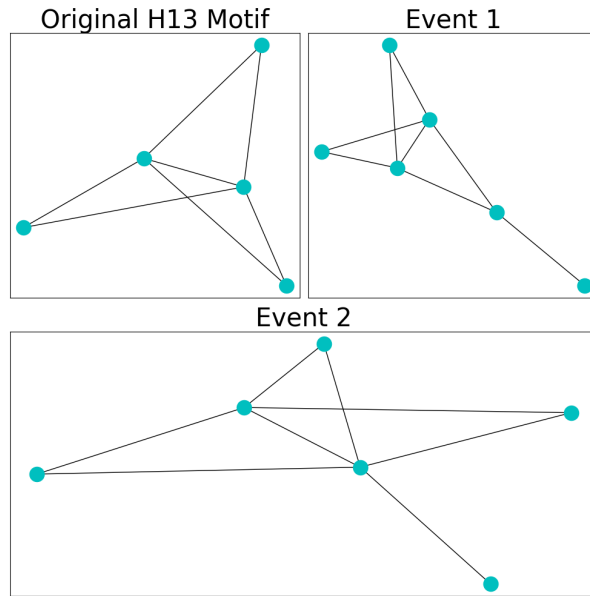


Figure 5.11. The H_{13} graph and possible node attachments up to symmetry.

Motif Count	Original Motif	Event 1	Event 2
H3	18	24	24
H4	8	14	9
H5	12	15	13
H6	3	3	3
H7	6	12	6
H8	6	12	10
H9	6	9	8
H10	0	0	4
H11	0	0	0
H12	0	0	0
H13	1	1	1

Table 5.11. Motif counts of the possible $T2$ events on the $H13$ motif

5.12 Summary of Preferential Attachment and $T2$ Event Motif Evolution

Motif development in the Barabási–Albert model is dependent on the initialization of nodes and the choice of k . If we only add $k = 1$ edges for every new node this limits the types of motifs that can appear. There will be no new $H6$'s, $H11$'s, $H12$'s, or $H13$'s generated. There is no possible way for them to form as there is no node of degree one in those motifs. Only upon taking $k > 1$ could those motif counts change over time. Some graphs still are more likely for $k = 2$ than others like the $H4$'s, $H7$'s, and $H8$'s.

This analysis also applies to the $T2$ event in the Thij model. The occurrence is similar to the preferential attachment model with $k = 1$ as it is simply the addition of a node which is then connected to a single existing node. The $T2$ event, unlike the BA model, selects a message tree and then uses a superstar attachment mechanism to attach to a node with probability $q = 0.9$. Even when the network is relatively small nodes will still overwhelmingly attach to the root message node. This mechanism is much more probable to generate $H4$'s as seen in chapter 3. If the root message node is the vertex of a C_3 then we may see $H7$ and $H8$ counts rapidly increase over time, correlating with the $H4$ count.

CHAPTER 6

Twitter Model Specific Motif Evolution

In chapter 3, we specified three possible events in the Thij model: a new root node, a new node and an attached edge, or a new edge between existing nodes (T_1 , T_2 , T_3 respectively). The only event specific to the Thij model are T_1 and T_3 events. T_1 events add a new message node, but they do not immediately affect any change in the motif counts. They could potentially with the right T_3 event or a series of T_2 events begin to have an impact on motif enumeration. The T_3 event we must consider, because a T_3 event can change the composition of the network in ways T_2 events cannot. Given that a T_3 event is occurring it follows first, the preferential-attachment mechanism for tree selection, then follows superstar probability for source node selection, and then finally uniform probability for target node selection. This makes it difficult to discuss the associated probabilities of a potential T_3 event. We may suspect a root message node within a graph based on its degree, but may not know without prior knowledge of the data. We can examine how each T_3 event will affect a given motif graph provided the T_3 event occurs between nodes in the motif.

6.1 H3

The H_3 motif only has two possible events. We see either an H_5 form by connecting an outer vertex to the opposite inner or the outer two vertices are connected forming a four-cycle. Future development of this new H_5 in the context of T_3 events is discussed in section 6.3.

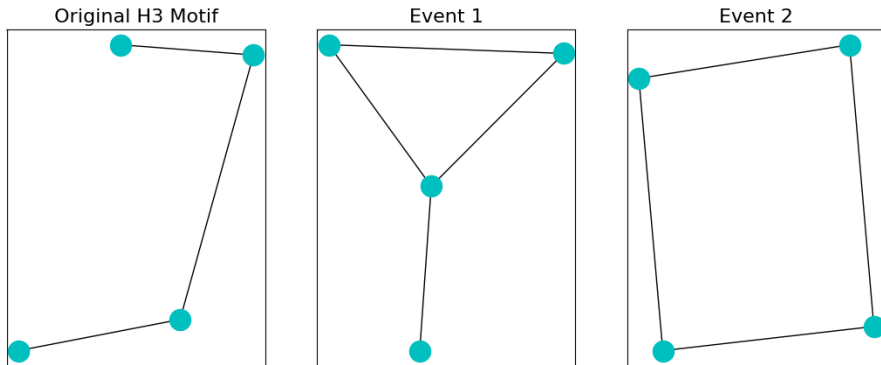


Figure 6.1. The possible graphs generated by adding an edge to the H_3 graph.

Motif Count	Original Motif	Event 1	Event 2
H3	1	2	4
H4	0	1	0
H5	0	1	0

Table 6.1. Motif counts of the possible T_3 events on the H_3 motif

6.2 H4

Due to the three symmetry of the H_4 , adding an edge between any two unconnected nodes creates a single H_5 . Therefore given some balance between T_2 and T_3 events we could see correlation between these two motifs.

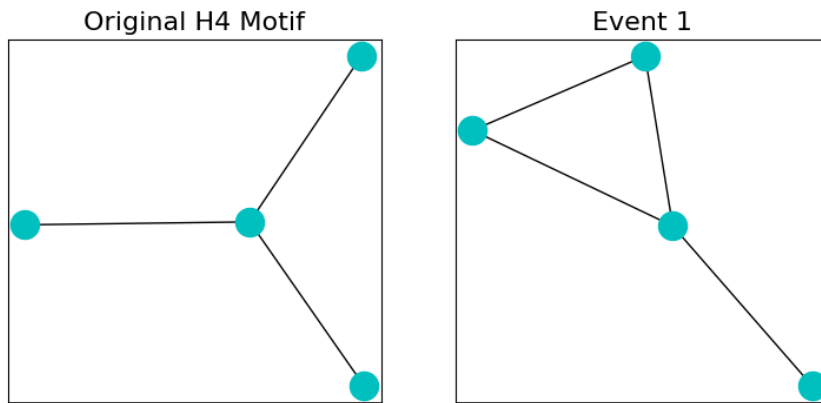


Figure 6.2. The possible graphs generated by adding an edge to the H_4 graph. By connecting the two outer edges we find a C_4 and by connecting an outer vertex to an inner vertex we generate a H_5 .

Motif Count	Original Motif	Event 1
H3	0	2
H4	1	1
H5	0	1

Table 6.2. Motif counts of the T_3 event on the H_4 motif

6.3 H5

The H_5 motif is symmetric. Connecting any two unconnected vertices of the H_5 produces an H_6 . A H_4 with a $T3$ event creates an H_5 graph. A $T3$ event occurs again on the same graph and a H_6 graph is produced.

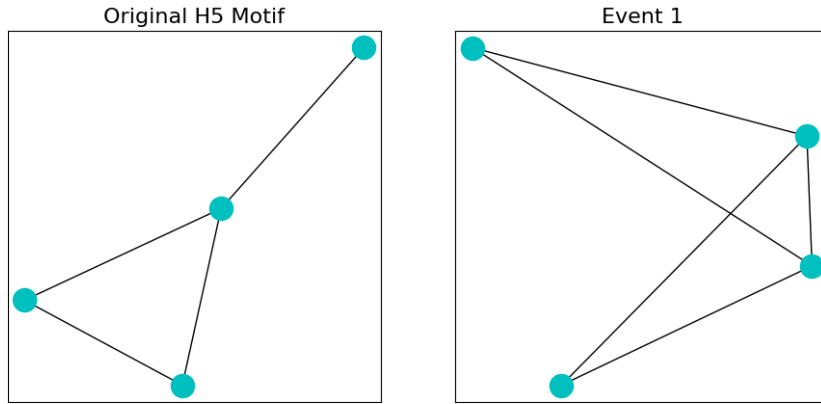


Figure 6.3. The possible graphs generated by adding an edge to the H_5 graph.

Motif Count	Original Motif	Event 1
H3	2	6
H4	1	2
H5	1	4
H6	0	1

Table 6.3. Motif counts of the graphs produced by a $T3$ event on the H_5 motif.

6.4 H6

Adding an edge to H_6 generates a complete graph of four nodes. This event is unlikely given a large graph, but not impossible. If a vertex of the H_6 is a message node then an edge could be added within the H_6 graph. However, an edge added between the H_6 appearance and the appearance of another motif is more likely.

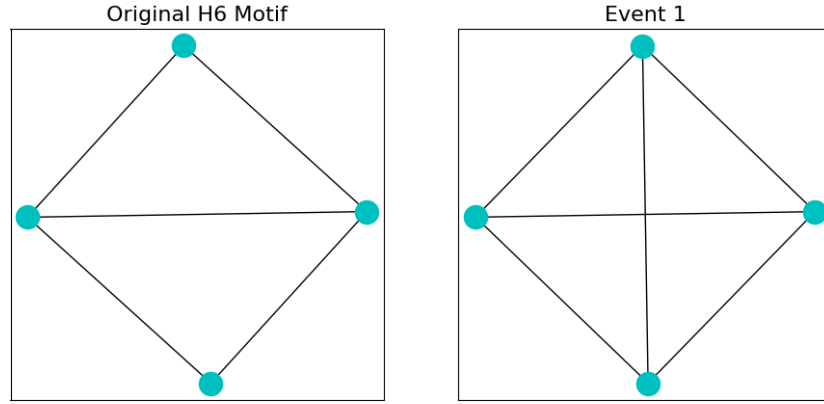


Figure 6.4. The possible graphs generated by adding an edge to the H_6 graph.

Motif Count	Original Motif	Event 1
H3	6	12
H4	2	4
H5	4	12
H6	1	6

Table 6.4. Motif counts of graph produced by a T_3 event on the H_6 motif.

6.5 H7

Adding edges, the H_7 motif gives only two non-isomorphic graphs as a consequence of the motif's symmetry. Given an event two in figure 6.5 the graph becomes an H_{11} . Both events do show that one could see a high H_7 count given enough clustering around a message node.

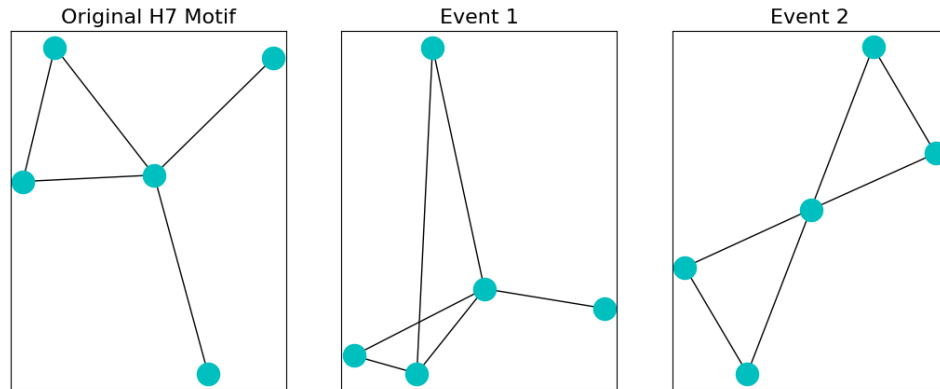


Figure 6.5. The possible graphs generated by adding an edge to the H_7 graph.

Motif Count	Original Motif	Event 1	Event 2
H3	4	10	8
H4	4	5	4
H5	2	6	4
H6	0	1	0
H7	1	2	2
H8	0	2	0
H9	0	1	0
H10	0	0	4
H11	0	0	1

Table 6.5. Motif counts of the two possible graphs produced by the T_3 event on the H_7 motif

6.6 H8

The H_8 motif here generates three different motifs depending upon the nodes which become connected. The H_8 motif is similar to the H_7 motif as clusters of triangles can contain many H_8 appearances.

Motif Count	Original Motif	Event 1	Event 2	Event 3
H3	5	10	10	10
H4	2	5	3	2
H5	2	6	5	2
H6	0	1	1	0
H7	0	2	0	0
H8	1	2	2	1
H9	0	1	1	2
H10	0	0	2	2
H11	0	0	1	0
H12	0	0	0	0

Table 6.6. Motif counts of the possible T_3 event on the H_8 motif

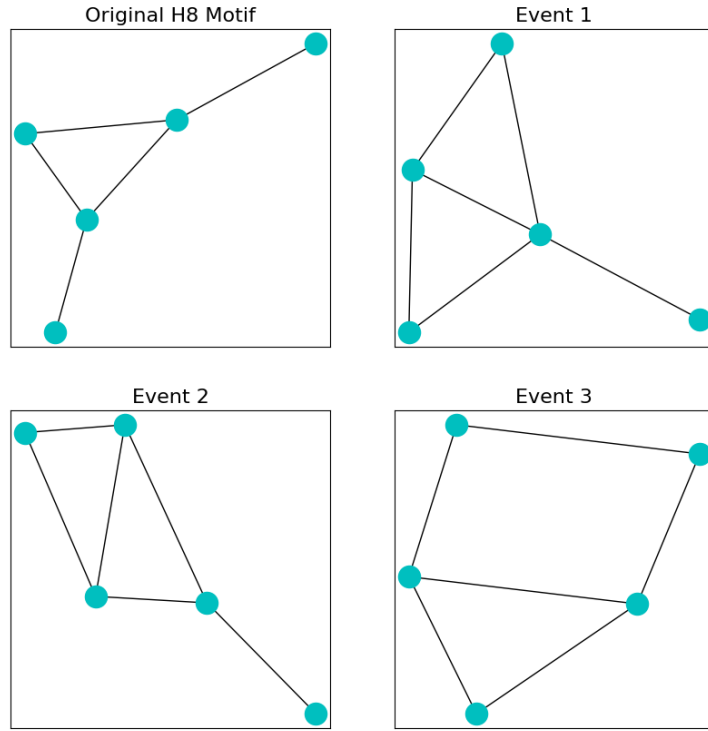


Figure 6.6. The possible graphs generated by adding an edge to the H_8 graph.

6.7 H9

An H_9 motif with an edge added anywhere does not produce a combinatorial jump in counts as other motifs might. The H_9 had an induced subgraph, isomorphic to the C_4 which means the graph requires more events or the right initialization to generate itself. Given a high $T3$ probability there relatively high H_9 counts as seen in figures 9.11 and 9.21.

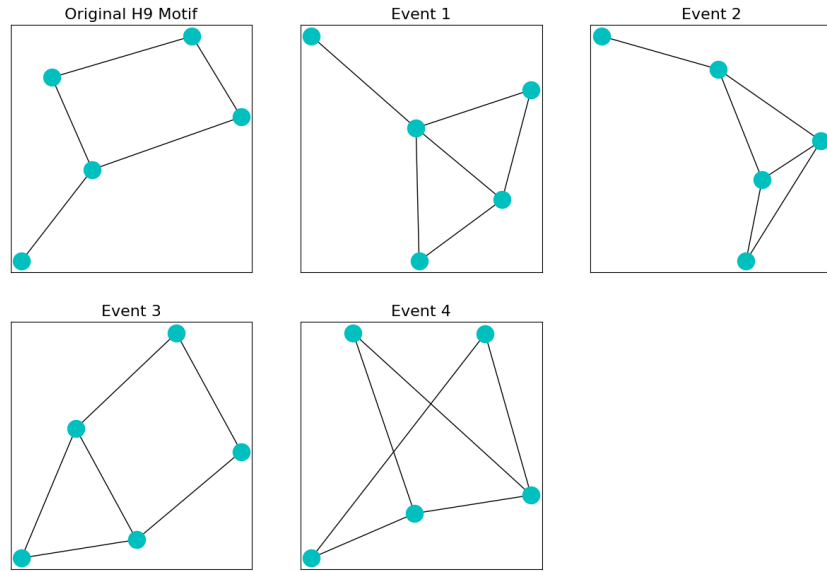


Figure 6.7. The possible graphs generated by adding an edge to the $H9$ graph.

Motif Count	Original Motif	Event 1	Event 2	Event 3	Event 4
H3	6	10	10	10	10
H4	1	5	3	2	2
H5	0	6	5	2	2
H6	0	1	1	0	0
H7	1	2	1	0	0
H8	0	2	2	1	1
H9	1	1	2	2	2
H10	0	0	2	2	2
H11	0	0	0	0	0
H12	0	0	0	1	1

Table 6.7. Motif counts of the possible $T3$ event on the $H9$ motif

6.8 H10

The H_{10} motif features in those Thij models with $p < 0.5$ line in figures 9.11 and 9.26, given that there is enough likelihood a $T3$ event occurs acting on an $H9$. For events two, three, and four below in Figure 6.8, attaching a node to the H_{10} motif produces a handful more of H_{10} 's.

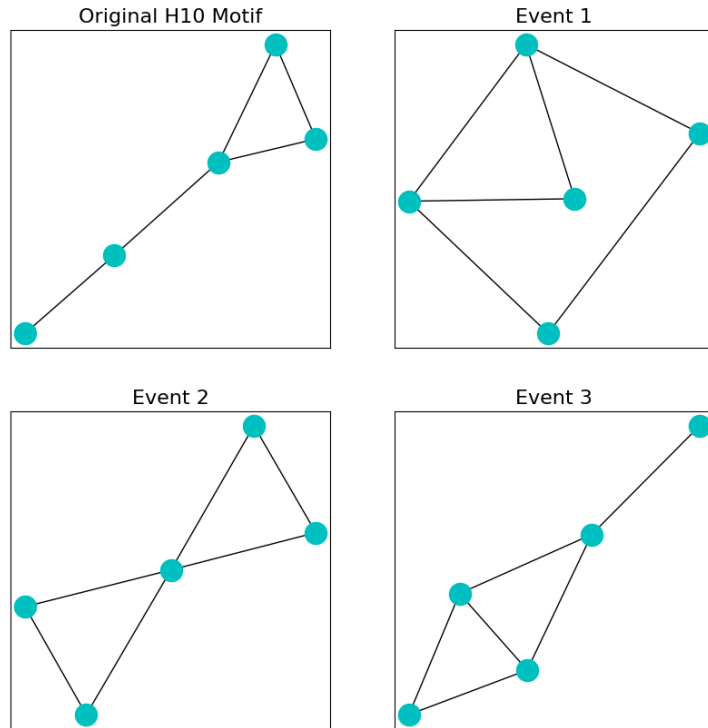


Figure 6.8. The possible graphs generated by adding an edge to the H_{10} graph.

Motif Count	Original Motif	Event 1	Event 2	Event 3
H3	4	10	8	10
H4	1	2	4	3
H5	1	2	4	5
H6	0	0	0	1
H7	0	0	2	0
H8	0	1	0	2
H9	0	2	0	1
H10	1	2	4	2
H11	0	0	1	0
H12	0	1	0	0

Table 6.8. Motif counts of the graphs given by a T_3 event on the H_{10} motif

6.9 H11

H_{11} 's do not appear prominently in any of the simulations because they are isomorphic to two C_3 's connect at a single vertex. To produce an H_{11} from an exiting H_{11} appearance, one would need to connect a new C_3 to one of the H_{11} vertices.

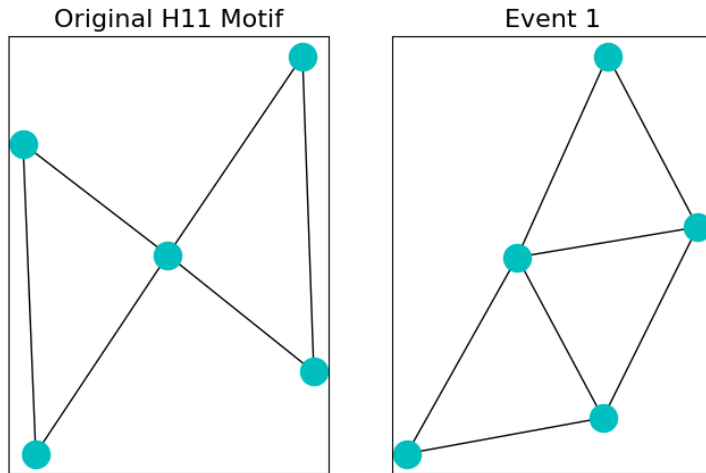


Figure 6.9. The possible graphs generated by adding an edge to the H_{11} graph.

Motif Count	Original Motif	Event 1
H3	8	17
H4	4	6
H5	4	10
H6	0	2
H7	2	3
H8	0	5
H9	0	4
H10	4	6
H11	1	1
H12	0	2
H13	0	0

Table 6.9. Motif counts of the single graph produced by a $T3$ event on the $H11$ motif

6.10 H12

As we discussed in section 5.10, the $H12$ motifs are not commonly found in the network simulations because they require a four-walk. In the Thij model, assuming the presence of an $H12$, one could generate more $H12$'s by a $T2$ event to a vertex of the four-cycle and then a $T3$ event to follow. In table 6.10 we see even a single $T3$ would suffice to produce two or even four new $H12$'s.

Motif Count	Original Motif	Event 1	Event 2
H3	10	17	18
H4	2	6	4
H5	2	10	6
H6	0	2	1
H7	0	3	0
H8	1	5	4
H9	2	4	8
H10	2	6	6
H11	0	1	0
H12	1	2	4
H13	0	0	0

Table 6.10. Motif counts of the possible $T3$ event on the $H12$ motif.

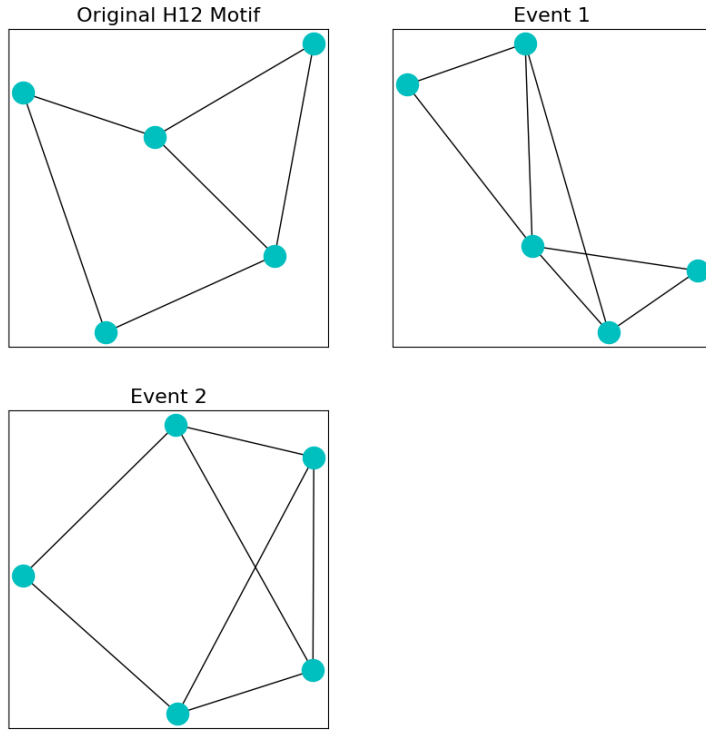


Figure 6.10. The possible graphs generated by adding an edge to the $H12$ graph.

6.11 $H13$

The $H13$ does not frequently appear in any of the simulations. $H13$ appearances are not readily generated from an existing $H13$ appearances. To generate new appearances, one requires exact $T2$ and $T3$ events. Contrast this to an $H7$ or an $H8$ which upon a $T3$ event alone can generate new $H7$ or $H8$ appearances. The $H13$ requires events to occur, which are not likely given the attachment mechanism.

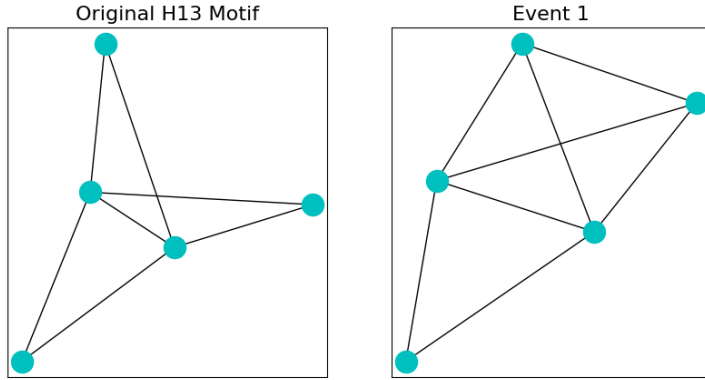


Figure 6.11. The possible graph generated by a T_3 event on the $H13$.

Motif Count	Original Motif	Event 1
H3	18	28
H4	8	10
H5	12	22
H6	3	8
H7	6	8
H8	6	14
H9	6	12
H10	0	12
H11	0	2
H12	0	6
H13	1	1

Table 6.11. Motif counts of the graph given by a T_3 event on the $H13$ motif.

6.12 In summary of the T_3 events

The T_3 event is a much more complex animal than the T_2 . For any of the motifs $H3-H13$, we see how T_3 events change the motif counts, but T_3 's can add edges *between* different motifs as well as on motifs. If two motifs are disjoint a T_3 bridges them and functions as one or more T_2 events occurring in a single time-step. This is still a simple case, but for the eleven motifs considered there are 55 different possibilities.

The T_3 ultimately opens up several possibilities for the model. C_3 's and C_4 's are more likely to form around root nodes. We may ultimately see more $H6$'s through $H13$'s. For $p = 0.2$, the Thij model exhibits significantly more clustering throughout time. Shedding light on the impact of the p parameter is for the tools of statistical analysis.

CHAPTER 7

Motif Correlation

Given the analysis in chapters 4 and 5, a $T2$ or $T3$ event applied to any motif graph will generate a given amount of new motif appearances. We naturally expect some motif counts like $H4$, $H7$, and $H8$ to correlate. We compute correlation and covariance matrices for the time-series generated by the motif counts. There is an order of magnitude difference in covariances between motif counts although all are strongly correlated. All covariance matrices are described on a log scale. We begin with a simulation of the Barabási–Albert model resulting in the heat maps in figures 7.1 and 7.2:

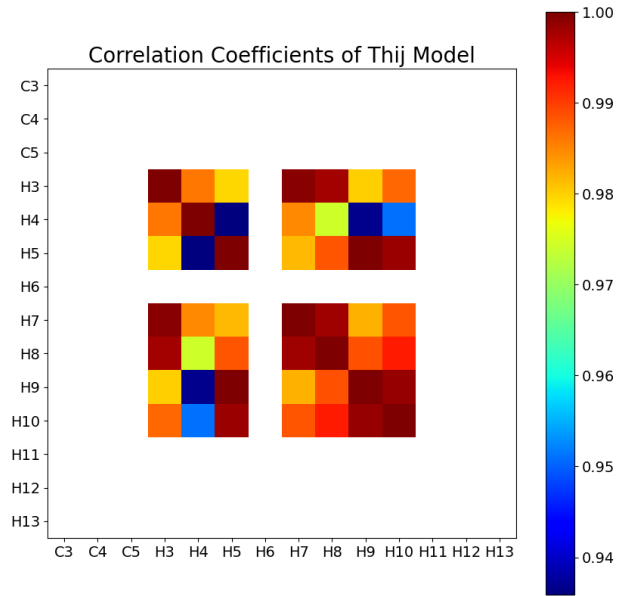


Figure 7.1. Barabási–Albert model with eight initial nodes and $m = 1$. The model is capable of only producing certain motifs due to the limitations of attaching a single edge and a single node at every time-step. We also see that $H7$'s and $H8$'s correlate together. However, appearances of those motifs depend upon the initialization of the graph itself.

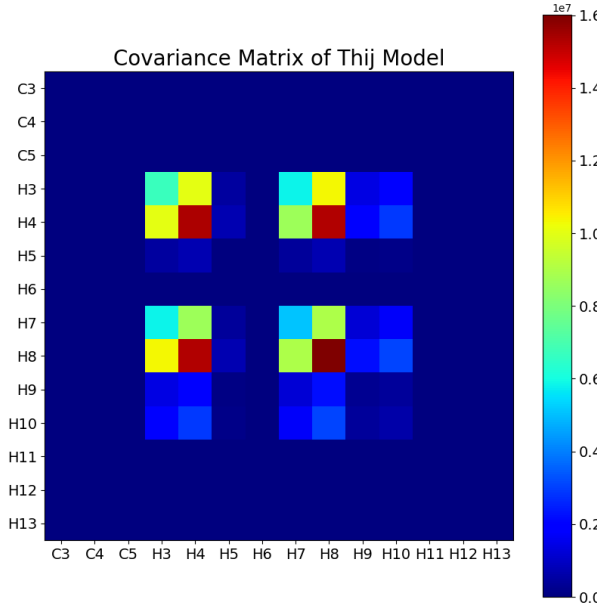


Figure 7.2. Barabási–Albert model with eight initial nodes and $m = 1$. Here we once again see that the H_7 and H_8 motifs have a much higher covariance than any other pair of motifs.

The Barabási–Albert model, for $m = 1$, is only capable of generating certain new motif appearances after the initialization as it only adds one edge at a time. Some motifs would require the introduction of an event similar to the T_3 events, which can add edges between existing nodes. The only motif counts that increase after the initialization of the $m = 1$ Barabási–Albert model are H_2 , H_4 , H_5 , H_7 , H_8 , H_9 , and H_{10} . There is an initial cluster of nodes at the center of simple cycles at the center. These counts are able to grow by attaching nodes to these cycles. In figures 7.3 and 7.4, we see that we can generate all motifs provided $m > 2$.

In figures 7.1 and ??, we have a Barabási–Albert simulation that resembles the Thij model for low λ and high p . For the Barabási–Albert model with $m = 2$, all motifs can now be generated via an attachment event. This allows for the formation of C_3 and C_4 subgraphs that are necessary for the motifs that also have C_3 and C_4 subgraphs. We also see that some of our a priori speculation in chapter 5 is supported by the correlation and covariance matrices.

We recall that for relatively high p we are more likely to attach a new node and a new edge. For relatively low p we attach a new edge between existing nodes. For relatively high λ we are likely to introduce a new message node without any

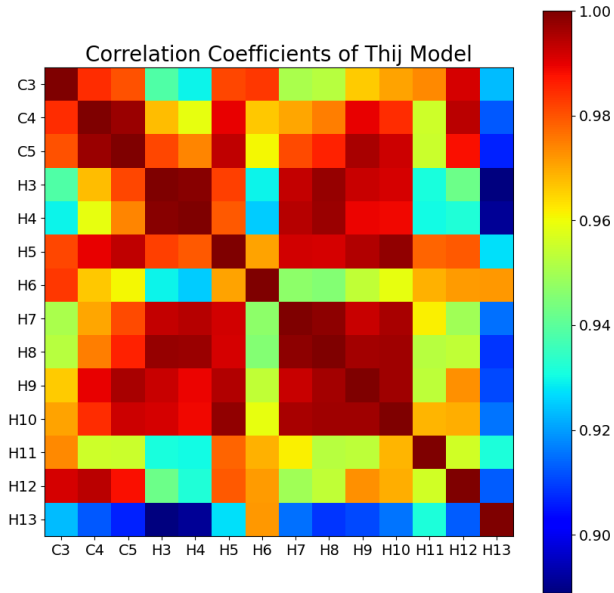


Figure 7.3. Here we have the Barabási–Albert model with $m = 3$ initial nodes and $k = 2$. Here we see that all motifs are present. They all have fairly high correlation coefficients, but we see that the H7's and H8's are highly correlated as is H7 and H8 with H3.

attachments. In chapter 4, we discussed that for high p we introduce a new node and attach it with a the superstar mechanism after selecting a message subgraph with the preferential attachment mechanism.

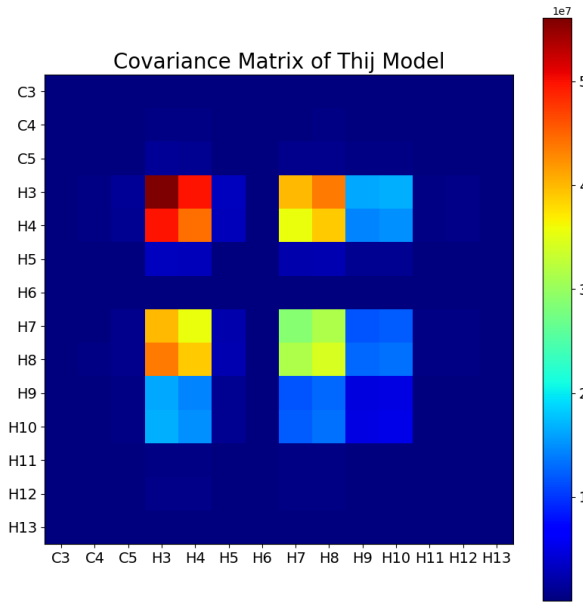


Figure 7.4. Barabási–Albert model with $m = 3$ initial nodes and $k = 2$. The covariance offers a different perspective from that of the correlation figure. The H_7 and H_8 motif counts exhibit high covariance, and once again there is a relationship between H_8 , H_7 , H_3 , H_4 . Other motifs have a much smaller covariances.

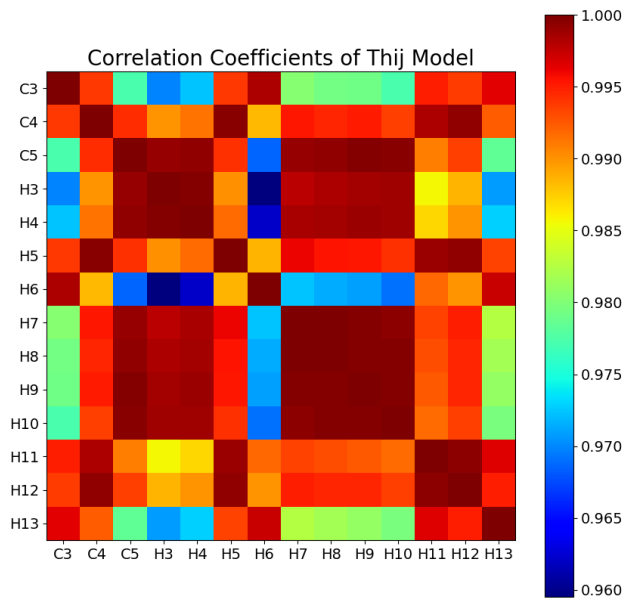


Figure 7.5. $\lambda = 0.2$ and $p = 0.2$. We recall low λ reduces the chance of only adding a new node (T1) and low p reduces the chance of adding a new node and a new edge. Thus probabilistically this simulation should be overall adding only edges between existing nodes.

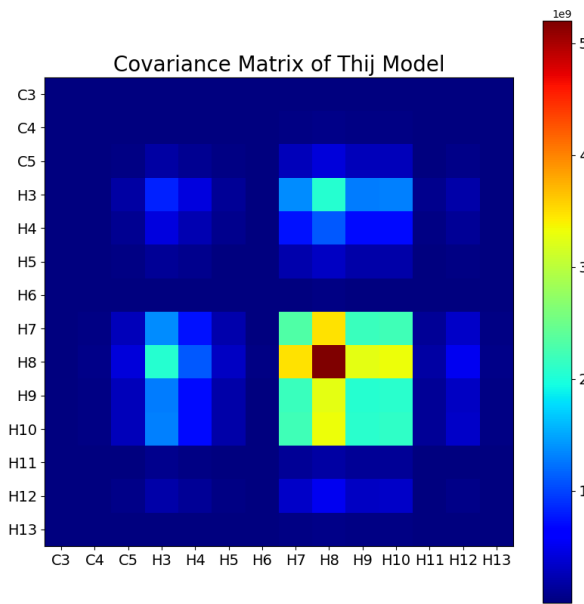


Figure 7.6. $\lambda = 0.2$ and $p = 0.2$. Here we see once again a strong covariance relationship between H_7 , H_8 , H_9 , H_{10} . In this particular graph it's insightful to see these correlate together given these parameters are less likely to produce the induced star subgraph we expect to see for higher p .

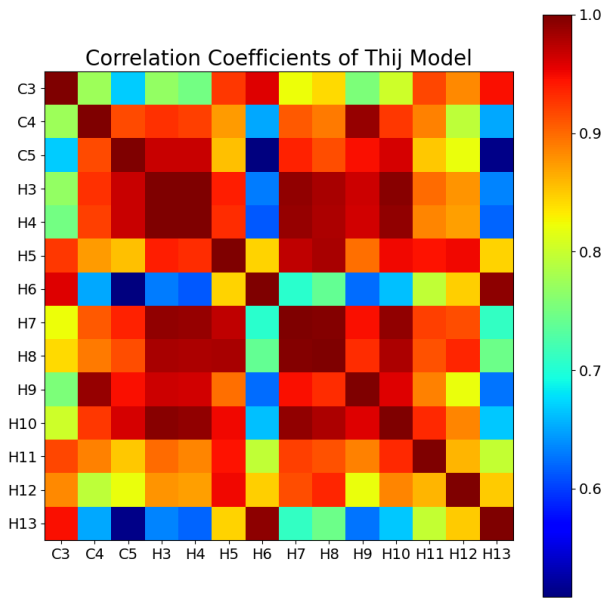


Figure 7.7. $\lambda = 0.2$ and $p = 0.8$. Here in the correlation coefficients we see that there is a strong correlation between $H7$, $H8$, but otherwise a much larger spread over the motifs. We also see that no $H6$ or $H13$ motifs appeared throughout this simulation.

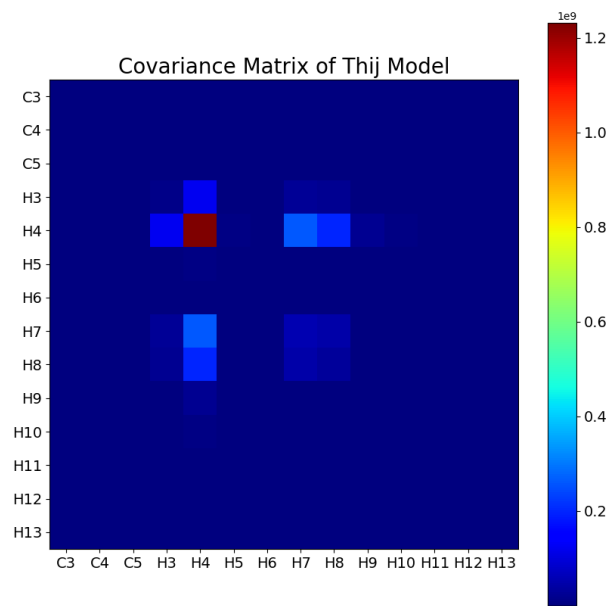


Figure 7.8. $\lambda = 0.2$ and $p = 0.8$. Here the covariance is relatively very small, except for the H4 variance. This is suggestive of the high p generating that induced star subgraph.

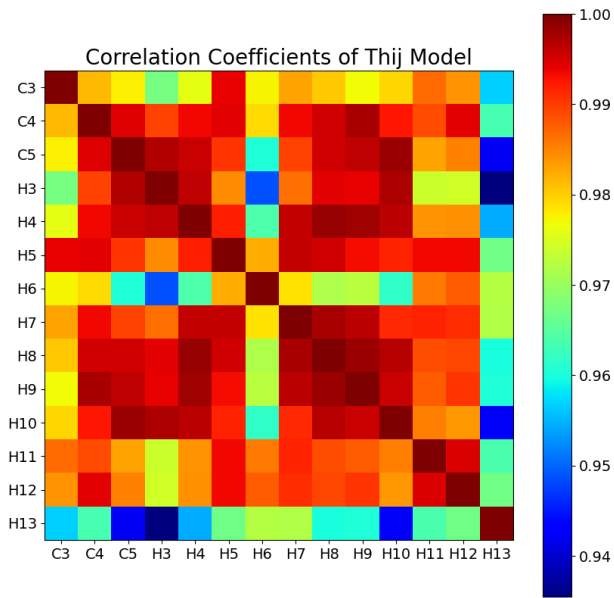


Figure 7.9. $\lambda = 0.8$ and $p = 0.2$. Once again we see a familiar structure in the correlation matrix. Here though we do see strong correlations across a wider selection of motifs: $C_3, C_4, C_5, H_3, H_4, H_5, H_7, H_8, H_9, H_{10}$. It appears the H_6 's are not easily produced by any of the parameters chosen or the Barabási–Albert model.

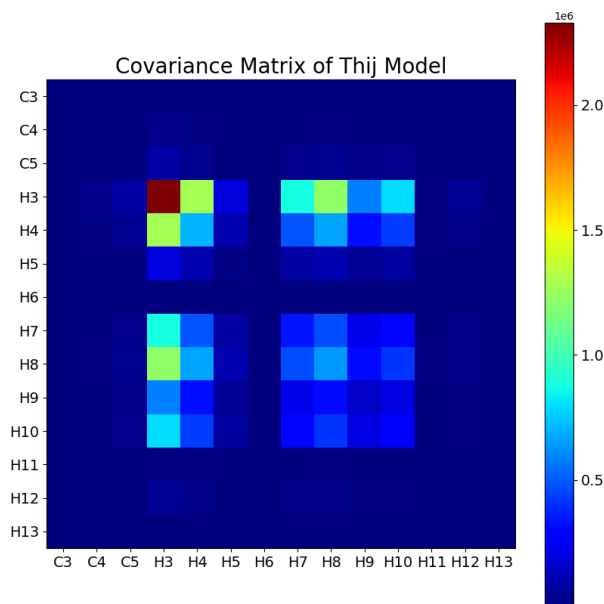


Figure 7.10. $\lambda = 0.8$ and $p = 0.2$. We do see strong covariance around the H_4 with other motifs. There is possibly multiple induced star subgraphs connected that could drive this phenomena generating many H_4 's along with other motifs.

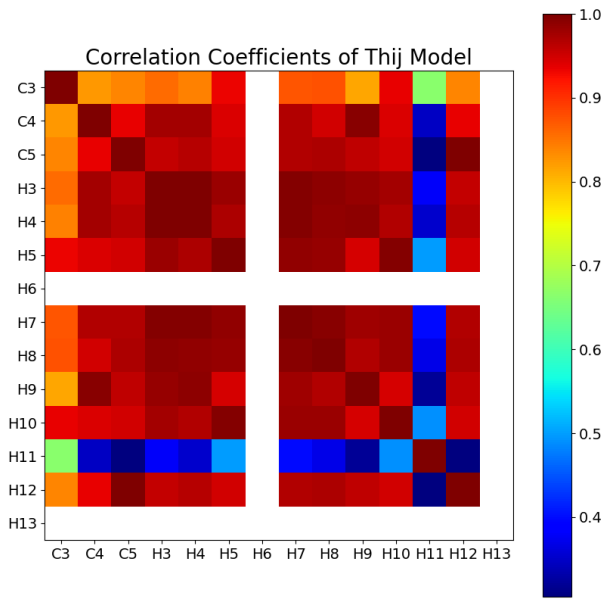


Figure 7.11. $\lambda = 0.8$ and $p = 0.8$. Here we have a higher likelihood of adding a new node or a new edge and node. Here we do not see any new H_6 's or H_8 's produced after the initialization of the graph. Any block structures that we saw in earlier correlation matrices are not as apparent, although there is still strong H_7 - H_8 correlation.

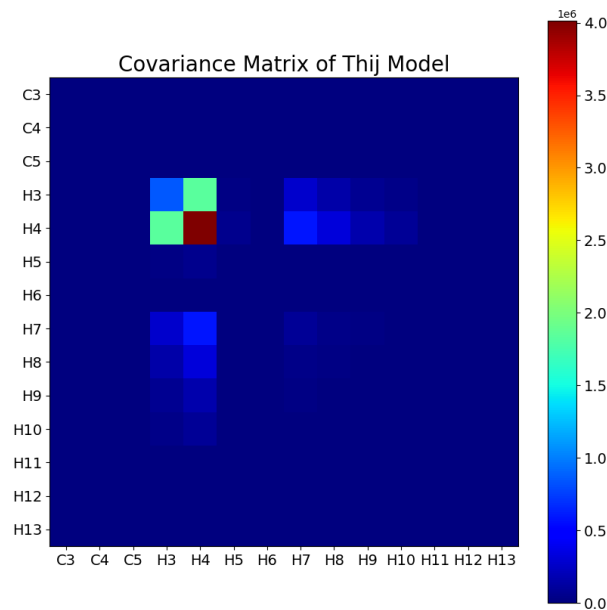


Figure 7.12. $\lambda = 0.8$ and $p = 0.8$. The covariances formed by this simulation suggest once again an overlapping of H_4 's, but there are clearly more nodes attached to the outer edges of this induced subgraph. This could lead to the covariance we see between H_3 and H_4

In figures 7.11 and 7.12, we see clearly evidence of the S_k , $k >> 1$ induced subgraph for high values of p . We see relatively high covariance between the $H7's$ and $H8's$ and with $H3$ and $H3$. $H13$ and $H6$ counts don't change at all because the probabilistically of $T2$ attachment through the superstar mechanism is high relatively high. In fact, this mechanism is what encourages the growth of those motifs. We expect to grow in a combinatorial manner around S_k induced subgraphs.

CHAPTER 8

Dynamic Mode Decomposition

In addition to using statistical methods, we can view the motif counts through the lens of dynamical systems. We achieve this through dynamic mode decomposition to find the modes and eigenvalues of the Koopman operator. The DMD algorithm produces spatiotemporal coherent structures (modes) which have associated temporal behavior: growth, decay, and oscillation. These modes provide insight into the underlying mechanics of the system.

8.1 The Koopman Operator

Suppose we have a continuous, finite-dimensional, non-linear dynamical system

$$\frac{dy}{dt} = f(y) \quad y(0) = x \in \mathbb{R}^N$$

with $N >> 1$. $y(t)$ is the state of the dynamical system at time t . Sampling the dynamical system every Δt we get the discrete time-series

$$y_{k+1} = F(y_k),$$

with $y_k = y(t_k) = y(k\Delta t)$. We would like a coordinate transformation to render the dynamics of the non-linear system much simpler. In this new coordinate system, the dynamics could be described linearly. We seek a φ such that $z = \varphi(y)$ where the dynamics are much easier to evaluate in the z -coordinates. In this context, we seek $y_{k+1} = Ky_k$.

We define a Hilbert space of observables, that is

$$L_2(O) = L_2(\mathbb{R}^N, \mathbb{R}, \mu),$$

with an associated norm

$$\int_{\mathbb{R}^N} |g(x)|^2 d\mu(x) < \infty,$$

where μ is some appropriately chosen measure. The Koopman operator K is a mapping between the Hilbert space unto itself,

$$K : L_2(O) \rightarrow L_2(O)$$

such that

$$Kg(x) = g(F(x)) = g(x_{k+1}) \quad g \in L_2(O)$$

The Koopman operator is an infinite-dimensional, linear operator which advances the dynamical system forward a single step in time. The infinite dimensionality of the Koopman operator introduces difficulties. Instead, we examine the spectral decomposition of the Koopman operator. For an eigenfunction $\varphi_k(x)$ of K and their associated eigenvalue μ we have

$$K(\varphi(x_k)) = \mu\varphi(x_k) = \varphi(x_{k+1})$$

A vector of observables g can be written in terms of a basis of eigenvectors ξ_j

$$g(x_k) = \sum_{j=1}^{\infty} \varphi_j(x_k) \xi_j$$

which implies we can evolve the system like so

$$g(x_{k+1}) = K(g(x_k)) = \sum_{j=1}^{\infty} \mu_j \varphi_j(x_k) \xi_j.$$

The eigenfunctions define a set of coordinates on which we can advance the measurements with a linear dynamical system. The eigenfunctions are exactly the nonlinear change of coordinates we sought out. However, finding the exact eigenfunctions, modes, and eigenvalues of K analytically is difficult for any meaningful problem as the Koopman mode is infinite-dimensional. We can, however, seek to approximate a finite number of Koopman eigenpairs. Thus we resort to numerics to find them via the Dynamic Mode Decomposition.

8.2 Dynamic Mode Decomposition

Similar to the previous section, we consider sampled data collected from a non-linear dynamical system of the form:

$$\frac{dx}{dt} = f(x, t; \mu)$$

where $x(t) \in \mathbb{R}^n$ is a vector representing the state of the dynamical system at time t and μ are parameter values. Our data is sampled at discrete points in time every Δt . Every sampling can be written as $x_k = x(k\Delta t)$. This discrete time-flow map we denote $x_{k+1} = F(x_k)$. We can then extend our collected data:

$$y_k = g(x_k)$$

where $g(k)$ is the set of observables formed from the state space. Here we use the Koopman operator theory to introduce a linear, infinite-dimensional operator A :

$$Ag = Ag(x_k) = g(x_{k+1}),$$

A advances measurements along the flow F by Δt . We calculate the Koopman operator of our dynamical system in the following manner [15]. Beginning with our data snapshot matrix composed of the relevant observables, we write

$$G = [g(x_0), g(x_1), g(x_2), \dots, g(x_n)] = [g_1, g_2, \dots, g_n],$$

which we can then break into two matrices:

$$\begin{aligned} G_+ &= [g_1, g_2, g_3, \dots, g_n] \\ G_- &= [g_0, g_1, g_2, \dots, g_{n-1}] \end{aligned}$$

The matrix G_+ is simply our matrix G_- taken forward one step in time. The matrix A we wish to find satisfies:

$$G_+ = AG_-$$

Subtracting AG_- from both sides, we have

$$G_+ - AG_- = 0$$

We would then like to find a \tilde{A} that

$$\tilde{A} = \arg \min_A \|G_+ - AG_-\|_F$$

where $\|\cdot\|_F$ denotes the Frobenius norm. We still have the matter of finding the \tilde{A} that minimizes the norm, which is our best approximation to A . We could use a least-squares fit or solve using Moore pseudo-inverse calculating $G_+G_-^\dagger$, but we use the r-rank singular value decomposition in the following way.

$$\begin{aligned}
G_+ &= \tilde{A}G_- \\
&= \tilde{A}U_rS_rV_r^T \quad \text{by singular value decomposition} \\
G_+V_rS_r^{-1}U_r^T &= \tilde{A}
\end{aligned}$$

Taking the r-rank of the SVD limits the number of modes and eigenvalues to a few that satisfy a threshold tolerance. This produces a low-rank model that still captures most of the information of the dynamical system. Finally, we use an eigendecomposition on the left-hand side to find the DMD modes ξ_j and eigenvalues μ_j . We can write a solution to the dynamical system for all time:

$$x_{k+1} \approx \sum_{n=1}^r b_n e^{\frac{\ln(\mu_n)t}{\Delta t}} \xi_n$$

Once we have the DMD modes and eigenvalues, we can begin to look at which DMD modes "contribute the most" throughout the snapshot matrix by examining the associated eigenfunctions and eigenvalues which describe their temporal behavior: growth, decay, or oscillation. We have not discussed how to choose g , how we build our dictionary of observables. If we choose g to be the identity mapping, then the method reduces to the standard DMD algorithm, where $g(x_i) = x_i$. Choosing any other function of g in a meaningful way requires prior knowledge of the system or challenge. A mapping g can extend the dictionary of observables beyond the state space using an appropriate basis. This is aptly called Extended Dynamic Mode Decomposition (EDMD) [23]. A quick example of such a choice might be:

$$Y = \{y_1, y_2, y_3, \dots, y_n\}, \quad y_i \in \mathbb{R}^N$$

with

$$y_i = y_{i,1}, y_{i,2}, \dots, y_{i,N}$$

then we might take g such that:

$$G(Y) = \{g(y_1), g(y_2), g(y_3), g(y_4), \dots, g(y_n)\}$$

$$g(y_i) = y_{i,1}, y_{i,2}, \dots, y_{i,N}, y_{i,1}^2, y_{i,1}y_{i,2}, \dots, y_{i,N}^2$$

This example of g is one of many possible functions. EDMD strengthens the connection between Dynamic Mode Decomposition and Koopman Operator Theory. In

fact, given a choice of g such that $\phi_j \in \text{span}\{g_k\}$ then the eigenvalues of the Koopman operator are the DMD eigenvalues [23].

8.3 Kernel Dynamic Mode Decomposition

EDMD can quickly generate a large set of observables and the computational complexity of the problem increases rapidly. It suffers from the dimensionality problem and works well provided many more snapshots than state-space variables. If one is analyzing, for instance, n-dimensional fluid flows, the flattened matrix-snapshot can easily have thousand of entries. Extending the state-space by building a dictionary with nonlinear combinations of the state space will generate very large matrices [35]. For that reason, one applies the kernel trick. Instead of evaluating the high dimensional state space directly, one can take inner-products of the state space using kernel functions to "collapse" the information of many nonlinear terms to a single value. In chapter 9, KDMD can produce modes with relatively low mode error [23]. We introduce the notion of the kernel.

Definition 14. *We define the kernel function*

$k : \mathbb{R}^n \times \mathbb{R}^n \rightarrow \mathbb{R}$, $k(x, \hat{x}) = \langle \phi(x), \phi(\hat{x}) \rangle$. k maps a pair of vectors to an inner product of observables of the data.

There are a variety of different kernels that we may choose. In this these we use the polynomial kernel.

$$k(x, x') = (1 + x^T x')^p$$

As mentioned, the kernel functions allow us to store a large amount of information in a single value. We generate matrices Φ^+ and Φ^- from the polynomial basis function. Given our snapshot matrix Y follows:

$$Y = \{y_1, y_2, y_3, \dots, y_n\}$$

$$k(y, \hat{y}) = (1 + y^T \hat{y})^p$$

We then construct the matrices $\Phi^+ \in \mathbb{C}^{n \times n}$ and $\Phi^- \Phi^+ \in \mathbb{C}^{n \times n}$.

$$\Phi_{i,j}^+ = k(Y_i^+, Y_j^-)$$

$$\Phi_{i,j}^- = k(Y_i^-, Y_j^-)$$

Then, for every element in $\Phi_{i,j}^+$ and $\Phi_{i,j}^-$, we have a kernel between two snapshots in time. We finally find our modes as outlined in [35].

Given our matrices Φ^+ , Φ^- we compute the singular value decomposition of $\Phi^- = U\Sigma V^T$. We then compute

$$\hat{A} = (\Sigma U^T) \Phi^+ (U^T \Sigma)$$

Finally, we find an eigenvector ξ of A by solving

$$\xi = V\hat{\xi}$$

where $\hat{\xi}$ is an eigenvector of \hat{A} .

8.4 Accuracy Criterion

For the DMD and KDMD algorithms, we evaluate how well the methods performed. We consider two different measures of accuracy. First, we define the one-step reconstruction error r . We define the matrix \tilde{G} where the j 'th column vectors of \tilde{G} are the one-step reconstructions of the state space at time $j + 1$ for $j = 0, 1, \dots, n - 1$.

$$\begin{aligned}\tilde{G}_j &= \sum_i \mu_k \varphi_k(x_j) \xi_k \\ r &= \frac{\|G_+ - \tilde{G}\|_F}{\|G_+\|_F}\end{aligned}$$

where $\|\cdot\|_F$ denotes the Frobenius norm.

We also wish to know if the approximated modes and eigenvalues are good approximations to Koopman modes. We define the Rowley Criterion [37]. Let ξ_j and μ be a Koopman mode for the dynamical system F and its corresponding eigenvalue. Provided that ξ_j and μ_j are a true eigenpair it follows:

$$\xi_j \circ F = \mu_j \xi_j$$

Now, letting $\|\cdot\|$ denote the $L2$ norm, we would like to calculate

$$\frac{\|\xi \circ F - \mu \xi\|}{\|\xi\|}$$

However, if we know F then DMD isn't a useful tool. We must estimate F using a finite number of data points. We take two data points $x_k, x_{k+1} \in X$. We can now write

$$\tilde{r}_j = \frac{\sum_k |\varphi_j(x_{k+1}) - \mu_j \varphi_j(x_k)|}{\sum_k |\varphi_j(x_k)|}$$

This equation measures how much each eigenfunction ϕ_j behaves like a Koopman eigenfunction. We can use this to evaluate each mode individually and could potentially use it to select modes for low-rank reconstruction [37]. If \tilde{r}_j is close to one the eigenpair is unreliable, because the difference in the eigenpair is of the same magnitude of the eigenfunction. Therefore a good eigenpair will have a mode error such that $0 < \tilde{r}_j \ll 1$.

CHAPTER 9

Results

9.1 Preprocessing Data

Dynamic Mode Decomposition is sensitive to noise in the data. We implement several techniques to better the errors of the DMD modes. First, we modify the data via a Poisson process such that the events do not occur at each snapshot, but events occur relative to a δt . Suppose we have

$$X = [x_1, x_2, x_3, \dots, x_n]$$

where x_i describes a feature vector at $i\Delta t = t$. We then allow

$$A = \frac{1}{2} \left(\frac{1}{\lambda} + \psi(x; \lambda) \right), \quad \psi(x; \lambda) = \lambda e^{-\lambda x}$$

$$\delta t = \min(A)$$

$\psi(x; \lambda)$ is an exponential probability distribution from which we draw a thousand samples with $\lambda = 10$. We then distribute events in the following way. Let \hat{A} denote a matrix that initially only contains the value x_1 . For $k = 1, 2, 3, \dots$ we calculate $k\delta t$. While $k\delta t < A_i$ we append x_i to \hat{A} . Thus we generate a new matrix \hat{A} that now contains $n = \sum_{i=1}^N A_i \bmod (\delta t)$ \hat{A} . This distributes the events according to a Poisson process. After we distribute events in time according to this process, we smooth the data with the window-average. This smoothing will help the DMD and KDMD generate better fits. Last, we center the data about its mean to improve the fit.

9.2 DMD: Barabási–Albert m=1

We now reach the results of the DMD algorithm applied to the motif counts of the simulated networks. We will first examine DMD applied to the Barabási–Albert motif counts. Thereafter, we examine several parameter choices for the Thij model. For all DMD and KDMD results, the Koopman modes and eigenvalues are as discussed in chapter 8. The $\varphi(x_k)$ eigenfunctions tell us how much energy the respective Koopman mode contributes at a given time step.

We can now consider DMD results of the Barabási–Albert motif counts. We show in this section the $m = 1$ and $m = 2$ case to observe differences and similarities between the approximated Koopman modes and eigenvalues.

For the $m = 1$ case, we know that a new node and edge are added at every time-step. Moreover from our correlation and covariance heat maps, we know the only motifs that change in the $m = 1$ case are as such:

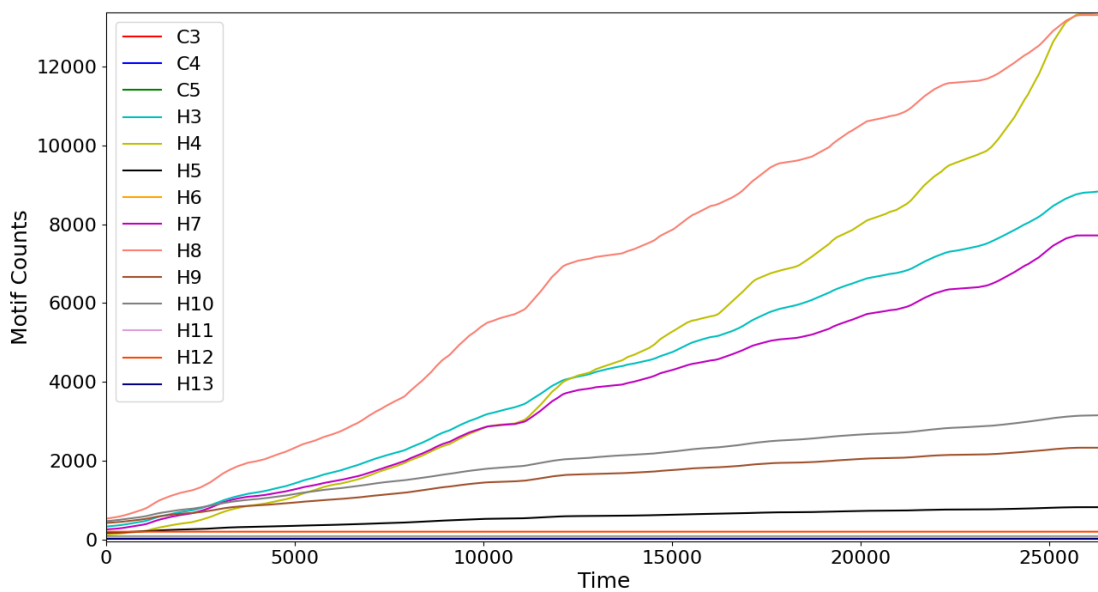


Figure 9.1. Smooth motif counts for Barabási–Albert model $k = 1$.

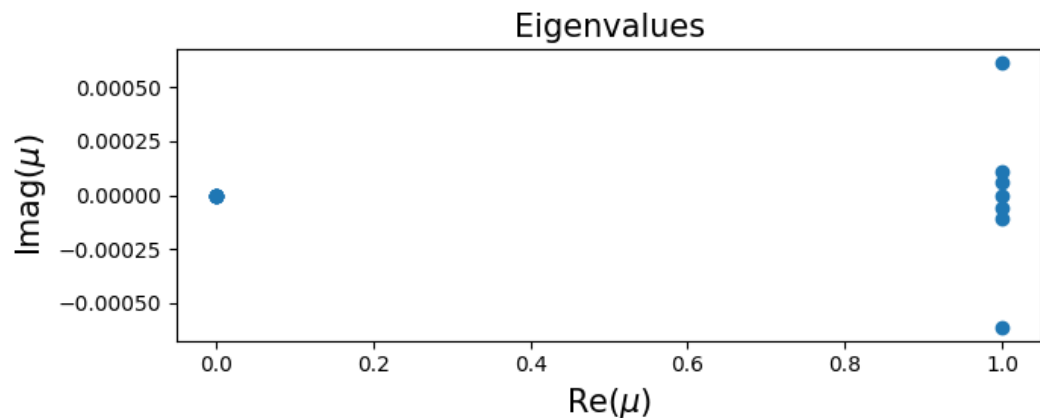


Figure 9.2. Mode eigenvalues for Barabási–Albert model with $k = 1$.

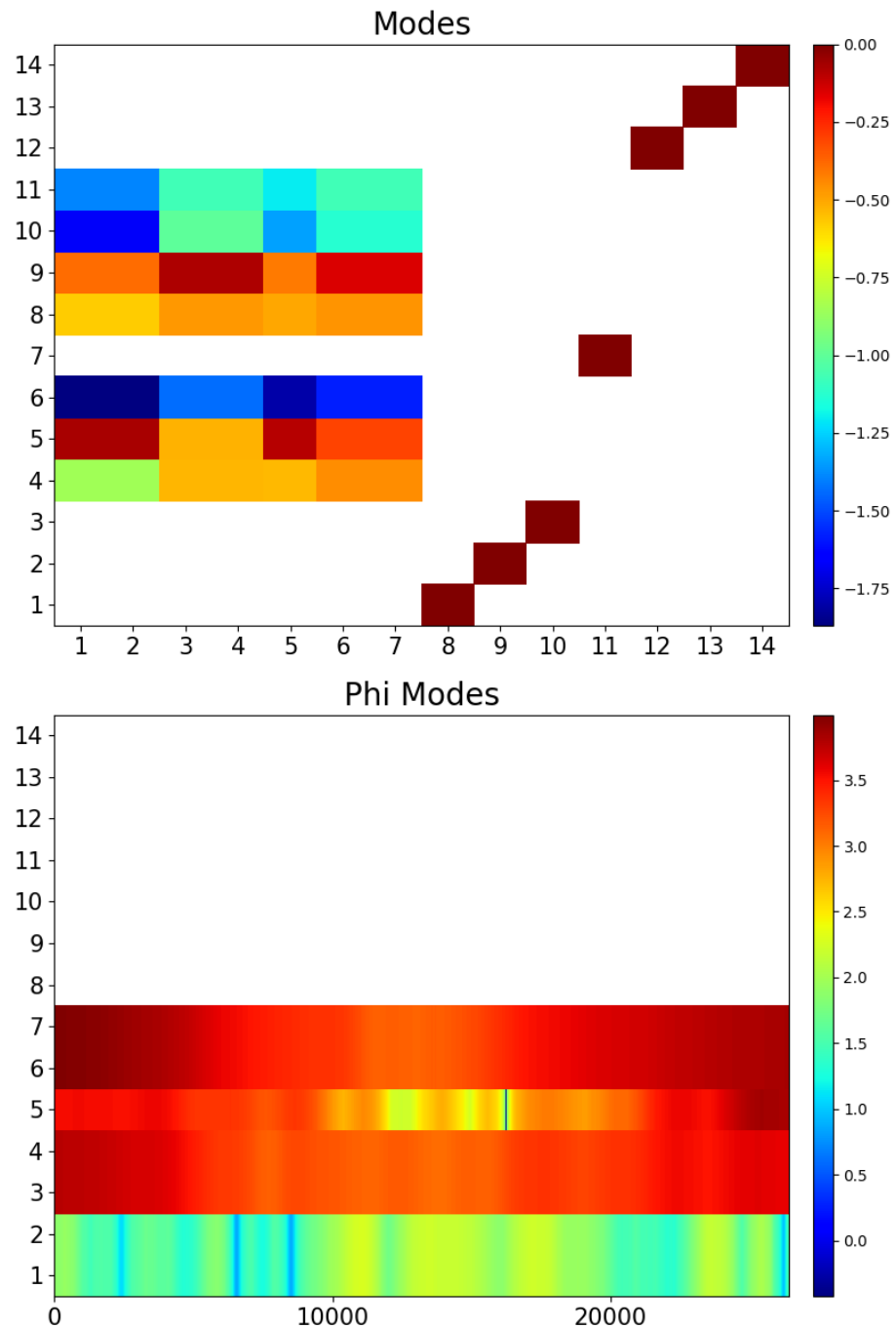


Figure 9.3. DMD modes for Barabási–Albert model with $k = 1$.

9.3 KDMD: Barabási-Albert m=1

We now examine the same simulations through the KDMD method.

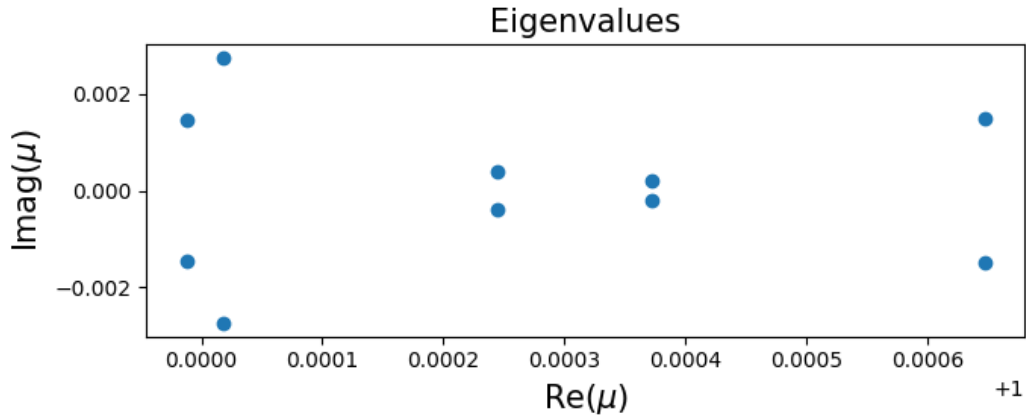


Figure 9.4. Mode eigenvalues by KDMD for Barabási–Albert model with $k = 1$.

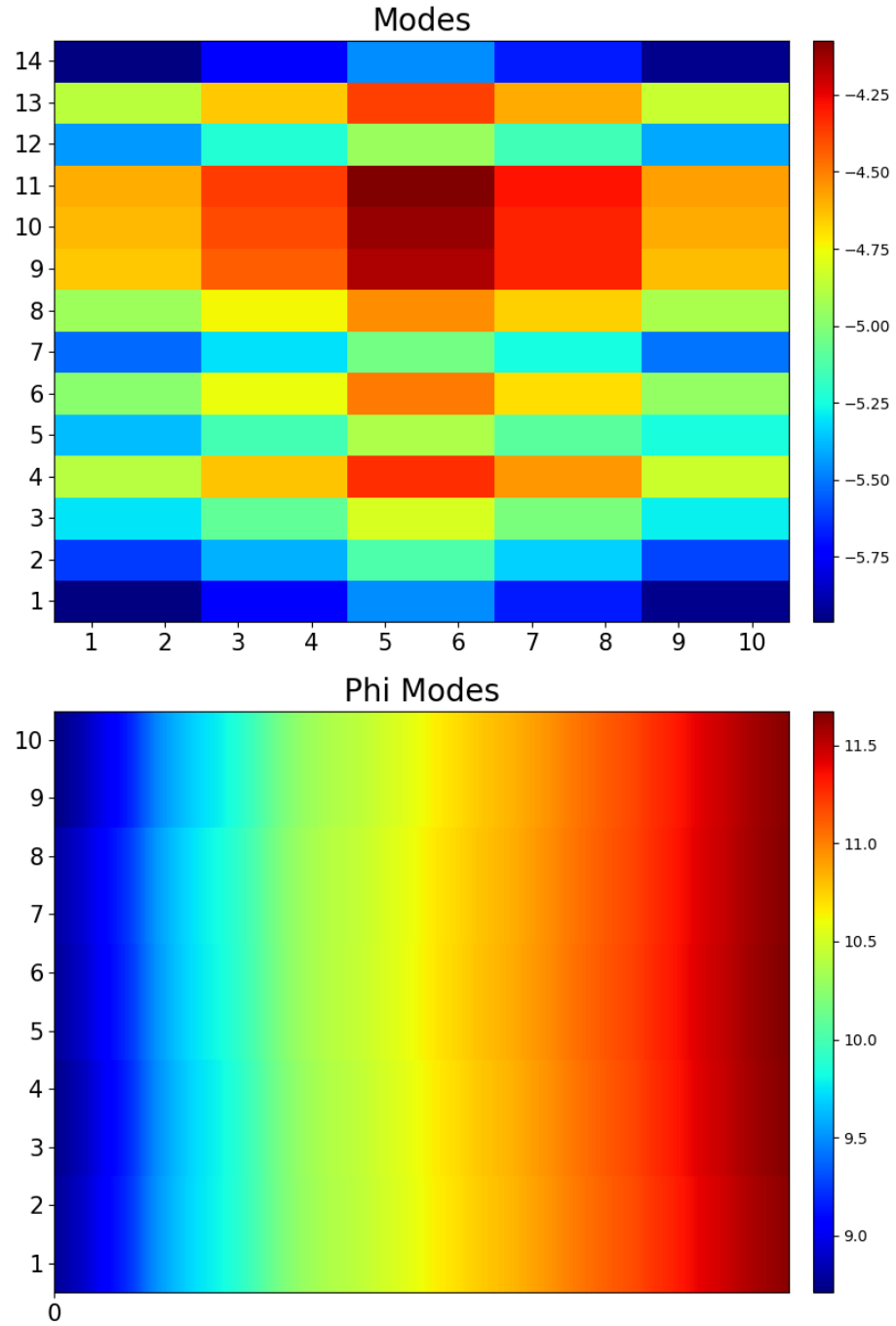


Figure 9.5. KDMD modes for Barabási–Albert model with $k = 1$.

9.4 DMD: Barabási–Albert m=2

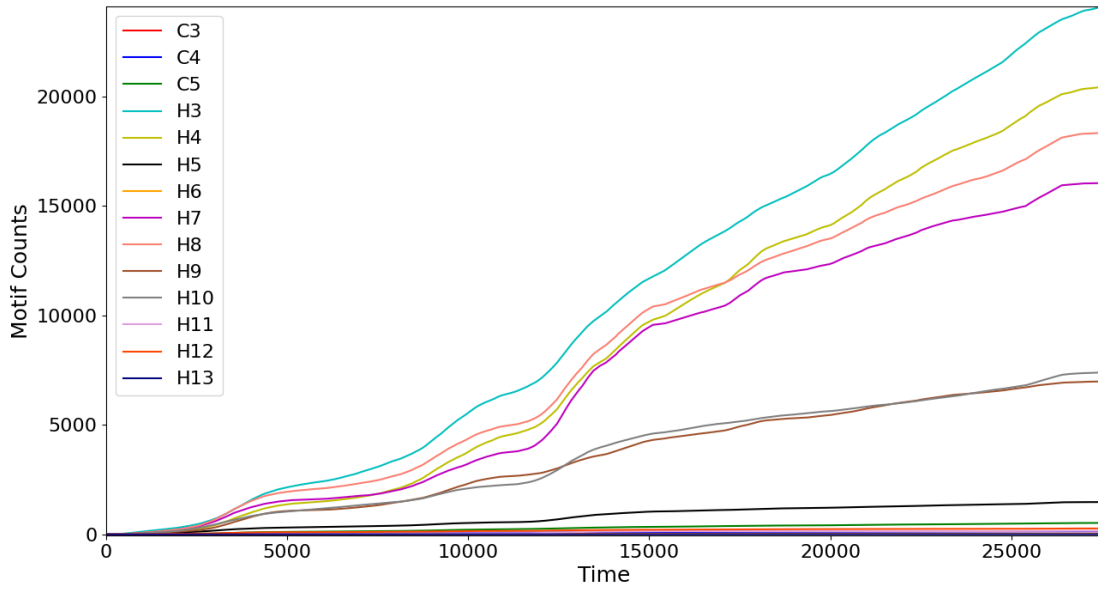


Figure 9.6. Smooth motif counts for the Barabási–Albert model with $k = 2$.

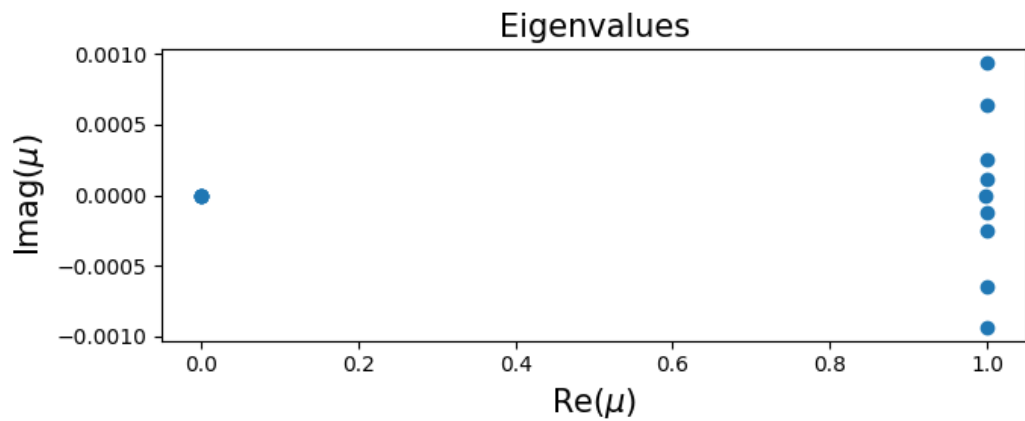


Figure 9.7. DMD modes for the Barabási–Albert model with $k = 2$.

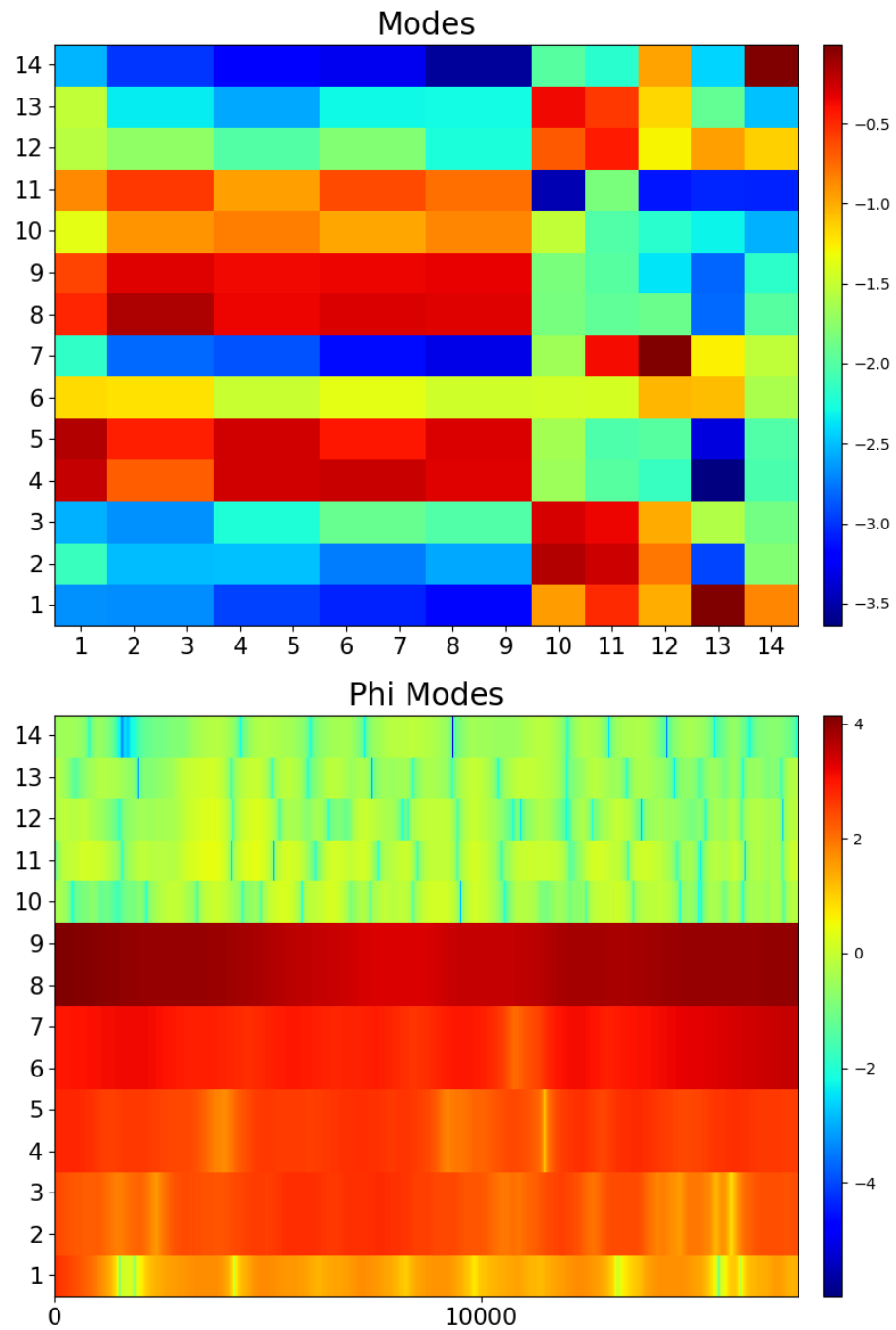


Figure 9.8. KDMD modes for the Barabási–Albert model with $k = 2$.

9.5 KDMD: Barabási–Albert m=2

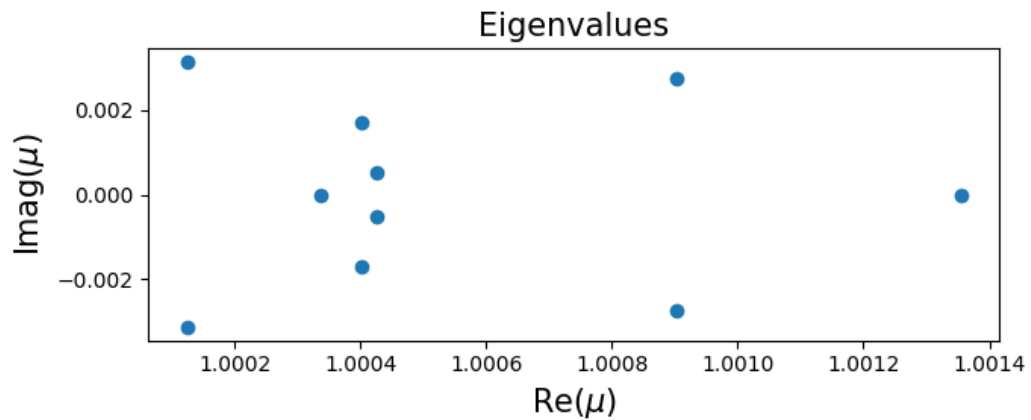


Figure 9.9. Mode eigenvalues by KDMD for the Barabási–Albert model with $k = 2$.

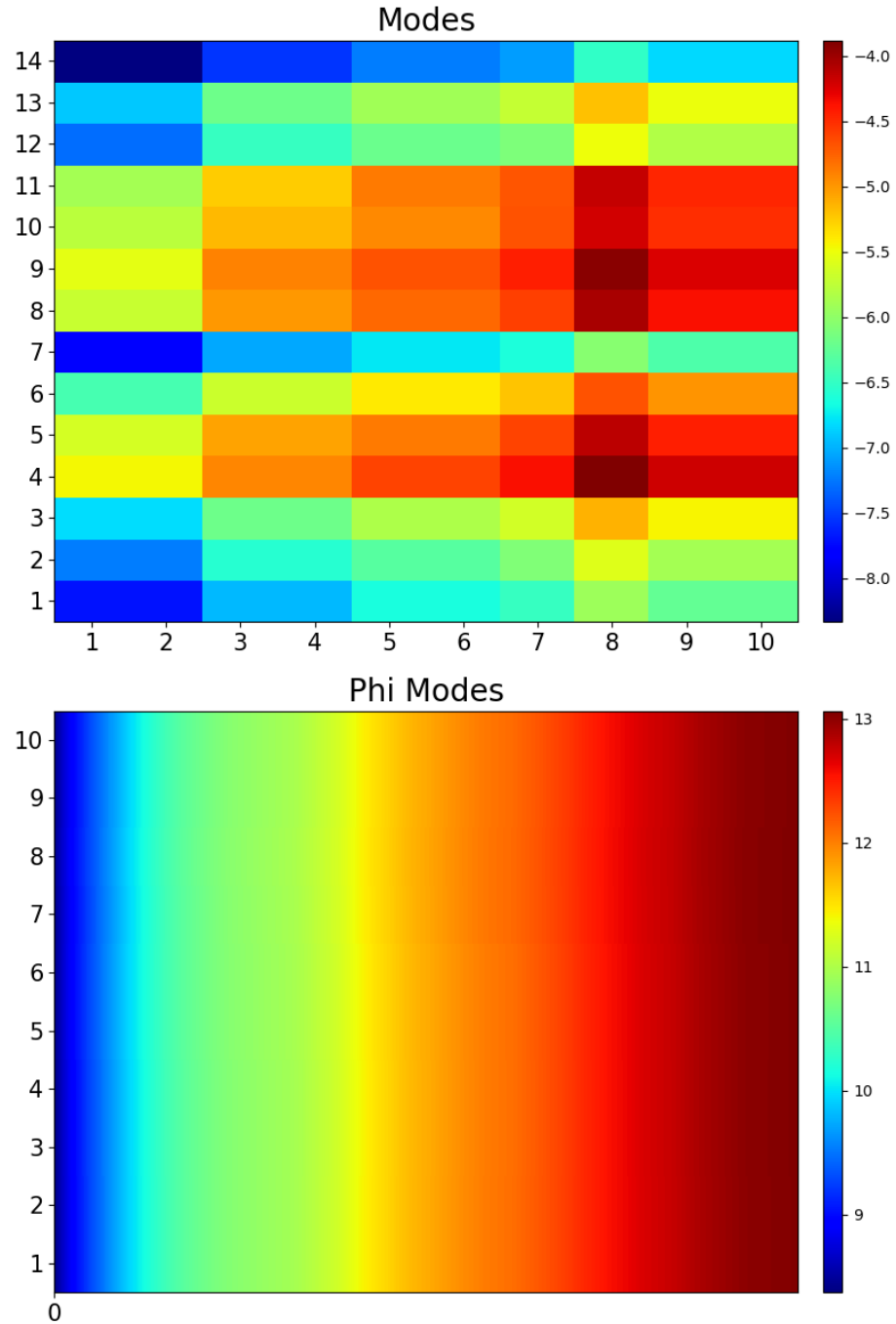


Figure 9.10. KDMD modes for the Barabási–Albert model with $k = 2$.

9.6 DMD: Thij Model with $\lambda = 0.2$, $p = 0.2$

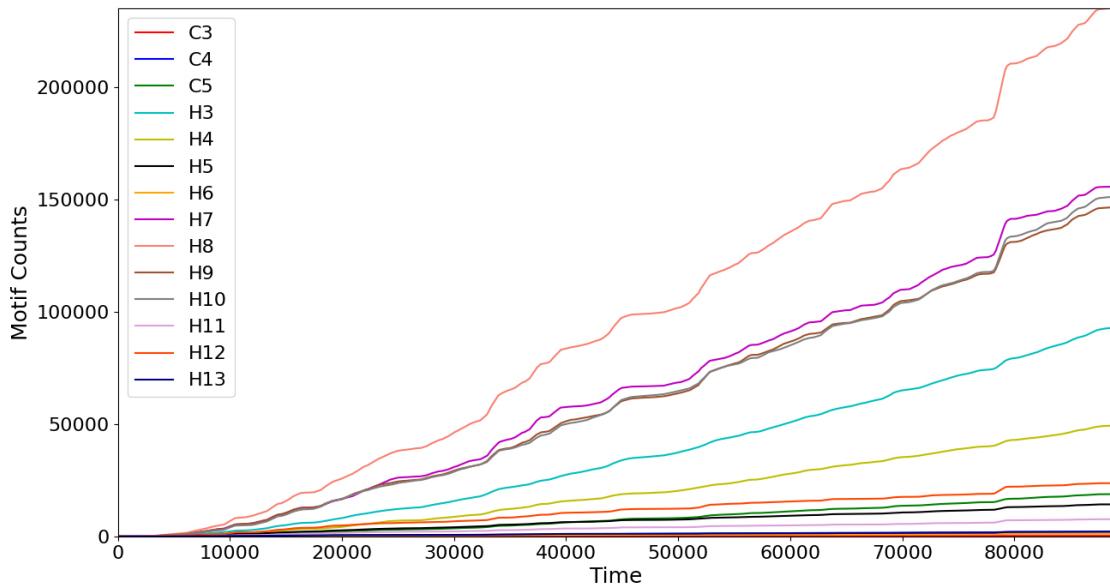


Figure 9.11. Smooth motif counts for the Thij model with $\lambda = 0.2$, $p = 0.2$.

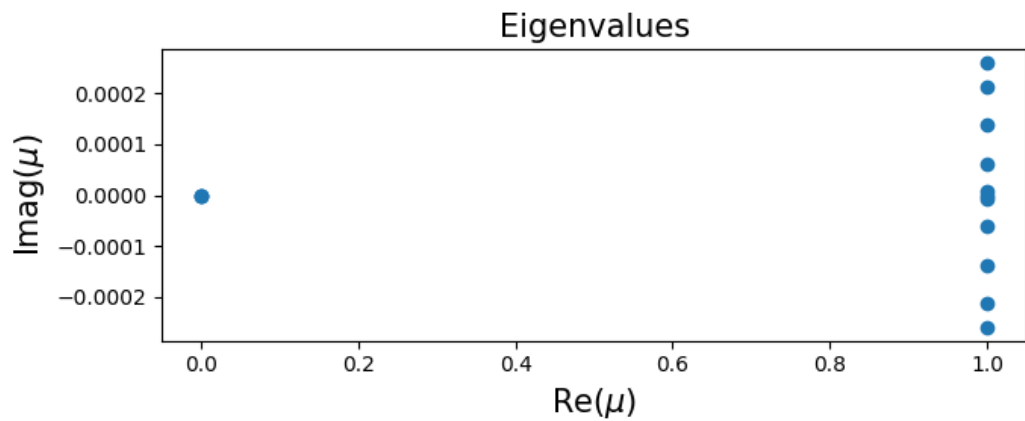


Figure 9.12. Mode eigenvalues by DMD for the Thij model with $\lambda = 0.2$, $p = 0.2$.

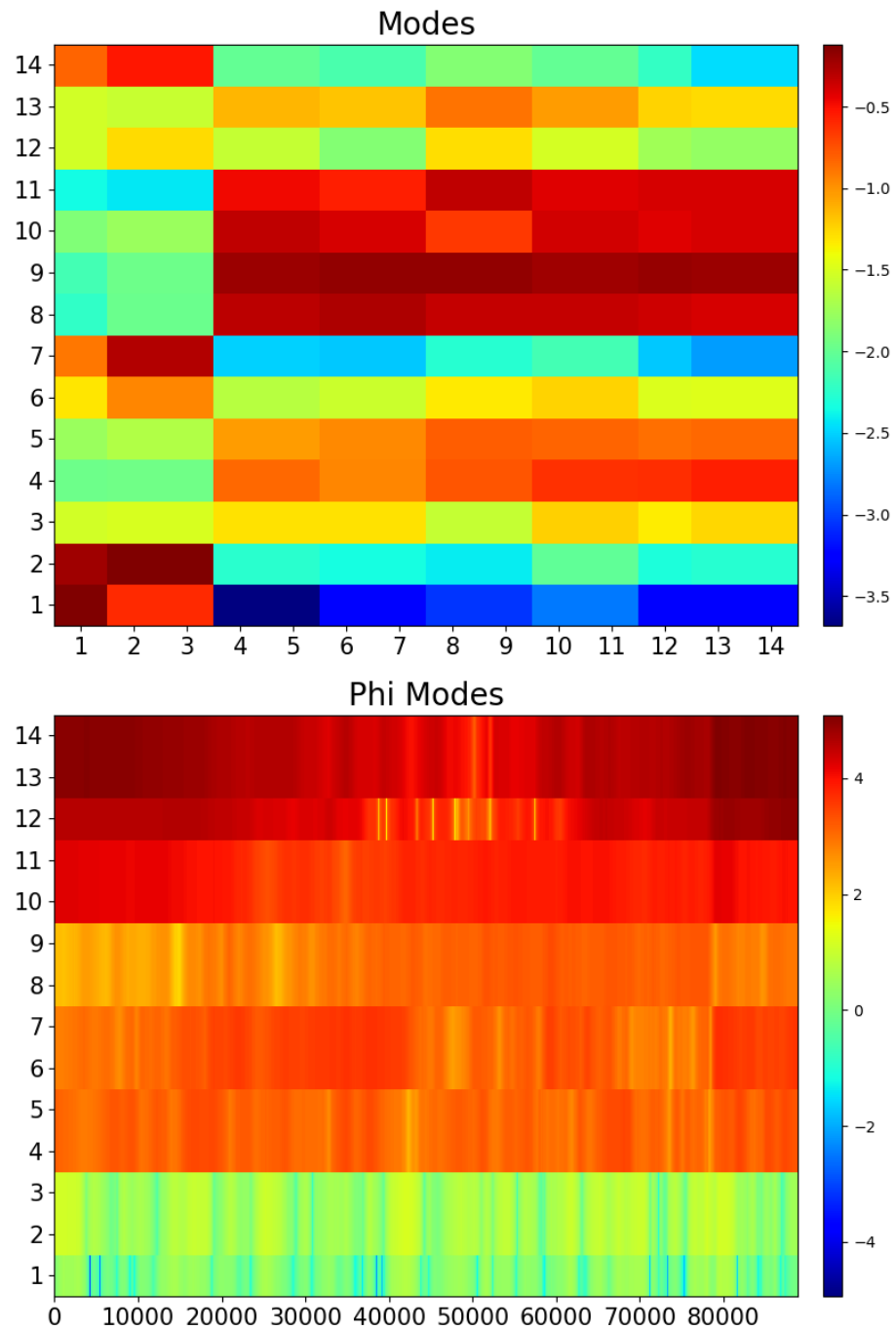


Figure 9.13. DMD modes for the Thij model with $\lambda = 0.2$, $p = 0.2$.

9.7 KDMD: Thij Model with $\lambda = 0.2$, $p = 0.2$

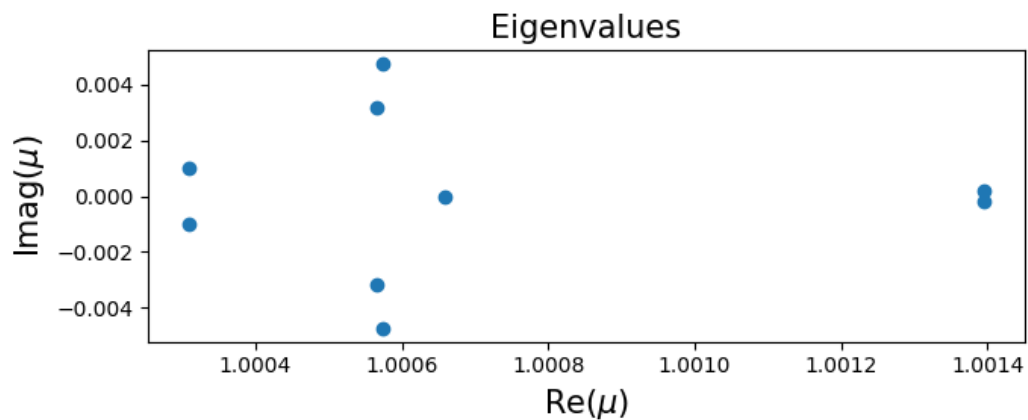


Figure 9.14. Mode eigenvalues by KDMD for the Thij model with $\lambda = 0.2$, $p = 0.2$.

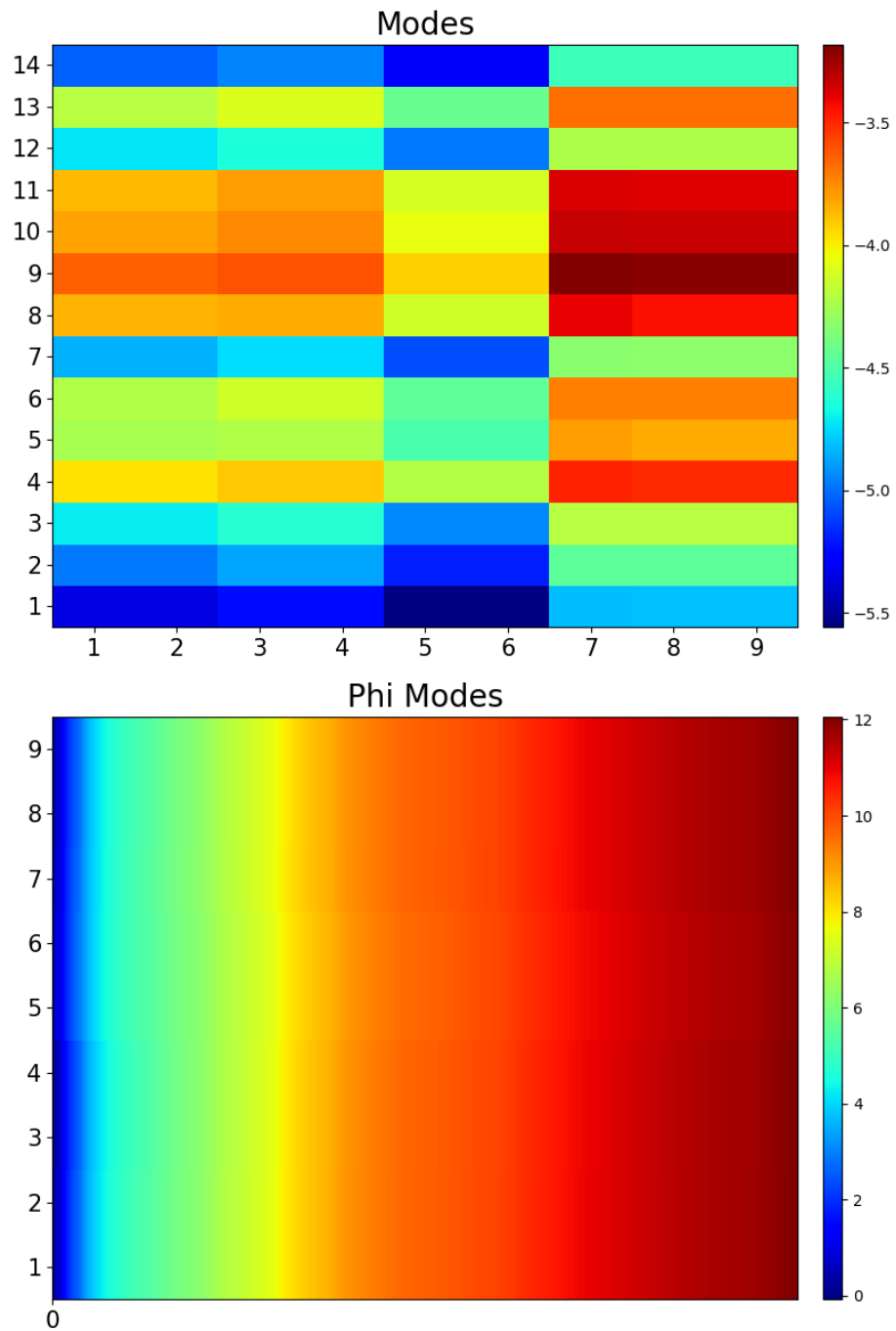


Figure 9.15. KDMD modes for the Thij model with $\lambda = 0.2$, $p = 0.2$.

9.8 DMD: Thij Model with $\lambda = 0.2, p = 0.8$

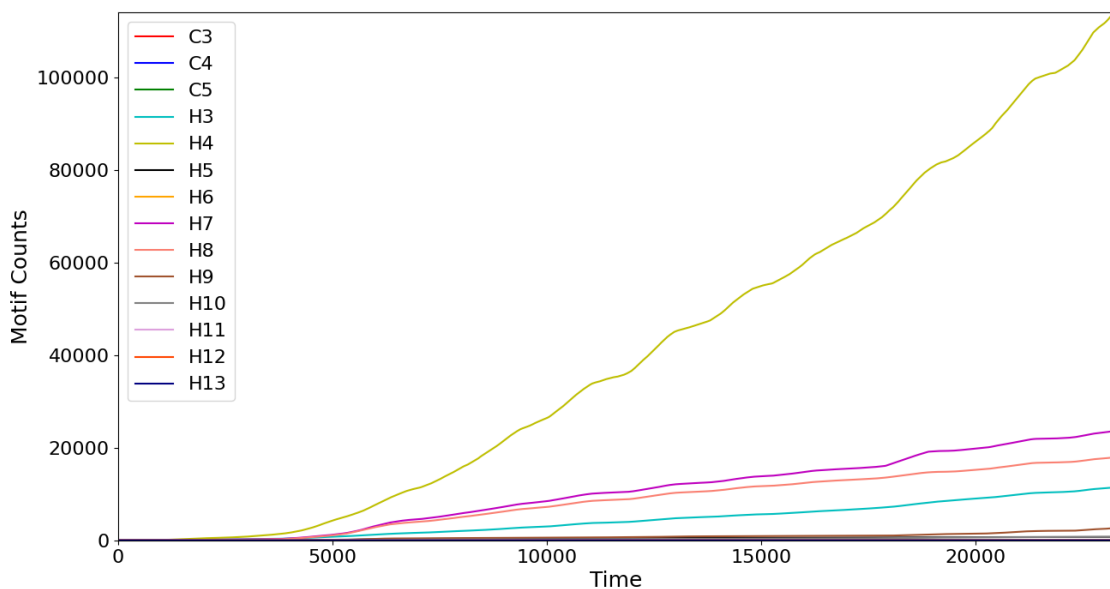


Figure 9.16. Motif counts for the Thij model with $\lambda = 0.2, p = 0.8$.

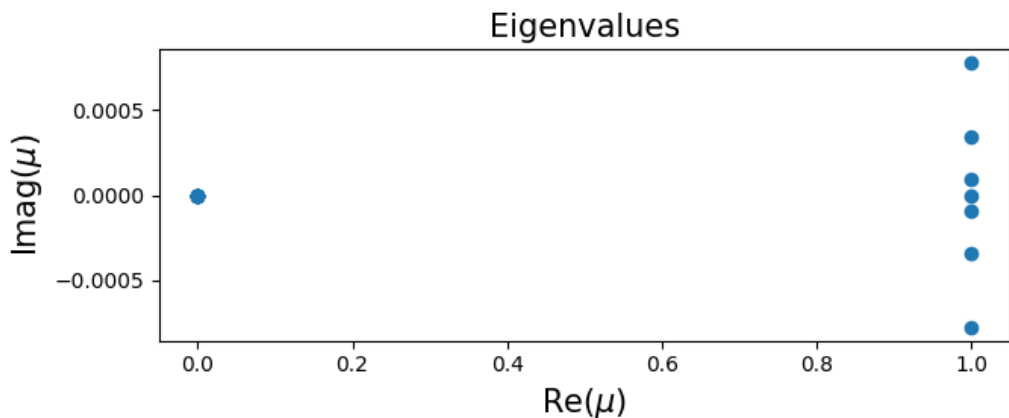


Figure 9.17. Mode eigenvalues by DMD for the Thij model with $\lambda = 0.2$, $p = 0.8$.

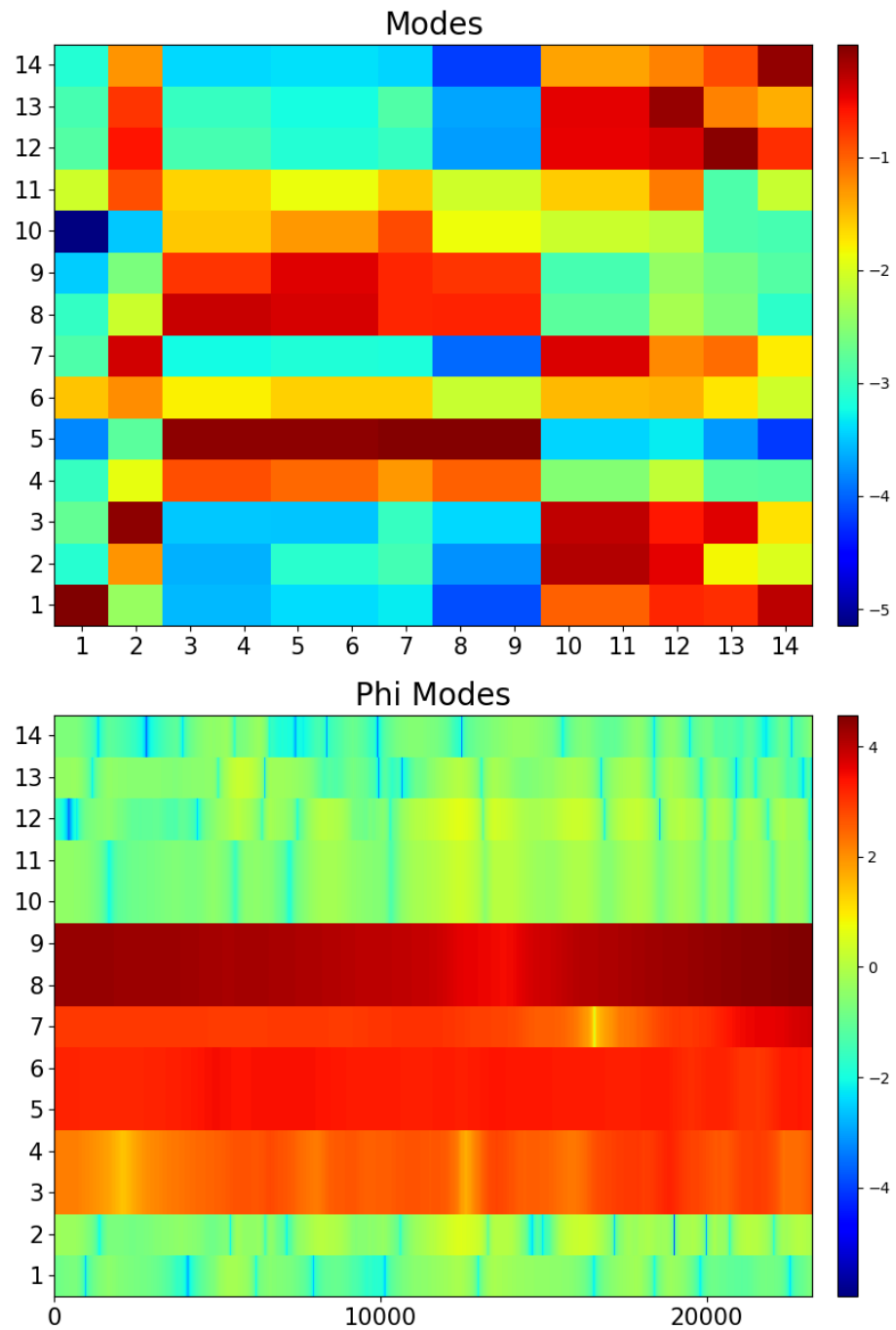


Figure 9.18. DMD modes for the Thij model with $\lambda = 0.2$, $p = 0.8$.

9.9 KDMD: Thij Model with $\lambda = 0.2$, $p = 0.8$

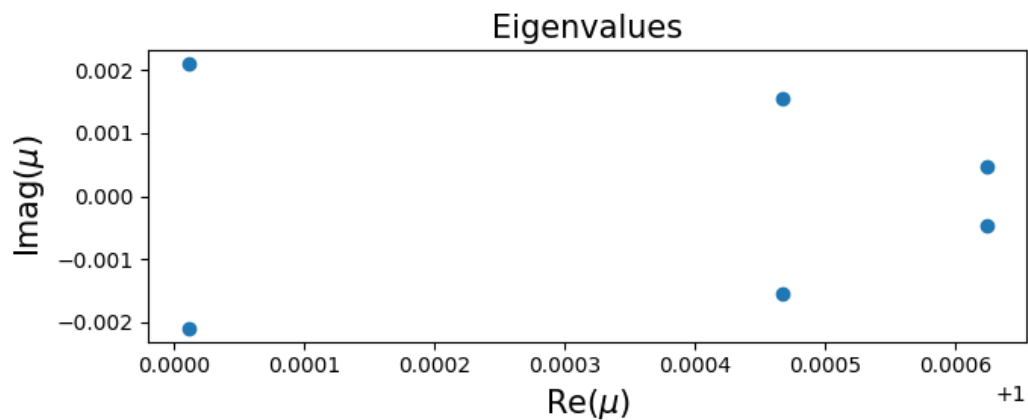


Figure 9.19. Mode eigenvalues by KDMD for the Thij model with $\lambda = 0.2$, $p = 0.8$.

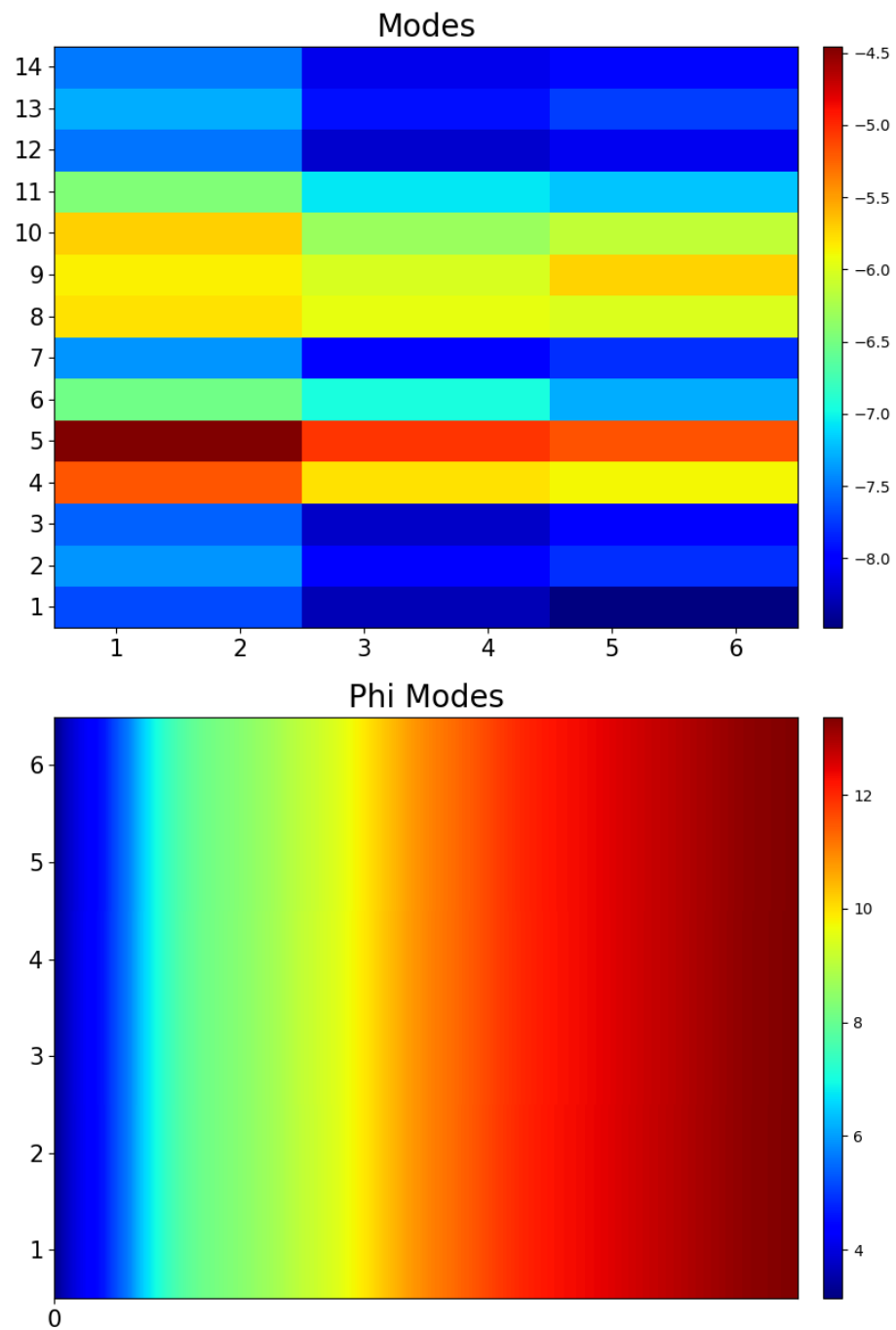


Figure 9.20. KDMD modes for the Thij model with $\lambda = 0.2$, $p = 0.8$.

9.10 DMD: Thij Model with $\lambda = 0.8$, $p = 0.2$

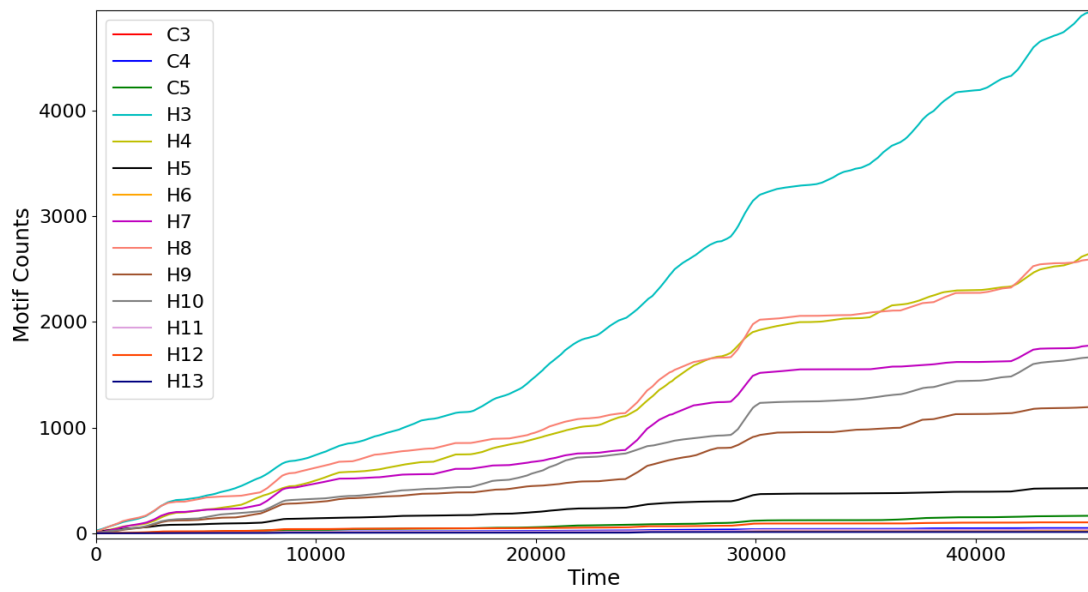


Figure 9.21. Motif counts for the Thij simulation with $\lambda = 0.8$, $p = 0.2$

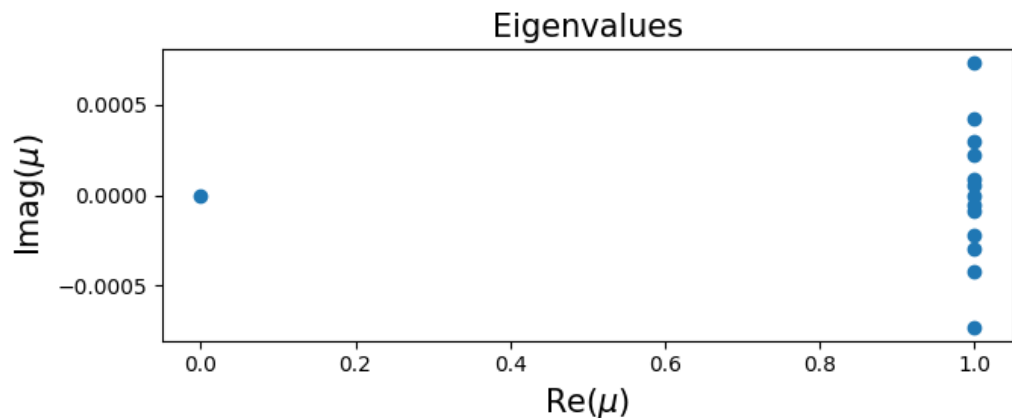


Figure 9.22. Mode eigenvalues by DMD for the Thij model with $\lambda = 0.8$, $p = 0.2$.

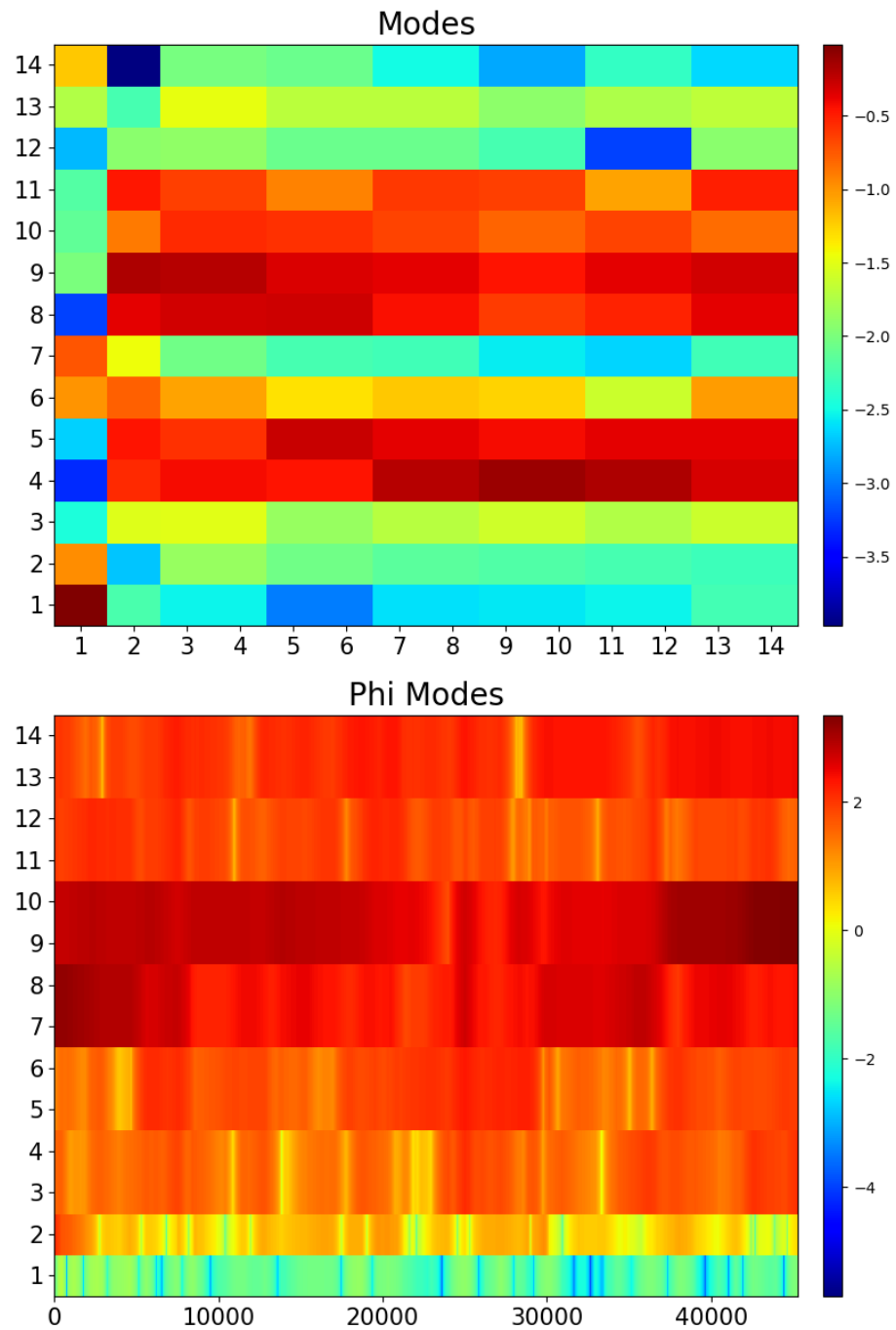


Figure 9.23. DMD modes for the Thij model with $\lambda = 0.8$, $p = 0.2$.

9.11 KDMD: Thij Model with $\lambda = 0.8$, $p = 0.2$

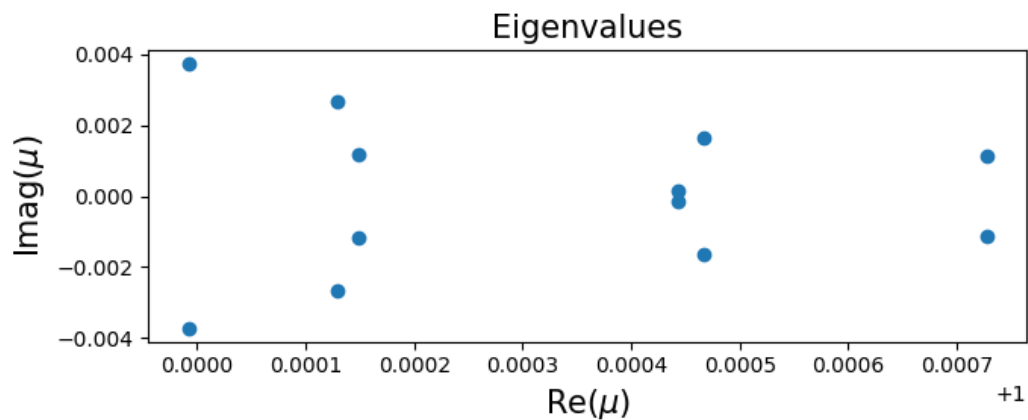


Figure 9.24. Mode eigenvalues by KDMD for the Thij model with $\lambda = 0.8$, $p = 0.2$.

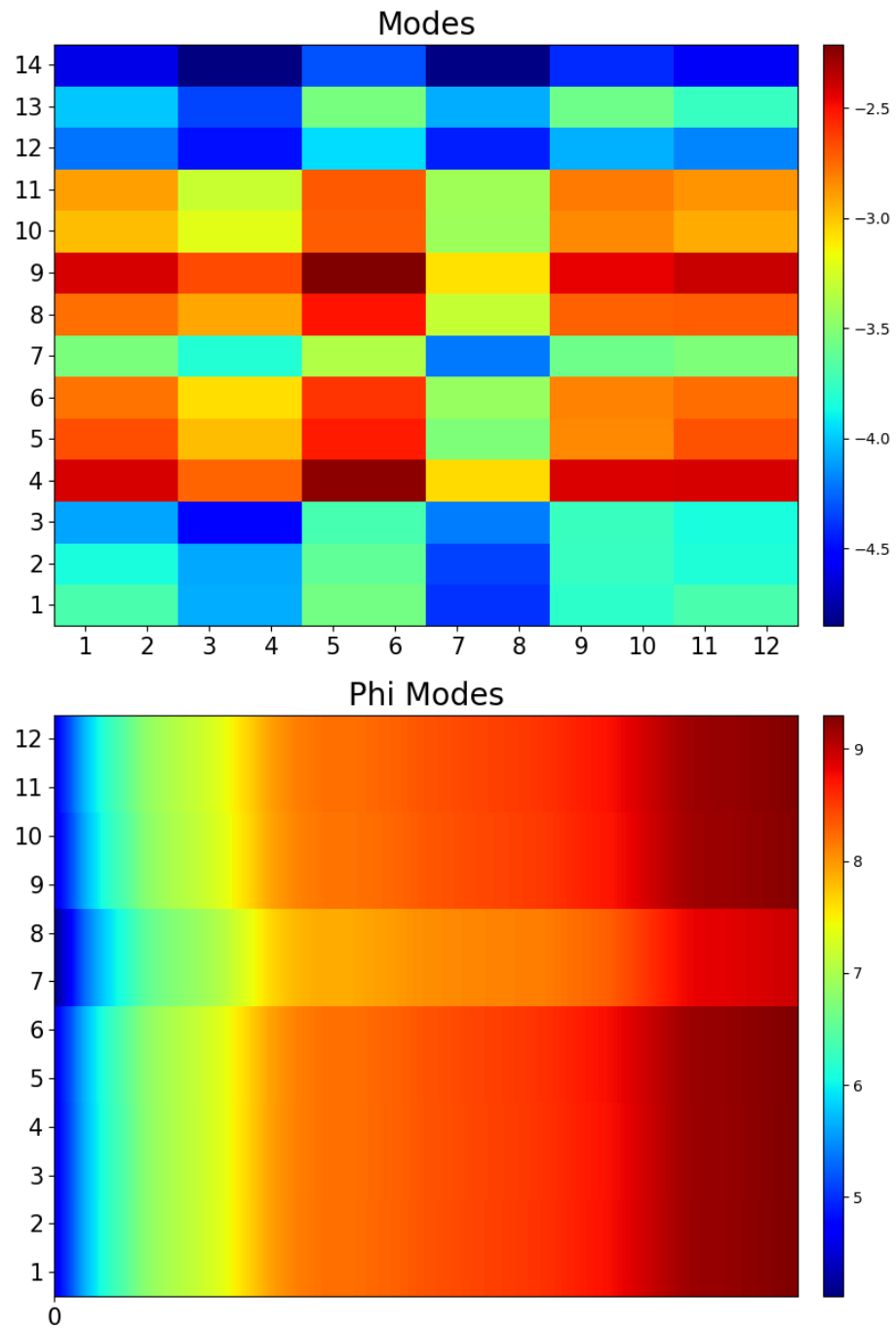


Figure 9.25. KDMD modes for the Thij model with $\lambda = 0.8$, $p = 0.2$.

9.12 DMD: Thij Model with $\lambda = 0.8$, $p = 0.8$

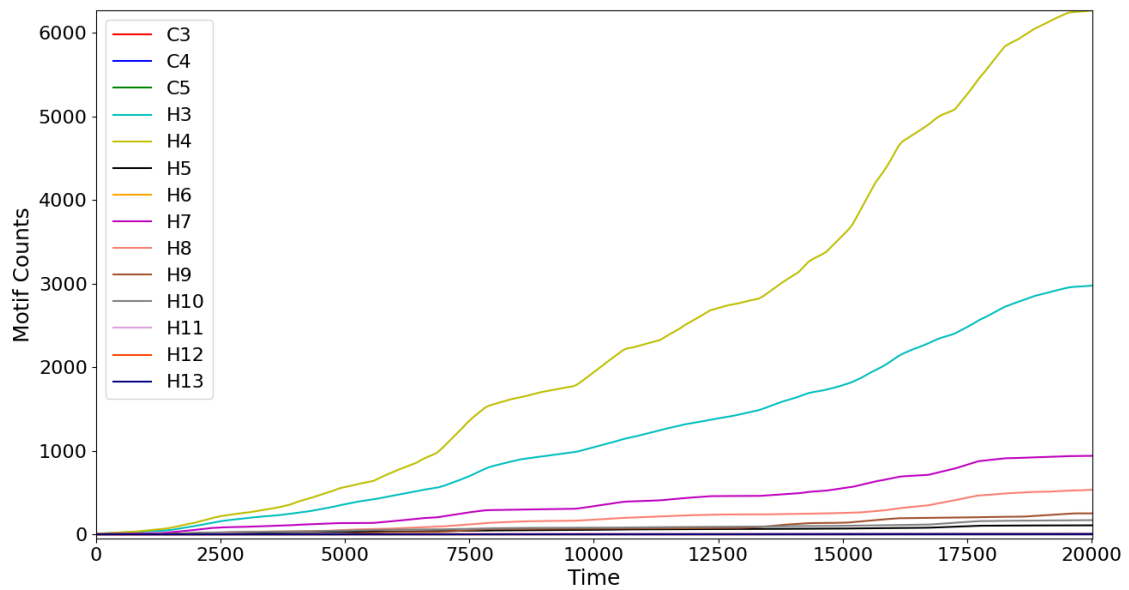


Figure 9.26. Motif counts for the Thij model with $\lambda = 0.8$, $p = 0.8$.

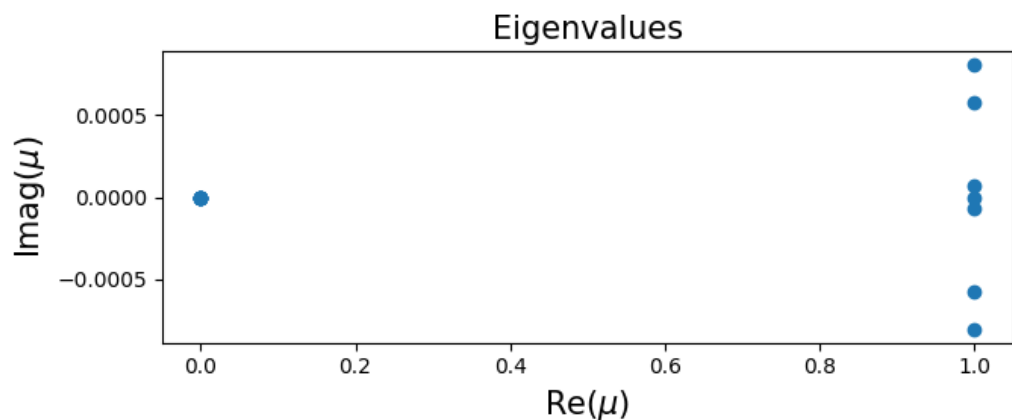


Figure 9.27. Mode eigenvalues by DMD for the Thij model with $\lambda = 0.8$, $p = 0.8$.

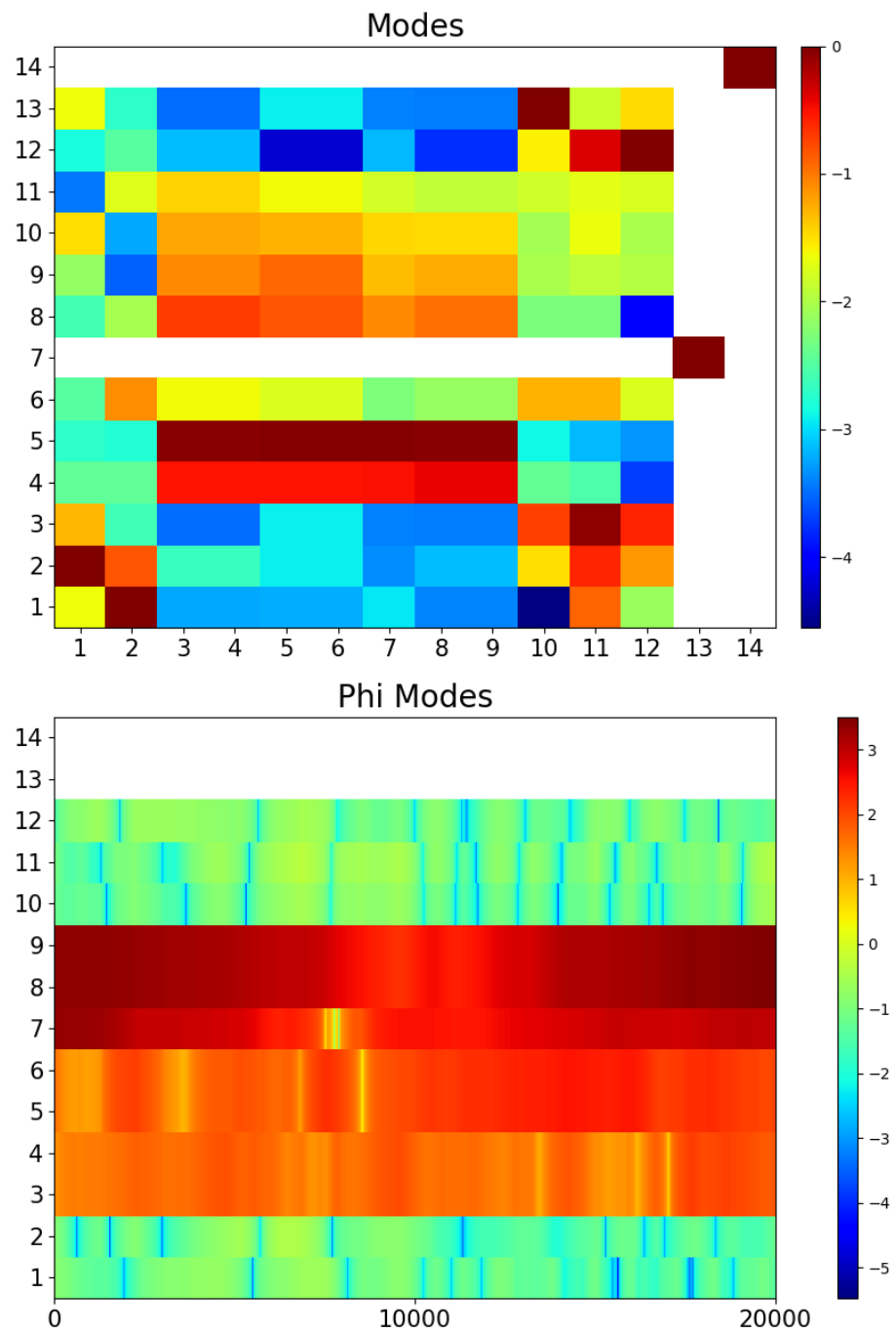


Figure 9.28. DMD modes for the Thij model with $\lambda = 0.8$, $p = 0.8$.

9.13 KDMD: Thij Model with $\lambda = 0.8$, $p = 0.8$

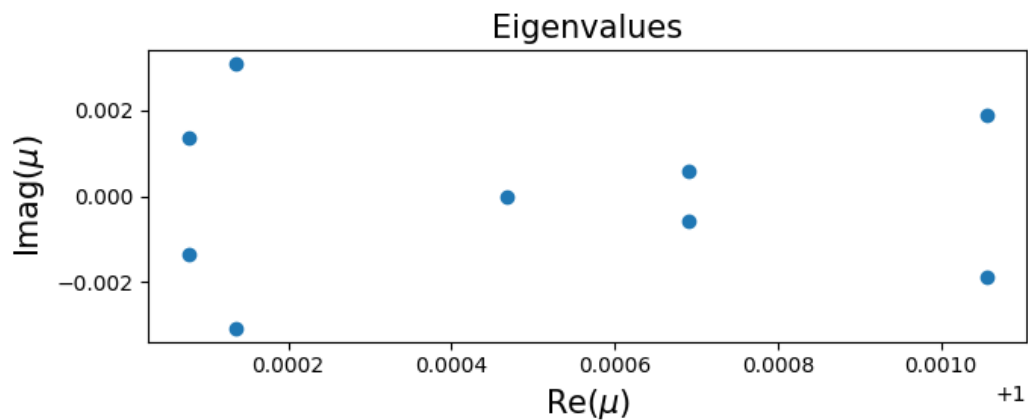


Figure 9.29. Mode eigenvalues by KDMD for the Thij model with $\lambda = 0.8$, $p = 0.8$.

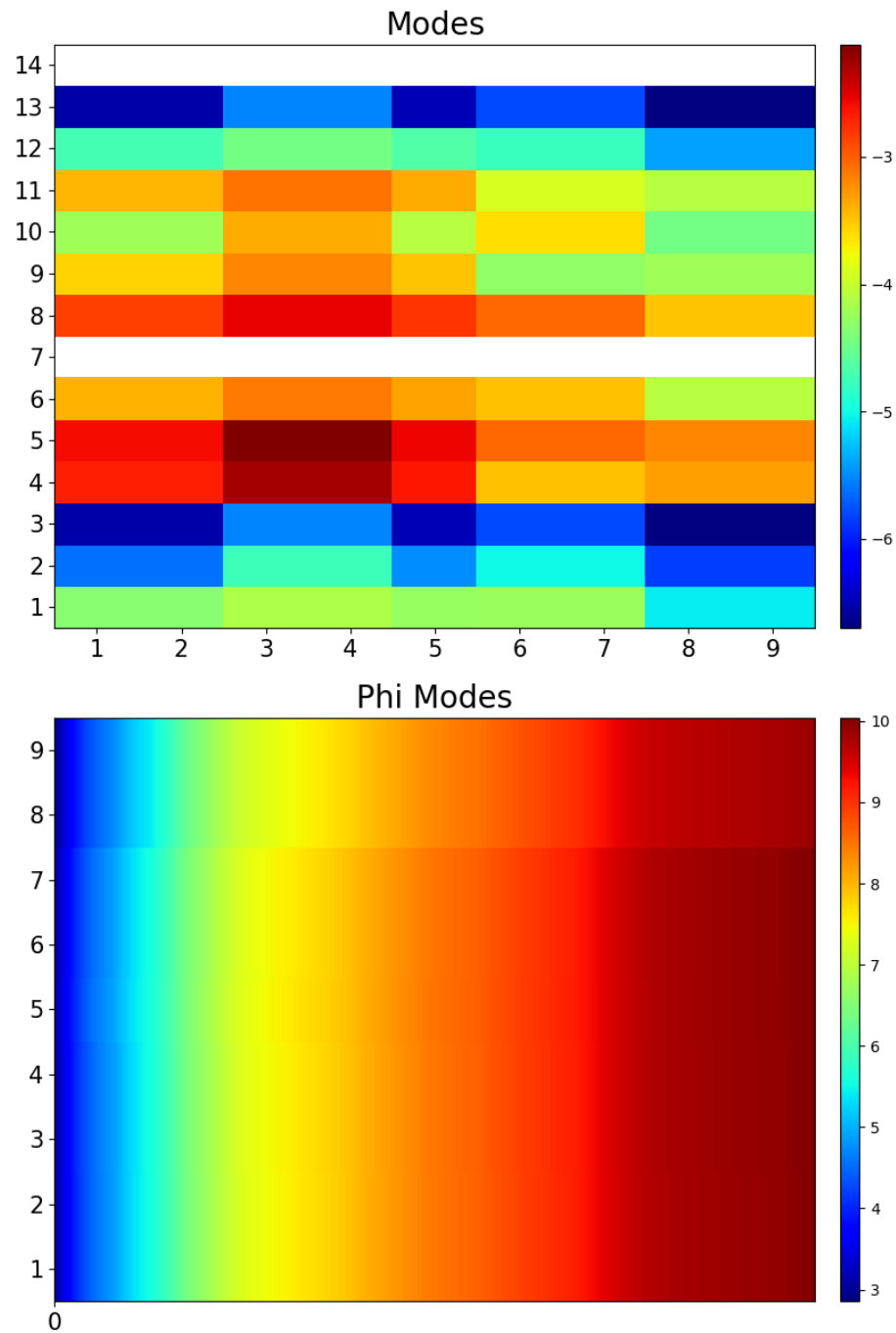


Figure 9.30. KDMD modes for the Thij model with $\lambda = 0.8$, $p = 0.8$.

9.14 Accuracy of Methods

We want to know how DMD handles different parameter simulations of the Thij model and how it compares to KDMD. We evaluate the two accuracy criterion described in section 8.2 across simulations and methods. We recall that we define the one-step reconstruction error, a measure of how well the modes and eigenvalues replicate the data. We also defined the mode error describing how well each DMD mode behaves like a true Koopman mode. We begin with the reconstruction error of the Barabási–Albert models.

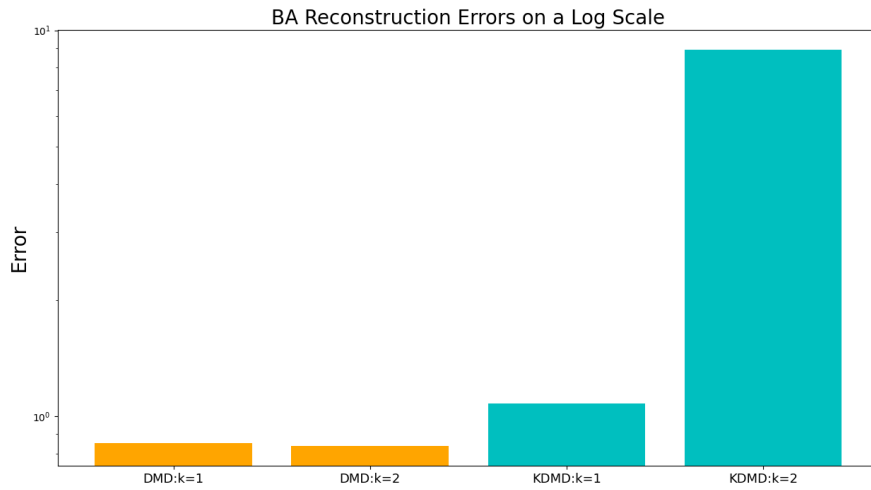


Figure 9.31. In orange, have the reconstruction error of the DMD results and in cyan the KDMD results. The DMD performs much better with regard to reconstruction error, by several scales of magnitude.

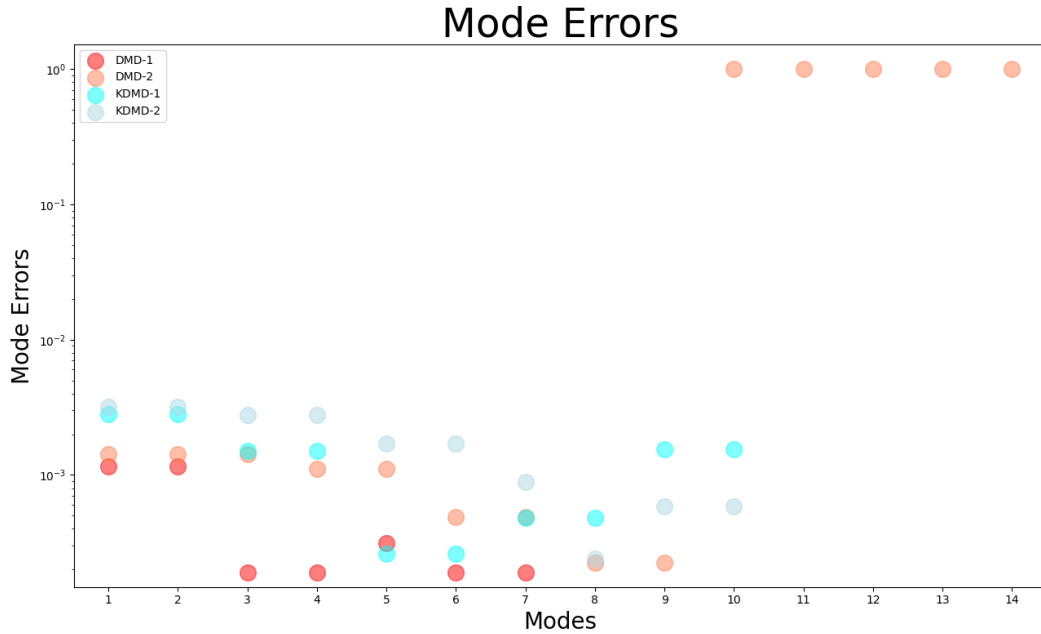


Figure 9.32. DMD also seems to produce modes with lower mode error. The scale on this figure is linear, so the differences are not as large as in figure 9.31.

Now we consider the performance of DMD and KDMD on the more complex Thij model.

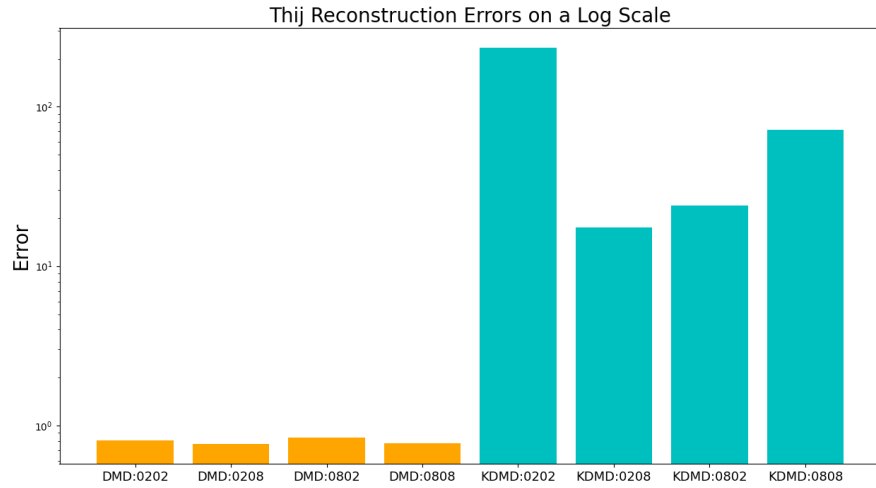


Figure 9.33. DMD and KDMD reconstruction errors across Thij simulations. DMD again has very low reconstruction errors compared to KDMD.



Figure 9.34. DMD and KDMD mode errors across simulations. DMD does seem to produce better results, but KDMD has the advantage of being able to produce more Koopman modes. The KDMD results for $\lambda = 0.2$, $p = 0.2$ is a noticeable outlier with very low mode error.

Examining these mode errors, we can see the modes from the standard DMD algorithm are just as accurate or more accurate than the KDMD modes. DMD also performs much better in terms of one-step reconstruction error over KDMD, which is not unexpected since DMD is a least-squares fit to the data. Overall the KDMD modes have low mode error.

CHAPTER 10

Discussion

From the results in the previous chapter, we are able to sift out differences in dynamic behavior by applying DMD to the motif counts. DMD produces modes that have associated temporal patterns: growth, decay, and oscillation. For many of these simulations, the real part of the DMD eigenvalues clusters around one or zero. We only see zero eigenvalues given that a mode does not exhibit any temporal behavior such as in the $k = 1$ Barabási–Albert simulation or the $p = 0.8$ Thij simulations. Otherwise, our observed eigenvalues tend to cluster in tight groups at the edge of the unit circle.

Examining the modes in chapter 9, we see block structure in the heatmaps in a pattern similar to those generated in the correlation and covariance matrices in chapter 7. If we look to figure 9.18 and 9.20 we can pick out in the former the strongest DMD modes reflect an association between $H3$, $H4$, $H7$, $H8$. In the latter simulation, KDMD produces modes of equal amplitude throughout time, but we can once again see the association between the same motifs.

For certain simulations, we have a readily available an a priori explanation of global network dynamics in the formation of large induced star subgraphs. The preferential attachment mechanism effectively acts as a positive feedback loop - the additional attachment of nodes to a node increases the likelihood of the future attachment to that same node. Even without such a tale DMD and KDMD are capable of extracting out underlying structure from these simulations.

A theory of induced star subgraphs on the network is most apt when there is a strong preferential attachment mechanism, but not so for $T3$ events. The $T3$ event opens up the possibility that there are attachments between appearances of motifs. A n selection of motifs means an $n!$ number of motif "joinings" to consider. In chapter 6, we considered the cases when the edge is added to the graph of a single motif. A complete investigation would have to consider dynamics of inter-motif reactions.

It's true that for any of the given simulations examined, the $H4$ motif was present if not outright central to the formation of the network's temporal development. That alone is not enough to suggest the formation of large S_k . In chapters 3 and 4, S_k induced subgraphs cause a relatively high abundance of $H4$ appearances and those motifs that have subgraphs isomorphic to the $H4$ graph provided the right initialization.

The correlation and covariance matrices of the motif counts show that all motifs strongly correlate with each other, but the covariances across different motifs vary greatly in magnitude. For Barabási-Albert model with $m = 1$, in figure 7.2, the motifs $H3, H4, H7, H8$ each have strong, positive covariances with one another. In figure 3.4, we see again the same covariance between those motif counts. In the Thij model, the covariances vary among parameter choices. For $\lambda = 0.2, p = 0.2$, in figure 7.6 $H8$ has high variance relative to other motif counts, and has strong covariance with the $H7, H9$, and $H10$ motif counts. In figure 7.8 for $\lambda = 0.2, p = 0.2$, the covariance matrix only shows high variance in the $H4$ motifs. Likewise in figure ??, we see the $H3$ motif has high, positive variance and covariance with the $H4, H7, H8, H9$, and $H10$ motif counts. Last, in figure 7.12, $H4$ has a very high, positive variance and high, positive covariance with the $H3$ motif count. The covariance and correlation matrices do not explain the DMD or KDMD modes, but they act as a companion to the sets of DMD and KDMD modes.

CHAPTER 11

Conclusion

The motif counts make valuable features to characterize the local structure of the network over time. Their dynamical behavior can be studied using traditional statistical methods as we have done above using correlation and covariance statistics. However DMD also provides a way to extract the spatiotemporal coherent structures associated with the motif counts. It is a different way of understanding how attaching nodes and edges to a graph, generates those new motifs.

The effects of adding nodes and edges can be understood through graph theory. As the attachment mechanisms become more complex the analysis becomes much more difficult. The connection of disjoint graphs can generate many new motifs quite suddenly. In the simplest case however the induced star subgraph offers a good explanation of why motifs correlate the way they do and could offer a way to interpret the DMD modes in the future. The study of motifs is young and better understanding of the dynamic interactions between motifs would greatly improve the ability to interpret the modes as physical phenomena.

The models above can be made more complex by introducing other mechanisms, such as an edge deletion mechanism. That mechanism would cause the deletion of certain motifs and could potentially introduce oscillatory behavior into the motif counts. These DMD and KMD modes may offer context to the modes we see above in chapter 8.

BIBLIOGRAPHY

- [1] I. ALBERT AND R. ALBERT, *Conserved network motifs allow protein–protein interaction prediction*, Bioinformatics, 20 (2004), pp. 3346–3352.
- [2] R. ALBERT AND A.-L. BARABÁSI, *Statistical mechanics of complex networks*, Reviews of Modern Physics, 74 (2002), p. 47–97.
- [3] J. ALLEN, B. HOWLAND, M. MOBIUS, D. ROTHSCHILD, AND D. J. WATTS, *Evaluating the fake news problem at the scale of the information ecosystem*, Science Advances, 6 (2020), p. eaay3539.
- [4] N. ALON, R. YUSTER, AND U. ZWICK, *Finding and counting given length cycles*, in Algorithms — ESA '94, J. van Leeuwen, ed., Berlin, Heidelberg, 1994, Springer Berlin Heidelberg, pp. 354–364.
- [5] S. APARICIO, J. VILLAZÓN-TERRAZAS, AND G. ÁLVAREZ, *A model for scale-free networks: Application to twitter*, Entropy, 17 (2015), pp. 5848–5867.
- [6] A.-L. BARABÁSI AND R. ALBERT, *Emergence of scaling in random networks*, Science, 286 (1999), p. 509–512.
- [7] A.-L. BARABÁSI AND M. PÓSFAI, *Network science*, Cambridge University Press, Cambridge, 2016.
- [8] A. BESSI, F. PETRONI, M. DEL VICARIO, F. ZOLLO, A. ANAGNOSTOPOULOS, A. SCALA, G. CALDARELLI, AND W. QUATTROCIOCCHI, *Homophily and polarization in the age of misinformation*, The European Physical Journal Special Topics, 225 (2016).
- [9] S. BHAMIDI, J. M. STEELE, AND T. ZAMAN, *Twitter event networks and the superstar model*, The Annals of Applied Probability, 25 (2015).
- [10] G. BLANK, *The digital divide among twitter users and its implications for social research*, Social Science Computer Review, 35 (2017), pp. 679–697.
- [11] J. BOLLEN, H. MAO, AND X. ZENG, *Twitter mood predicts the stock market*, Journal of Computational Science, 2 (2011), pp. 1–8.
- [12] A. BOVET AND H. A. MAKSE, *Influence of fake news in twitter during the 2016 us presidential election*, Nature communications, 10 (2019), pp. 1–14.
- [13] R. BROWNE, *Bitcoin spikes 20% after elon musk adds #bitcoin to his twitter bio*. "<https://www.cnbc.com/2021/01/29/bitcoin-spikes-20percent-after-elon-musk-adds-bitcoin-to-his-twitter-bio.html>", March 2020. [Online; accessed 15-March-2021].
- [14] R. BROWNE, *Tweets from elon musk and other celebrities send dogecoin to a record high*. "<https://www.cnbc.com/2021/02/08/>

- [tweets-from-elon-musk-and-celebrities-send-dogecoin-to-a-record-high.html](https://www.cnbc.com/2020/05/01/tesla-ceo-elon-musk-says-stock-price-is-too-high-shares-fall.html)", February 2020. [Online; accessed 19-March-2021].
- [15] S. L. BRUNTON, M. BUDIŠIĆ, E. KAISER, AND J. N. KUTZ, *Modern koopman theory for dynamical systems*, 2021.
 - [16] J. BURSZTYNSKY, *Tesla shares tank after elon musk tweets the stock price is ‘too high’*. "<https://www.cnbc.com/2020/05/01/tesla-ceo-elon-musk-says-stock-price-is-too-high-shares-fall.html>", March 2020. [Online; accessed 15-March-2021].
 - [17] C. CURTIS, R. CARRETERO-GONZALEZ, AND M. POLIMENO, *Characterizing coherent structures in bose-einstein condensates through dynamic-mode decomposition*, Physical Review E, 99 (2019).
 - [18] E. FERRARA, *# covid-19 on twitter: Bots, conspiracies, and social media activism*, arXiv preprint arXiv:2004.09531, (2020).
 - [19] V. R. K. GARIMELLA AND I. WEBER, *A long-term analysis of polarization on twitter*, in Proceedings of the International AAAI Conference on Web and Social Media, vol. 11, 2017.
 - [20] J. H. TU, C. W. ROWLEY, D. M. LUCHTENBURG, S. L. BRUNTON, AND J. NATHAN KUTZ, *On dynamic mode decomposition: Theory and applications*, Journal of Computational Dynamics, 1 (2014), p. 391–421.
 - [21] A. JAZAYERI AND C. C. YANG, *Motif discovery algorithms in static and temporal networks: A survey*, Journal of Complex Networks, 8 (2020). cnaa031.
 - [22] K. KLEMM AND V. M. EGUILUZ, *Growing scale-free networks with small-world behavior*, Physical Review E, 65 (2002).
 - [23] J. N. KUTZ, S. L. BRUNTON, B. W. BRUNTON, AND J. L. PROCTOR, *Dynamic Mode Decomposition*, Society for Industrial and Applied Mathematics, Philadelphia, PA, 2016.
 - [24] R. MILO, S. SHEN-ORR, S. ITZKOVITZ, N. KASHTAN, D. CHKOVSII, AND U. ALON, *Network motifs: Simple building blocks of complex networks*, Science, 298 (2002), pp. 824–827.
 - [25] M. MOSLEH, G. PENNYCOOK, A. A. ARECHAR, AND D. G. RAND, *Cognitive reflection correlates with behavior on twitter*, Nature communications, 12 (2021), pp. 1–10.
 - [26] A. PARANJAPE, A. R. BENSON, AND J. LESKOVEC, *Motifs in temporal networks*, in Proceedings of the Tenth ACM International Conference on Web Search and Data Mining, WSDM ’17, New York, NY, USA, 2017, Association for Computing Machinery, p. 601–610.
 - [27] F. PIERRI, C. PICCARDI, AND S. CERI, *Topology comparison of twitter diffusion networks reliably reveals disinformation news*, (2019).
 - [28] R. J. PRILL, P. A. IGLESIAS, AND A. LEVCHENKO, *Dynamic properties of*

- network motifs contribute to biological network organization*, PLOS Biology, 3 (2005), p. null.
- [29] N. PRZULJ AND I. JURISICA, *Modeling interactome: Scale-free or geometric?*, Bioinformatics (Oxford, England), 20 (2005), pp. 3508–15.
 - [30] Y. RUAN, A. DURRESI, AND L. ALFANTOUKH, *Using twitter trust network for stock market analysis*, Knowledge-Based Systems, 145 (2018), pp. 207–218.
 - [31] C. SHAO, G. L. CIAMPAGLIA, O. VAROL, K.-C. YANG, A. FLAMMINI, AND F. MENCZER, *The spread of low-credibility content by social bots*, Nature Communications, 9 (2018).
 - [32] D. SHEN, A. URQUHART, AND P. WANG, *Does twitter predict bitcoin?*, Economics Letters, 174 (2019), pp. 118–122.
 - [33] M. TEN THIJ, T. OUBOTER, D. WORM, N. LITVAK, H. BERG, AND S. BHULAI, *Modelling of trends in twitter using retweet graph dynamics*, 01 2015.
 - [34] M. O. WILLIAMS, I. G. KEVREKIDIS, AND C. W. ROWLEY, *A data-driven approximation of the koopman operator: Extending dynamic mode decomposition*, Journal of Nonlinear Science, 25 (2015), p. 1307–1346.
 - [35] M. O. WILLIAMS, C. W. ROWLEY, AND I. G. KEVREKIDIS, *A kernel-based approach to data-driven koopman spectral analysis*, 2015.
 - [36] S. WOJCIK AND A. HUGHES, *Sizing up twitter users*, PEW research center, 24 (2019).
 - [37] H. ZHANG, S. T. M. DAWSON, C. W. ROWLEY, E. A. DEEM, AND L. N. CATTAFESTA, *Evaluating the accuracy of the dynamic mode decomposition*, 2017.